High-Precision Linewidth Tunable Light Source with Optical Phase Modulation for Linewidth Dependence Evaluation of Optical Systems

光システムの線幅依存性評価のための光位相変調を用いた高精度線幅可変光源に関する研究

February, 2024

Yu ZHOU
周　宇

High-Precision Linewidth Tunable Light Source with Optical Phase Modulation for Linewidth Dependence Evaluation of Optical Systems

光システムの線幅依存性評価のための光位相変調を用いた高精度線幅可変光源に関する研究

February, 2024

Waseda University Graduate School of Fundamental Science and Engineering

Department of Electronic and Physical Systems, Research on Radio and Optical Converged Systems

Yu ZHOU
周　宇

Abstract

Laser linewidth refers to the range of frequencies over which a laser emits light. Ideally, a laser produces light at a single frequency, which would mean it has zero linewidth. However, in reality, various physical phenomena, such as quantum noise, thermal fluctuations, and technical noise, cause lasers to emit light over a spectrum of frequencies. The extent of this frequency spread, known as linewidth, reveals the spectral purity of the laser, a smaller linewidth indicates lower noise levels, often associated with higher precision and coherence in numerous technological applications. Consequently, the linewidth is a critical factor in the functioning of optical atomic clocks, coherent optical systems, and frequency-modulated continuous wave (FMCW) light detection and ranging (LiDAR).

The laser linewidth is typically quantified by the full width at half maximum (FWHM), which is a significant factor in determining the laser precision, operational range, and sensitivity. Hence, a detailed analysis of system tolerance to laser linewidth is essential for improving performance. Additionally, noise does not only widen the laser linewidth but also influences its line shape. For example, white Gaussian noise tends to produce a Gaussian line shape. The line shape, in turn, substantially affects systems that are sensitive to linewidth variations, such as FMCW LiDAR with coherent receivers. Therefore, it is not

just the amount of noise that matters but also its type. Understanding the impact of different types of laser noise on system performance necessitates a detailed examination of laser noise characteristics.

A noise source is often introduced to assess the impact of noise on a system. In electrical experiments, this is typically an electrical noise source. However, such noise sources are not readily available for lasers. Previously, researchers would change the laser diode or employ internal phase modulation to investigate phase noise in lasers. These methods are costly, time-consuming, do not allow the precise control of laser phase noise, and result in unstable output power and wavelength. A novel approach using an external lithium niobate (LN) phase modulator is suggested for addressing these challenges and providing an efficient means to measure laser phase noise in coherent systems. This new method enables more precise, stable, and cost-effective characterization of laser phase noise. It simplifies the process of incorporating and analyzing the effects of laser phase noise on coherent systems within experimental setups.

The external LN phase modulator is employed to induce phase changes in the laser, effectively simulating laser phase noise. This modulator is advantageous due to its stable output power and its ability to linearly modulate phase in response to the input electrical signal. Due to these benefits, two noise types are utilized: random walk noise with limited walls and white Gaussian noise. The random walk noise is limited in its low-frequency components; hence, white Gaussian noise is used to compensate for this deficiency. Combining these two

distinct noises and carefully controlling them enables operating the laser line shape into various forms. The effectiveness of this innovative method is first established through detailed theoretical equations, followed by simulations, and then confirmed by practical experiments, providing a solid confirmation of the validity of the technique.

Field-programmable gate arrays (FPGAs) are utilized to generate two specific types of noise: random walk noise with limited walls and white Gaussian noise. FPGAs are chosen for their cost-effectiveness, compact size, and, crucially, their ability to produce customizable electrical noise signals. These advantages enable a more accurate replication of actual laser phase noise, which aids in a deeper understanding of real-world laser noise characteristics. Furthermore, the precise noise generation capability of FPGAs allows for high-precision control over the laser linewidth and line shape. This precision enables experiments to capture slight variations in phase noise and offers a more detailed understanding of the impact of laser phase noise on coherent systems. Essentially, the assessment of laser linewidth is the most crucial element within optical systems, particularly in coherent systems. The method previously discussed enables precise control over the laser linewidth and line shape, which allows for an in-depth investigation of their effects on FMCW LiDAR systems equipped with coherent receivers. With this high-precision control, the optical phase noise within such coherent systems can be thoroughly understood, guiding the selection of an appropriate laser to reduce system costs. Equally important is understanding

the influence of laser line shape on the system. This knowledge can inform us about the various impacts of noise on the system and serve as a reference for optical phase noise considerations. The system's tolerance to optical phase noise can be quickly and accurately determined using lasers with variable linewidth and line shape; this enhances the understanding of LiDAR technology and promotes its wider adoption.

The findings and discussions outlined in this dissertation provide a critical resource for creating high-precision, variable light sources incorporating optical phase modulation. They also deliver essential insights for assessing the impact of laser linewidth on the performance of optical systems, which is particularly relevant in the context of coherent detection technologies like FMCW LiDAR. These contributions are instrumental in advancing the field of photonics, where the control of linewidth and phase noise are vital for the enhancement of optical communication and sensing technologies.

Keywords:

variable linewidth laser, variable lineshape laser, external lithium niobate (LN) phase modulator, white Gaussian noise, random walk noise with limited walls, Frequency-modulated continuous wave (FMCW) light detection and ranging (LiDAR), coherent receiver, Field-programmable gate array (FPGA), and meticulous precision.

Table of Contents

Chapter 1 Introduction **1**

1.1 Overview of laser and laser linewidth 1

1.2 Historical review and research motivation 5

1.2.1 Variable linewidth and lineshape laser 5

1.2.2 FPGA for signal generation 7

1.2.3 FMCW LiDAR Using Coherent Receiver 9

1.3 Dissertation structure 13

Chapter 2 Variable linewidth and lineshape lasers **15**

2.1 Introduction 15

2.2 The theory of the variable linewidth laser 17

2.2.1 Random walk noise for the variable linewidth laser 18

2.2.2 Equations for the laser linewidth 21

2.2.3 Equations for the line shape of the laser spectrum 28

2.3 Experimental setup 29

2.4 Results and discussions 31
2.4.1 Simulation results of variable linewidth laser 31
2.4.2 Experimental results of the variable linewidth laser 37
2.4.3 Simulation results of the variable line shape laser 44
2.4.4 Experimental results of the variable lineshape laser 46
2.5 Summary 49

Chapter 3 FPGA-based variable linewidth and lineshape laser 51

3.1 Introduction 51
3.2 White Gaussian noise for variable linewidth laser in FPGA 54
3.2.1 The principle of white Gaussian noise generation in FPGA 54
3.2.2 Experimental setup 57
3.2.3 Results and discussions 59
3.3 Random walk noise for variable linewidth laser in FPGA 64
3.3.1 The principle of the random walk noise generation in FPGA 64
3.3.2 Experimental setup 67
3.3.3 Results and discussions 68
3.4 Varibale linewidth and line shape laser based on two FPGAs . . . 77
3.4.1 Experimental Setup 82
3.4.2 Random numbers for noise generation 84
3.4.3 Results and discussions 90
3.5 Summary 106

Chapter 4 Exploring the Impact of Laser Linewidth on FMCW LiDAR **108**

4.1 Introduction 108

4.2 Experimental setup 112

4.2.1 Low-frequency compensation using digital noise source . 112

4.2.2 Low-frequency compensation using an analog noise source 115

4.3 Results and discussions 116

4.3.1 Results of digtial noise 116

4.3.2 Results of analog noise 127

4.4 Summary 134

Chapter 5 Conclusion **136**

REFERENCES **139**

Acknowledgements **151**

Publication List **153**

List of Figures

1.1 The simple principle of theFMCW LiDAR [48] 9

1.2 Linear chirp modulation of a signal, and the beat frequencies it produces through interference between the transmitted and reflected signal. [48] 10

2.1 The schematic diagram of (a) random walk and (b) random walk with limit wall 19

2.2 Experimental setup of the laser linewidth measurements using the coherent interference. 29

2.3 Simulation results on the laser spectrum of different cutoff frequency with same power. 32

2.4 The respective noise PSD of different cutoff cutoff frequencies with the same. 33

2.5 Simulation results on the laser spectrum of different power with same cutoff frequency. 34

2.6 The respective noise PSD of different power with the same cutoff frequency. 35
2.7 Simulation results on the laser spectrum of the random walk without a limited wall and with a limited wall. 36
2.8 The respective noise PSD of the random walk without a limited wall and with a limited wall. 37
2.9 Results of the half-wave voltage of the phase modulator. 38
2.10 Results of laser spectrum for the different powers of white Gaussian noises. 39
2.11 Results of laser spectrum for the different cutoff frequencies of white Gaussian noises. 40
2.12 Spectrum results of laser for the noise of different cutoff frequencies. 41
2.13 Laser spectrum of the white Gaussian noise compensation. 42
2.14 The noise spectrum of the mixed noise. 43
2.15 Simulation results of different white Gaussian noise power and cutoff frequency on the Lorentz components. 45
2.16 Laser spectrum of only white Gaussian noise. 46
2.17 Laser spectrum of white Gaussian noise mixed random walk noise. 47

3.1 Principle of the programmable white Gaussian noise using the FPGA with DACs. 54

3.2 Principle of generating white Gaussian noise using the FPGA with DACs. 57
3.3 Spectrum of white Gaussian noise with a 200 kHz cutoff frequency and varying standard deviations. 60
3.4 Laser spectrum linewidth under different standard deviations of white Gaussian noise. 61
3.5 Spectrum of the original normal distribution of white Gaussian noise with different standard deviations. 62
3.6 Spectrum of normal distribution of white Gaussian noise with different standard deviations. 63
3.7 Principle of generating random walk noise with a limit wall using the FPGA with DACs. 65
3.8 Experimental scheme of the variable linewidth laser and laser linewidth measurement. 67
3.9 Random walk noise in the frequency domain: 0.09 V SL with 600 MHz SR and 0.01 V SL with 50 MHz SR. 69
3.10 Spectrum of random walk noises mixed with WGN of 120-140 kHz. 70
3.11 Laser spectrum linewidth affected by random walk noises mixed with WGN of 120-140 kHz. 72
3.12 Spectrum of random walk noises mixed with WGN of 150-170 kHz. 73

3.13 Laser spectrum linewidth affected by the random walk noises mixed with WGN of 150-170 kHz. 74
3.14 Principle of the new random number generation method. 78
3.15 Principle of generating white Gaussian noise using the FPGA with DACs with novel random number generating method. 79
3.16 Principle of generating random walk noise with limited wall using the FPGA with DACs with new random number generating method. 81
3.17 Experimental scheme of the variable linewidth laser and laser linewidth measurement with FPGA system. 82
3.18 The simulation results of the white Gaussian distribution. 85
3.19 The simulation results of the white Gaussian distribution number mixed with pseudorandom number. 86
3.20 The random number results of the analog noise from ADCs. . . . 87
3.21 The results of the mixed random number from analog noise and pseudorandom number. 88
3.22 Noise power density spectrum of white Gaussian noise with different STDs. 90
3.23 Laser spectrum of white Gaussian noise with different STDs. . . . 91
3.24 Relationship of laser spectrum and white Gaussian noise with different STDs. 92
3.25 Spectrum of white Gaussian noise with a 200 kHz cutoff frequency and different generation methods. 93

3.26 Spectrum of normal distribution of white Gaussian noise with different STDs of the original one. 94
3.27 Spectrum of normal distribution of white Gaussian noise with different STDs of the actual one. 95
3.28 Spectrum of white Gaussian noise with different STDs and a 200 kHz cutoff frequency. 97
3.29 The laser spectrum linewidth of with white noise having different STDs. 98
3.30 Spectrum of the 0.2029 V STD white Gaussian noise with different cutoff frequencies. 99
3.31 The laser spectrum linewidth of the 0.2029 V STD white Gaussian noise with different cutoff frequency. 100
3.32 Measured linewidth results with different STDs having different cutoff frequencies of the white Gaussian noise. 101
3.33 The noise spectrum of the two FPGA methods and FPGA with AWG method. 103
3.34 The laser spectrum linewidth using the two FPGA method and FPGA with AWG method. 105

4.1 The experimental scheme of a phase-diversity coherent FMCW LiDAR using variable laser linewidth. 113
4.2 Experimental scheme of phase-diversity coherent FMCW LiDAR using variable linewidth and variable line shapes laser. . . 115

4.3 The relationship between the laser linewidth and the intensity of the velocity signal. 116
4.4 The relationship between the laser linewidth and the linewidth of the velocity signal. 117
4.5 The relationship between the laser linewidth and the position of the velocity signal. 120
4.6 The laser spectrum of the low-frequency compensation method. . 121
4.7 The laser spectrum of the mirror method. 123
4.8 The velocity signal spectrum of the low-frequency compensation method. 124
4.9 The velocity signal spectrum of the mirror method. 126
4.10 Relationship between laser linewidth and laser line shape. 128
4.11 Relationship between laser linewidth, laser line shape, and velocity signal intensity. 130
4.12 Relationship between laser linewidth, laser line shape, and velocity signal linewidth. 131
4.13 Velocity signal spectrum of white Gaussian noise. 132
4.14 Velocity signal spectrum of white Gaussian noise mixed random walk noise. 132
4.15 Relationship between laser linewidth, laser line shape, and velocity signal DFSs. 133

List of Tables

3.1 Dependence of theoretical and actual laser linewidths on the random walk SL and WGN. 75

Chapter 1 Introduction

1.1 Overview of laser and laser linewidth

Laser is an abbreviation for ”Light amplification by stimulated emission of radiation” and lasers function on the principle of stimulated emission [1].

Different types of lasers exhibit varying linewidth characteristics [1, 2, 3, 4]:

1. Fiber lasers: Fiber lasers use an optical fiber as the gain medium, with the core doped with rare-earth elements like erbium. Their long interaction length and the waveguiding nature result in narrower linewidths. Known for high power, excellent beam quality, and relatively narrow linewidths, these lasers are particularly effective as single-frequency fiber lasers. The typical linewidth of it is under 100 Hz, and the lineshape predominantly observed is Lorentzian in nature.

2. External cavity lasers (ECL): ECLs employ an external optical resonator for feedback, instead of the natural facets of a laser diode. The extended cavity length of ECLs contributes to significantly reduced linewidths. They

are capable of producing extremely narrow linewidths and are widely used in precision spectroscopy and sensing.The typical linewidth of it is under 1 kHz, and the lineshape predominantly observed is Lorentzian in nature.

3. Distributed feedback (DFB) lasers: DFB lasers are semiconductor lasers featuring a periodic structure, typically a Bragg grating, within their active region. This grating ensures selective feedback for a certain wavelength, rendering DFB lasers single-frequency sources. They are valued for their narrow linewidth and stability, making them popular in telecommunications. The typical linewidth of it is about several MHz, and the lineshape mainly observed is Lorentzian.

4. Vertical external surface-emitting lasers (VCSELs): VCSELs emit light perpendicularly to the semiconductor plane, differing from edge-emitting lasers. They usually have a shorter cavity length, leading to broader linewidths. However, they are advantageous in power efficiency, integration into arrays, and beam profiles. The typical linewidth of it is about hundreds MHz, and the lineshape is observed as Lorentzian and Gaussian

The laser linewidth is a parameter that quantifies the spectral width over which a laser operates, indicating the frequency range where the laser emits most of its power [1].

Ideally, a laser would emit light at a single frequency, resulting in a zero

linewidth. However, real-world lasers emit over a range of frequencies owing quantum noise, thermal fluctuations, and technical noise. This frequency spread, or linewidth, is a measure of the laser's spectral purity [1, 2, 5]. The previously mentioned laser types −fiber laser, ECL, DFB, and VCSEL −each have different linewidths that are reflected in their specific applications.

A narrower linewidth typically indicates a more monochromatic source, often equated with precision and coherence in various applications [6]. Laser linewidth is crucial in fields like optical atomic clocks, coherent optical systems, and Frequency-Modulated Continuous-Wave (FMCW) Light Detection and Ranging (LiDAR). The full width at half maximum (FWHM) of the laser significantly affects its precision, range, and sensitivity [7, 8, 9, 10, 11, 12]. A thorough assessment of system tolerance in relation to laser linewidth is crucial for reducing costs and improving performance [13]. Especially as the demand for autonomous driving grows, the focus shifts to implementing cost-effective, high-quality sensors [14].

Furthermore, the laser line shape characterizes the distribution of its emitted power across the frequency spectrum, explaining how the intensity varies at different frequencies [15, 16, 17]. While the linewidth indicates the width of this spectrum, the lineshape reveals its form, which can be Lorentzian, Gaussian, or a Voigt profile. These profiles arise from various broadening mechanisms and factors in laser design [18, 19]. The lineshape also has its effects in fields like spectroscopy, optical communication, and frequency metrology. It significantly

influences resolution, data transmission, and precision measurements, thereby serving as a key parameter in advanced laser applications [20, 21].

Exploring the trends of laser linewidth and lineshape in optical systems is crucial for deepening the understanding of optical noise and its various forms. In electrical engineering, the abundance of noise sources has led to extensive experimental research on the impact of electrical noise on system performance. However, in the optical domain, the lack of similar optical noise sources poses a significant challenge for researchers aiming to conduct analogous studies. Developing a laser with tunable linewidth and lineshape, capable of high-precision control and continuous variation, marks a significant breakthrough, serving effectively as an optical noise source in laser systems. This innovation paves the way for detailed investigations into the effects of optical noise in experimental setups, offering a tool for generating continuous, controlled disturbances. With the ability to precisely adjust this optical noise source, researchers can now simulate a broad range of real-world interferences.

Hence, the related works are also included in this dissertation for the variable lineshape laser.

1.2 Historical review and research motivation

1.2.1 Variable linewidth and lineshape laser

The laser linewidth, typically characterized by its full width at half maximum (FWHM), defines the spectral range where most of the laser output power is concentrated [22]. It is an indicator of the laser coherence properties, with a narrower linewidth indicating higher temporal coherence [23]. FWHM is a parameter that reveals the spread of the laser power spectrum [24], and is vital for numerous optical applications, making its measurement essential in photonics research and practical applications [20].

In laser production, linewidth often becomes a fixed characteristic after manufacturing [25]. While variable linewidth lasers exist, they face challenges, particularly in precision, often resulting in undesirably broad linewidths [19, 26]. There is a divide between research, which favors narrow linewidths fiber laser under 100 Hz , and practical applications, where cost-effective but broader linewidth lasers are common [27, 28]. Thus, there is a pressing need for a variable linewidth laser that is not only responsive but also maintains high precision [29].

Additionally, understanding the laser line shape, which is influenced by various noise sources within the laser system, is crucial. The line shape, indicative of the laser spectral distribution, offers insights into its stability and potential disturbances [30]. Simulating different line shapes, dictated by specific noise profiles, is essential for aligning lasers with application-specific needs.

A comprehensive examination of both laser linewidth and line shape provides deep insights into the impact of laser noise on various systems [31]. A holistic approach, considering both parameters, enables a better understanding of system disturbances and optimization opportunities.

1.2.2 FPGA for signal generation

The development of variable linewidth lasers necessitates customizing noise profiles like low-frequency white Gaussian noise and high-frequency random walk noise, closely resembling real laser noise. In addition these profiles must enable the generation of specific parameters, such as standard deviation (STD) in white Gaussian noise. Alongside this, a need for a lighter, low-cost system is imperative. Consequently, field-programmable gate arrays (FPGAs) are considered essential due to their advanced digital signal processing architectures, effectively bridging the analog and digital domains [32].

Analog-to-digital converters (ADCs) play a key role in this process, converting continuous analog waveforms into quantized digital forms and preserving the original signal's nuances [33]. Once in the FPGA digital realm, digital signal processing techniques like decimation and filtering refine the digital representation, particularly emphasizing essential low-frequency components that often get overshadowed by higher frequencies [34, 35]. These components are crucial for simulating actual laser noise, which is influenced by temperature and other factors [36, 37, 38, 39].

FPGAs often incorporate Look-up tables (LUTs) and Direct Digital synthesis (DDS) modules to generate specific low-frequency waveforms [40, 41, 42]. LUTs store predefined waveforms for precise replication [43], while DDS modules enable dynamic waveform creation through phase increment control.

Digital-to-analog converters (DACs) are essential in the final stage,

transforming processed digital data back into continuous analog waveforms [44]. This step is useful, especially for low-frequency signals, where precision ensures waveform integrity.

The cooperation of FPGA, ADC, and DAC offers a complex mechanism for capturing, refining, and regenerating low-frequency signals, representing the fusion of analog and digital technologies [44].

Integrating of FPGAs with DACs and ADCs has led to significant advancements in generating specialized noise patterns. Utilizing LUTs and DDS within FPGAs enables the synthesis of low-frequency white Gaussian noise and high-frequency random walk noise within defined boundaries [41, 42]. This noise generation not only improves the precision control of variable linewidth lasers but also signifies a shift towards more cost-effective and compact system designs.

1.2.3 FMCW LiDAR Using Coherent Receiver

Frequency-Modulated Continuous-Wave (FMCW) LiDAR, utilizing linearly frequency-modulated (LFM) waveforms, is a leading technology in remote sensing [45]. Its low peak power, wide dynamic range, and excellent ranging resolution make it vital for 3D imaging, remote sensing, and autonomous navigation [46, 47, 48, 49]. FMCW LiDAR adaptability for multi-domain information measurement, allowing simultaneous extraction of distance and velocity, marks its true potential.

The typical principle of FMCW LiDAR is showed in the Figure 1.1 [48].

It works by emitting a continuous laser signal with a gradually changing frequency, similar to how a siren's pitch changes as it moves past. When the laser light bounces back from an object, the system compares the frequency of the reflected light to that of the current signal. This comparison reveals any shifts caused by the distance the light traveled. The system calculates how far away the object is by measuring these shifts.

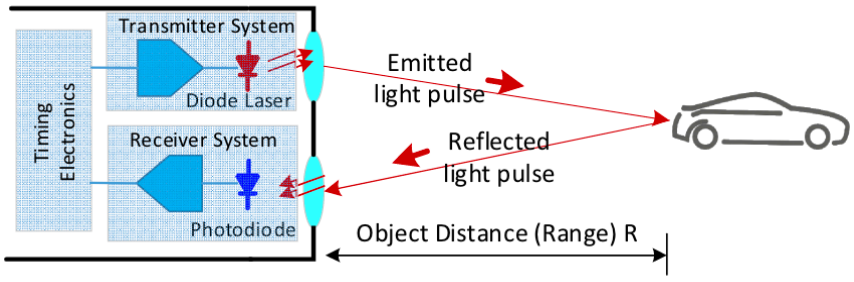

Figure 1.1: The simple principle of theFMCW LiDAR [48]

In this system, the antenna emits radio waves with a frequency that linearly increases from a base frequency f_0 to a maximum frequency $f_{\max}$ (referred to as "upchirp") over a certain period T. This is followed by a decrease in frequency from $f_{\max}$ back to f_0 over the same period T, known as "downchirp" (Figure 1.2) [48].

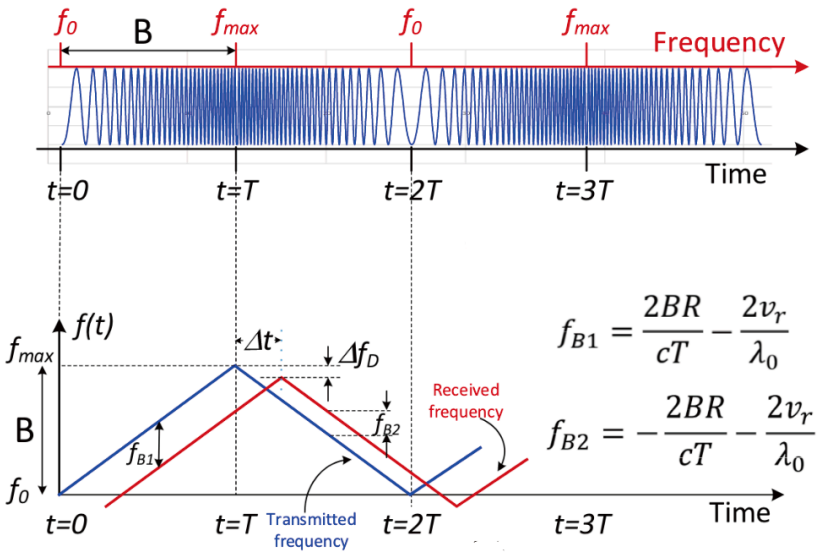

Figure 1.2: Linear chirp modulation of a signal, and the beat frequencies it produces through interference between the transmitted and reflected signal. [48]

Consider a scenario where the wave emitted at $t = 0$ encounters an object at a distance R, moving with a radial velocity v_r. After a time delay $\Delta t = \frac{2R}{c}$, the back-reflected wave returns to the transmitter-receiver, where it interferes with the wave emitted at that moment. The frequency of the received wave differs

from the emitted wave at that instant due to two factors: the round-trip travel time Δt, which depends on the range R of the object, and the Doppler shift Δf_D caused by the reflection from a moving object. This interference results in a beat frequency f_{B1} on the upchirp side and f_{B2} on the downchirp side of the frequency modulation [48].

However, its multifunctionality introduces the challenge of signal aliasing, necessitating innovative solutions [50, 51, 52]. Proposed solutions include integrating diverse probe signals and designing specific waveforms like dual-sideband modulation, though they face issues like negative frequency measurements and potential ambiguities [53].

A transformative approach in LiDAR technology is integrating FMCW LiDAR with a phase-diversity coherent receiver [54, 55]. This integration overcomes existing challenges and opens new possibilities. The phase-diversity coherent receiver discerns both intensity and phase of optical signals, enhancing FMCW LiDAR's bandwidth and enabling concurrent distance and velocity measurements [56]. It also mitigates atmospheric-induced optical phase fluctuations, including turbulence-induced Doppler frequency shifts [57, 58, 59], enhancing LiDAR quality.

However, laser linewidth, indicating optical phase noise, affects FMCW LiDAR precision. The absence of continuous variable linewidth lasers for high-precision control aggravates this issue. Even minor changes in laser linewidth significantly impact LiDAR performance. Employing a variable linewidth

laser through this method is essential for understanding the laser lineshape and linewidth effects on FMCW LiDAR when combined with a coherent receiver. This approach assists in understanding the laser's tolerance within the FMCW LiDAR system. Exploring this relationship helps in identifying cost reduction opportunities and fully comprehending the system. These insights are important for optimizing existing methodologies and expanding the technology applications and scalability.

1.3 Dissertation structure

Chapter 1 sets the foundation by offering an insightful overview of the historical development and advancement in technologies related to lasers with variable linewidth and lineshape. It examines the academic value, describing the motivation and research objectives that guide this dissertation.

Chapter 2 provides a comprehensive examination of lasers with variable linewidth and lineshape. It lays down a framework that seamlessly integrates theoretical models, high-performance computing (HPC) simulations, and experimental validations. This multifaceted approach enhances the depth of the theoretical foundations of the study. The chapter demonstrates the feasibility and efficacy of lasers with variable linewidth and lineshape through a blend of theoretical predictions and practical experiments. This chapter validates the operational viability of variable linewidth and lineshape lasers by combining these concepts with both computational and experimental evidence.

Chapter 3 focuses on the pioneering application of FPGAs in developing an efficient, cost-effective, and high-precision control system for modulating laser linewidth and lineshape. It highlights how integrating FPGAs enables the generation of noise profiles closely resembling actual laser noise, facilitating a more realistic simulation of laser behaviors. The chapter details the design and implementation of a dual-FPGA setup, which is instrumental in realizing a laser with variable linewidth capabilities. This discussion emphasizes the significant steps made in technological development and the succeeding enhancements in

operational efficiency.

Chapter 4 presents an in-depth analysis of the use of lasers with variable linewidth and lineshape in the field of FMCW LiDAR systems, specifically those employing coherent detection techniques. This chapter explores the intricate relationship between the properties of laser linewidth and the overall performance and efficacy of LiDAR systems. It comprehensively examines both the traditional approach of employing analog noise sources and the method of using digital noise sources, such as function generators (FG). The chapter provides a study of these two methods, highlighting their respective impacts on LiDAR system performance. This exploration indicates how the manipulation of laser linewidth and lineshape can significantly influence LiDAR system capabilities, offering insights into potential advancements and optimizations in this technology.

The concluding chapter, Chapter 5, integrates the key findings and technological breakthroughs presented in the earlier chapters. It summarizes the significant contributions of this research to laser technology and outlines potential avenues for future investigation.

This dissertation is structured to not only organize the research journey but also to emphasize the methodical approach employed in dealing with challenges associated with lasers having variable linewidth and lineshape. It represents an integrated and scholarly exploration of the topic.

Chapter 2 Variable linewidth and lineshape lasers

2.1 Introduction

Historically, attempts to test optical phase noise in systems such as electrical noise sources in standard experiments using variable linewidth lasers have adopted various methods [4]. A common technique involves directly modifying the laser diode [28]. While this offers some flexibility, it faces challenges such as the need for multiple lasers, inconsistent output power, and limitations in achieving continuous changes in linewidth, leading to discrete linewidth values instead of a continuous range [28].

An alternative approach uses internal modulation to control the laser linewidth. This method allows for continuous linewidth adjustment but requires a complex feedback system for current and temperature control, resulting in a costly setup [28]. Moreover, it is limited to linewidth variations above 3 MHz, making it unsuitable for applications requiring ultra-narrow linewidths [50].

Addressing these challenges, this research focuses on external modulation techniques, especially modifying optical phase noise to imitate laser-induced phase fluctuations [60]. The first part of this approach is the lithium niobate (LN) optical phase modulator, which offers linear optical phase modulation, consistent output power, and a simple, compact, and cost-effective design [61].

Furthermore, the modulator design enables the introduction of various noise profiles, enabling the simulation of different laser noise characteristics. This capability not only provides dynamic linewidth modulation but also opens up possibilities for creating lasers with variable line shapes [62]. This comprehensive method promises significant advancements in laser modulation, impacting both linewidth and spectral properties and marking a new era in photonics research and applications.

2.2 The theory of the variable linewidth laser

Optical phase noise significantly influences laser linewidth, making it an imperative element in laser physics [22, 24]. The interaction of optical phase noise with its source —the electrical noise, especially within an LN phase modulator setup, is of great importance [60]. The careful selection of the noise profile is essential, as establishing a clear relationship between the electrical noise and the resultant laser linewidth could revolutionize precision control in laser modulation [63, 64].

This study primarily explores two types of noise: random walk noise and white Gaussian noise. The choice of these noise prototypes is influenced by their properties and ability to reveal the complex dynamics between electrical inputs and optical outputs, thereby enhancing the control over the laser linewidth and its broader implications [60].

2.2.1 Random walk noise for the variable linewidth laser

This approach uses random walk noise as the fundamental noise model, exemplifying basic random walk models [60, 61]. This model, based on a 50% probability for each step direction and a uniform step length (l), is illustrated in Figure 2.1 (a). As time (t) progresses, the step magnitude increases; however this model faces a challenge as the walk boundaries expand infinitely over time, making it unrealistic for phase modulators that require low input powers [60].

To address this, the implementation of a ”limit wall” occurs to confine the random walk within specific parameters, as shown in Figure 2.1 (b) [60, 61]. This boundary ensures any excursion beyond it results in a reflective action, keeping the walk within manageable limits. This ”mirror method” not only maintains signal capacity but also ensures the input power into the phase modulator remains at optimal levels, balancing efficiency and safety in the modulation process.

The implementation of random walk noise with a limiting ”wall” is an innovative approach, but it encounters specific challenges. One significant issue is the high number of reflections within the system, which leads to a marked reduction in low-frequency components. This reduction harmfully affects the modulation of the optical signal low-frequency aspects, resulting in a notable 3 dB decrease in the linewidth [60, 61]. The plan is to explore deeper into these complex dynamics in the following subsections.

To mitigate the shortage, the incorporation of white Gaussian noise, complemented with a low-pass filter, was done to provide the necessary

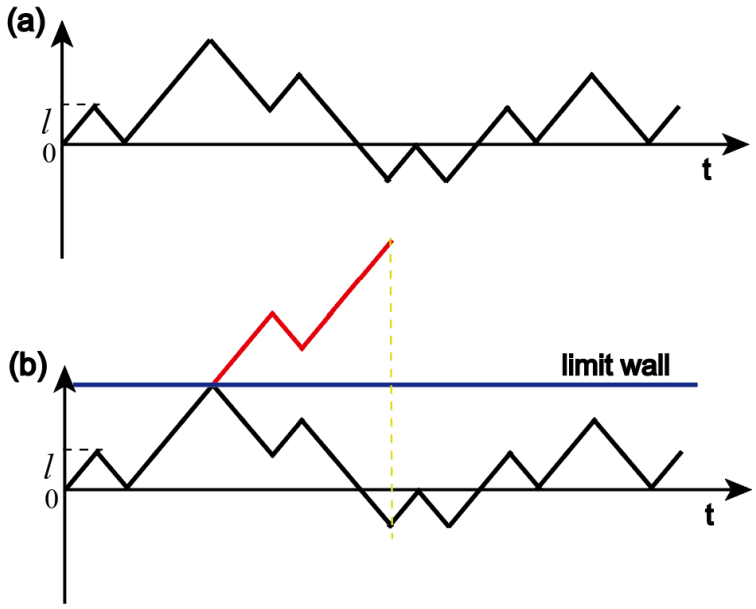

Figure 2.1: The schematic diagram of (a) random walk and (b) random walk with limit wall

low-frequency modulation [61, 65]. This approach effectively addresses the challenges related to carrier frequency modulation. Additionally, it introduces a new layer of complexity to the laser linewidth as it begins to change various line shapes due to the integration of different noise types. The effects of this effect, with its diverse impacts on linewidth and line shape, will be analyzed in the upcoming subsections.

Optical phase noise, a key factor in laser physics, significantly increases the laser linewidth [22, 24]. In the context of an LN phase modulator, it is crucial to understand the relationship between optical phase noise and its source, the electrical noise [60]. Therefore, selecting an appropriate noise profile is critical.

Establishing a clear relationship between electrical noise and laser linewidth enabled the achievement of a new level of precision in laser modulation [63, 64].

This study primarily explores two types of noise: random walk noise and white Gaussian noise. Their selection is based on their inherent properties and potential to explain the dynamics between electrical inputs and optical outcomes, enhancing the understanding and control of laser linewidth and its broader implications.

2.2.2 Equations for the laser linewidth

Establishing a precise mathematical relationship between introduced noise and the resulting laser spectrum linewidth is crucial to accurately regulate laser linewidth [63, 64]. The initial focus is on defining the equation connecting random walk noise to the laser linewidth, dropping light on the interaction between noise characteristics and the spectral behavior of the laser.

A key aspect of this correlation is the V_π (half-wave voltage) of the phase modulator, which is assumed to be a standard 1 V for simplicity and consistency in this theoretical framework. Another fundamental element is the power spectral density (PSD), which is essential for assessing power distribution across frequencies [63]. PSD is crucial for understanding the relationship between laser characteristics and noise dynamics.

In this context, two critical parameters must be considered: phase fluctuation (S_ϕ) and frequency fluctuation (S_F). S_ϕ (rad^2/Hz) provides insights into phase noise, while S_F (Hz^2/Hz) focuses on frequency noise. These parameters are vital for characterizing noise within optical systems.

The β-separation theory [22] in laser linewidth analysis suggests that noises with a high modulation index significantly affect the laser linewidth, whereas those with a low modulation index mainly impact the wings of the spectrum. However, this theory sometimes diverges from the observations of actual laser linewidths.

It is necessary to quantitatively examine the relationship between different

types of noise and the laser linewidth to understand these differences. Preliminary analysis indicates that white frequency noise and white Gaussian noise are major influencers that affect the core and wings of the laser spectrum linewidth, respectively. The random walk noise model is a suitable representation for white-frequency noise. An essential part of this study involves establishing a clear relationship between the PSD of phase and frequency noises, which can be formulated as follows [63, 64]:

$$S_F(f) = f^2 S_\phi(f) \tag{2.1}$$

Following the foundational analysis of noise sources, it is necessary to introduce a conceptual framework for the laser light field, thereby setting a critical link with the laser linewidth.

$$\mathrm{E(t)} = \mathrm{E_0} \exp\left[\mathrm{i}\left(2\pi \mathrm{v_0 t} + \phi(\mathrm{t})\right)\right] \tag{2.2}$$

Understanding the laser light field and its connection to laser linewidth involves introducing a conceptual framework that characterizes the laser light field using a specific expression. In this framework, $\mathrm{E_0}$ represents the amplitude of the optical field, $\mathrm{v_0}$ indicates the carrier frequency and $\phi(\mathrm{t})$ reflects the phase fluctuation.

According to the Wiener-Khintchine theorem, essential for spectral analysis, a clearer understanding of the spectral representation of the laser linewidth, $S_E(f)$ is attainable, as detailed in [63]. This is achieved by using the autocorrelation

function and a Fourier transform, represented as $(\mathcal{F}(\mathrm{E(t)}) \times \mathcal{F}^*(\mathrm{E(t)}))$. This approach provides a detailed mathematical description of the linewidth behavior.

$$S_E(f) = \int_{-\infty}^{+\infty} R_E(\tau) \exp(-i2\pi f\tau) d\tau \tag{2.3}$$

In this context, τ is chosen as the time interval, and $R_E(\tau)$ symbolizes the autocorrelation function, which is essential for understanding time-dependent phenomena. It is important to note that $\Delta\phi$(t), which denotes phase fluctuations, follows a stationary distribution, highlighting its consistent statistical characteristics over time. When compared to $S_F(f)$—the spectral function that depicts frequency variations—the autocorrelation function, $R_E(\tau)$, is effectively described by the following equation [63, 64].

$$\begin{aligned} \mathrm{R_E}(\tau) =< \mathrm{E(t+\tau)E^*(t)} >= \mathrm{E_0^2} \exp\left[\mathrm{i2\pi v_0 \tau}\right] < \exp \mathrm{i}[\phi(\mathrm{t}-\tau) - \phi(\tau)] >= \\ \mathrm{E_0^2} \exp\left[\mathrm{i2\pi v_0 \tau}\right] \cdot \exp\left(-2 \int_0^{\infty} \mathrm{S_F(f)} \sin^2(\pi \mathrm{f}\tau)/\mathrm{f^2 df}\right) \end{aligned} \tag{2.4}$$

In this analytical framework, the parameter $\langle \exp \mathrm{i}[\phi(\mathrm{t}-\tau) - \phi(\tau)] \rangle$ is used to represent phase fluctuations, denoted as $S_\phi(f)$, in the context of spectral density. For computational purposes, it is critical to treat these phase fluctuations as a Gaussian process with a zero mean. This approach aligns well with numerous empirical findings. This treatment is supported by the central limit theorem, which states that the sum of numerous independent identically distributed random variables will approximate a Gaussian distribution, regardless of the original distribution shape. Hence, the Gaussian probability density is adopted for the

calculations.

$$\begin{cases} < [\phi(t+\tau)\phi(\tau)] >= \int_0^\infty S_\phi(f)\cos(2\pi f\tau)df = R_\phi(\tau) \\ < [\phi(t+\tau)]^2 >=< [\phi(\tau)]^2 >= R_\phi(0) \end{cases} \tag{2.5}$$

Using Eq. (2.5)Eq. (2.4) can be further expressed as

$$R_E(\tau) = E_0^2 \exp\left[i2\pi v_0\tau\right] \exp\left(-\int_0^\infty S_\phi(f)[1-\cos(2\pi f\tau)]df\right) \tag{2.6}$$

By considering the carrier frequency, which determines the wave fluctuation behavior, the Power Spectral Density (PSD) of phase fluctuations, denoted as $S_y(f)$, can be reformulated as $S_\phi(f)$ by considering the carrier frequency, which determines the wave fluctuation behavior. This step involves considering the temporal derivative of the phase fluctuations, expressed as $(2\pi\Delta v(t) = \frac{d}{dt}\Delta\phi(t))$. With these considerations, the foundational Equation (2.1) can be reformulated for a more detailed understanding.

$$S_y(f) = \left(\frac{f}{v_0}\right)^2 S_\phi(f) \tag{2.7}$$

The PSD $S_E(v-v_0)$ in the carrier frequency domain can also be written as:

$$S_E\left(v-v_0\right) = E_0^2 \int_{-\infty}^{\infty} \exp - \left[i2\pi\left(v-v_0\right)\tau\right] \exp\left(-\int_0^\infty S_\phi(f)[1-\cos(2\pi f\tau)]df\right) d\tau \tag{2.8}$$

Random walk noise, a particular type of white-frequency noise, exhibits a complex interaction in optical physics. In the context of the PSD of phase

fluctuations, $S_\phi(f)$, this noise is characterized as $v_0^2 h_0 f^{-2}$. The parameter h_0 is influenced by the step length and the time interval between steps, providing insight into the dynamics of the noise. The term f^{-2} indicates that the noise process follows power laws with integer exponents, highlighting the deterministic yet arbitrary nature of the system [63]. Therefore, in situations involving white frequency noise, the PSD $S_E(v - v_0)$ in the carrier frequency domain can be described by the following mathematical expression:

$$S_E\left(v - v_0\right) = E_0^2 \int_{-\infty}^{\infty} \exp - \left[i2\pi\left(v - v_0\right)\tau\right] \exp\left(-\pi^2 h_0 v_0^2 |\tau|\right) d\tau = 2{E_0}^2 \frac{h_0 \pi^2 v_0^2}{{h_0}^2 \pi^4 {v_0}^4 + 4\pi^2 \left(v - v_0\right)^2} \tag{2.9}$$

The ”modest random walk” model is particularly relevant in optical noise analysis.. This model assumes that each incremental step has an equal probability (50%) of being an increase (walking up) or a decrease (walking down). Each step is defined by a fixed step length ΔL, occurring at regular time intervals Δt. In optical signal processing, the step is the conversion of electrical signals into phase fluctuations. Here, the electrical noise signal is precisely defined as $\left(\mathrm{S_{VR}}\left(\mathrm{V}^2 \cdot \mathrm{Hz}^{-1}\right)\right)$. Following this definition, the signal undergoes phase modulation. During this process, the half-voltage V_π of the phase modulator (PM) plays a significant role and must be carefully considered. The relationship that connects the electrical noise signal S_{VR} with the phase noise $S_\phi(f)$ is detailed in a complex mathematical equation [63]:

$$S_\phi(f) = \pi^2 S_{VR}/V_\pi^2 \tag{2.10}$$

In the field of optical signal characterization, the PSD of phase fluctuations, represented by $S_\phi(f)$, can be rewritten as $\frac{\pi^2 \Delta \mathrm{L}^2}{2\pi^2 \Delta \mathrm{t} \mathrm{V}_\pi^2 \mathrm{f}^2}$. Employing this revised equation for phase fluctuations enables a clear relation of the PSD in the carrier frequency domain. Importantly, this representation adopts a Lorentzian shape:

$$S_E\left(v - v_0\right) = 2E_0^2 \frac{\Gamma/2}{(\Gamma/2)^2 + 4\pi^2 \left(v - v_0\right)^2} \tag{2.11}$$

with $\Gamma \equiv 2\pi \left[\frac{\pi^2 \Delta \mathrm{L}^2}{2\pi \Delta \mathrm{t} \mathrm{V}_\pi^2}\right]$. The FWHM Lorentzian linewidth is expressed as:

$$\mathrm{FWHM}_{\mathrm{Loerntz}} = \frac{\pi \Delta \mathrm{L}^2}{2\Delta \mathrm{t} \mathrm{V}_\pi^2} \tag{2.12}$$

In the detailed realm of optical signal processing, it is essential to consider various factors for an accurate depiction. In this situation, assume the cutoff frequency of white Gaussian noise is represented as f_c, and the PSD of this noise is characterized by $\left(\mathrm{S}_{\mathrm{VW}}\left(\mathrm{V}^2 \cdot \mathrm{Hz}^{-1}\right)\right)$. Integrating this information with Equations (2.3), (2.4), and (2.10) becomes crucial. The PSD in the carrier frequency domain can be accurately defined by synthesizing these diverse variables [64].

$$S_E\left(v - v_0\right) = E_0^2 \int_{-\infty}^{\infty} - \exp\left[i2\pi \left(v - v_0\right)\tau\right] \cdot \exp\left[-S_{VW} f_c \left(1 - \mathrm{sinc}\left(2 f_c \tau\right)\right)\right] d\tau \tag{2.13}$$

The complex relationship between the laser spectrum linewidth and the two types of noise is detailed in Equations (2.12) and (2.13). The effect of white

Gaussian noise in the laser spectrum linewidth is a deliberate decision influenced by both the cutoff frequency and the resulting output power.

In a thorough analysis of laser spectral properties affected by random-walk noise, two key parameters are pivotal: the step length and the time interval. These related factors contribute to the characteristic Lorentzian spectrum linewidth. In addition, the half-voltage of the LN PM significantly impacts this spectrum and must be carefully considered in any analytical study.

A significant challenge arises with an unbounded random walk, which inherently lacks a defined limit. To address this issue, the ’mirror method’ has been introduced to address this issue. This approach effectively manages the power input limitations of the PM, maintaining its functionality.

Yet, this method leads to an unintended effect: large step sizes in the random walk enhance reflections, causing the white frequency noise to lose its low-frequency component. This loss results in an unmodulated central part of the laser linewidth, presenting a problem that needs resolution.

White Gaussian noise plays a crucial role in this context. It compensates for the missing low-frequency component, restoring spectral unmodulation. However, this is not the end of the story. The various noise sources and their interactions shape the morphology of the laser linewidth, a subject that deserves further detailed examination.

2.2.3 Equations for the line shape of the laser spectrum

In the complex arena of laser linewidth spectra, it is widely recognized that different noise types create distinct spectral shapes. In this regard, white Gaussian noise is utilized to address the lack of low-frequency components. Meanwhile, the influence of random walk noise is paramount, as it shapes the spectral line into a Lorentzian profile [22]. Conversely, the impact of white Gaussian noise is observed in a Gaussian-shaped line profile [24].

Addressing the complex interaction between various noise types and their spectral outcomes requires an analytical method. Thus, the proposal is to use the PseudoVoigt model, a model recognized for its precision and complexity. This model provides a comprehensive framework to understand the relationship between spectral line shapes and the noise sources behind them. Specifically, the PseudoVoigt model can be mathematically represented as [15]:

$$f\left(x, A, v_0, \sigma, \alpha\right) = \frac{(1-\alpha)A}{\sigma_g\sqrt{2\pi}} e^{-\frac{(x-v_0)^2}{2\sigma_g^2}} + \frac{\alpha A}{\pi}\left[\frac{\sigma}{\left(x-v_0\right)^2+\sigma^2}\right] \tag{2.14}$$

Here, x denotes a particular point on this spectrum, A denotes the amplitude or power of the laser linewidth, and v_0 is used to denote the carrier frequency, a key factor in the laser performance.

Next, σ indicates the FWHM, a significant measure of the linewidth. The Gaussian equivalent of this parameter is expressed as $\sigma_{\mathrm{g}} = \sigma/\sqrt{\ln 2}$ [15]. Furthermore, the coefficient α represents the Lorentzian component influence, playing a role in defining the spectral profile shape.

2.3 Experimental setup

Figure 2.2 provides a schematic overview of the experimental setup used for measuring the laser linewidth. The experiment employed two narrow linewidth fiber laser diodes (NKT Photonics Koheras BASIK) with wavelengths of 1550.075 nm and 1550.090 nm respectively. For precise modulation, the inherent optical power of these diodes was carefully attenuated using optical attenuators (Anritsu MN935A2) along a specific optical path. Simultaneously, polarization dynamics were precisely controlled using a dedicated polarization controller (PC).

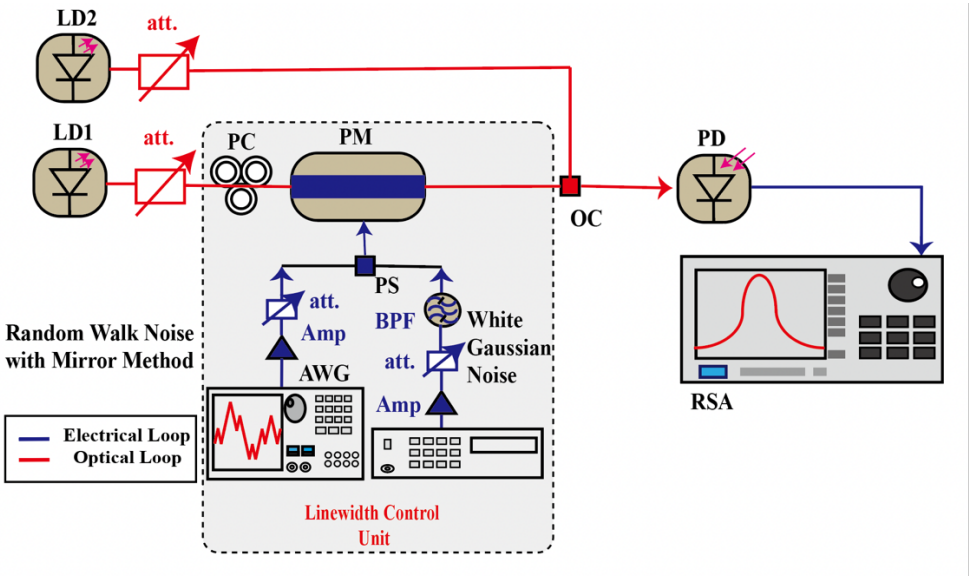

Figure 2.2: Experimental setup of the laser linewidth measurements using the coherent interference.

A key element in the setup was the external LN PM (Sumitomo Osaka

Cement T.PMH1.55 S), which was responsible for modulating the light phase. This modulation was further enhanced by introducing random walk and white Gaussian noise signals. These were generated using a high-resolution arbitrary waveform generator (Tektronix AWG 7102) and an analog noise source (Noisecom UFX 7107).

A series of amplifiers (SHF 115BP, NF BA4805, FEMTO DHPVA-101) and electrical attenuators (Agilent 8494 B, Fairview microwave SA 4090) were integrated to preserve the fidelity and amplitude of the noise. Additionally, a low-frequency variable bandpass filter (NF 3628), coupled with an electrical amplifier, enabled precise control over the cutoff frequency of the white Gaussian noise.

The combination of these two types of noise was achieved using a power splitter (PS, Mini-Circuits, ZFRSC-183-S+), forming a complex linewidth control unit. The bounded random walk noise, with parameters like 0.015 Vpp step length and 0.1 ns temporal interval, was amplified across a range of 1 to 23 dB. This was contrasted with dynamically varied white Gaussian noise in terms of both cutoff frequency and power.

Following the merging of the two optical paths by a precision optical coupler (OC), a coherent interference method discerned a wavelength of 0.015 nm, which was accurately detected by the photodetector (PD, Sevensix Inc 12.5 Gb/s Optical Receiver). Finally, a real-time spectrum analyzer (RSA, Tektronix RSA 3308A) processed the received signal, providing an assessment of the laser linewidth within the spectral domain.

2.4 Results and discussions

2.4.1 Simulation results of variable linewidth laser

In photonics research, numerical simulations are essential for unraveling the complex relationship between noise sources and laser linewidth behavior. The half-wave voltage of the PM was set to 1 V in the simulations, and the insights gained from the subsequent figures are highly informative.

Figure 2.3 illustrates the variation in laser linewidth as influenced by different cutoff frequencies of the white Gaussian noise. Notably, a cutoff frequency of 100 kHz, represented by a striking red curve, yields a linewidth of 328 kHz. In contrast, a blue curve, indicative of a 50 kHz cutoff frequency, results in a narrower linewidth of 162 kHz. It is important to mention that both noise conditions were maintained at a PSD of -48 $dBrad^2/Hz$ and a resolution bandwidth (RBW) of 1 Hz. This suggests that an increase in the cutoff frequency of white Gaussian noise leads to a corresponding increase in the resulting laser linewidth.

Figure 2.4 presents the PSD profiles for the previously discussed noise conditions. In this illustration, the blue and red curves distinctly represent the 50 kHz and 100 kHz cutoff frequencies, respectively. The PSD resolution for both situations is consistently maintained at 1 Hz.

Figure 2.5 illustrates the effects of varying the PSD of the noise.

In this detailed examination, the red and brown curves represent PSD values

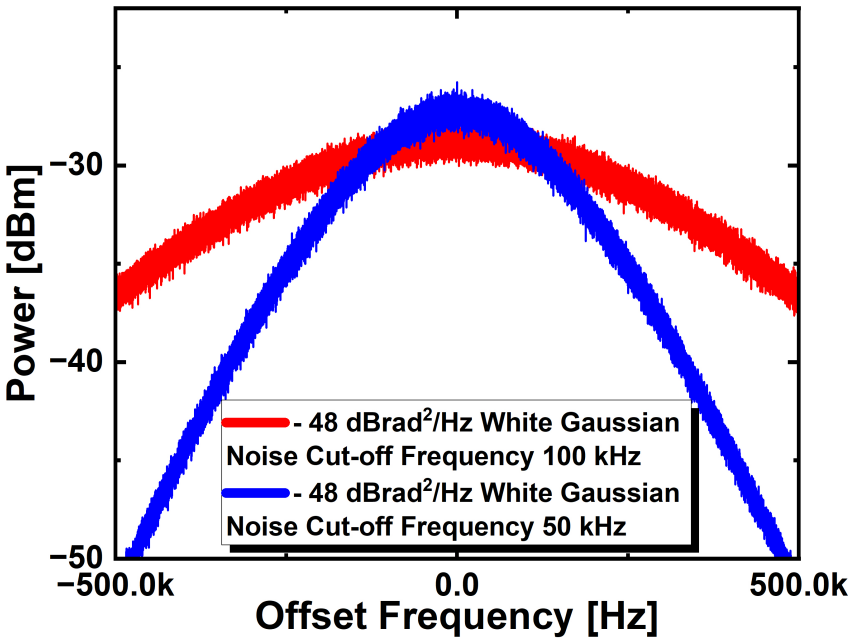

Figure 2.3: Simulation results on the laser spectrum of different cutoff frequency with same power.

of -48 and -128 $dBrad^2/Hz$, respectively, for the white Gaussian noise. The corresponding PSDs for these noise conditions are further illustrated in Figure 2.6.

A key observation emerges from the analysis: with minimal noise PSD, as shown by the brown curve, the carrier frequency of the laser linewidth remains essentially unmodulated. In contrast, the red curve exhibits a significant increase to a linewidth of 328 kHz.

In conclusion, these findings highlight the critical influence of noise PSD

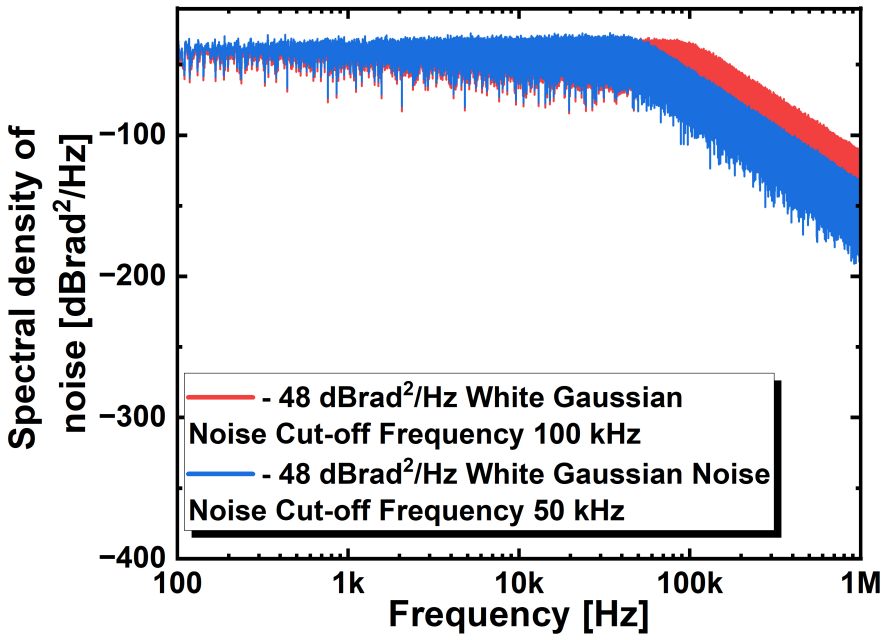

Figure 2.4: The respective noise PSD of different cutoff cutoff frequencies with the same.

on the modulation ability of the carrier frequency in the laser linewidth. Precise calibration of the noise PSD is essential to achieve a laser linewidth with a distinct central component. Additionally, the width of the laser linewidth, particularly under conditions of high noise PSD, is directly affected by the cutoff frequency of the white Gaussian noise—with a higher frequency leading to a wider linewidth.

In studies of lasers with variable linewidth, random walk noise was incorporated into the experimental setup. The random walk is naturally constrained owing to the inherent power limitations of the PM. This caused the

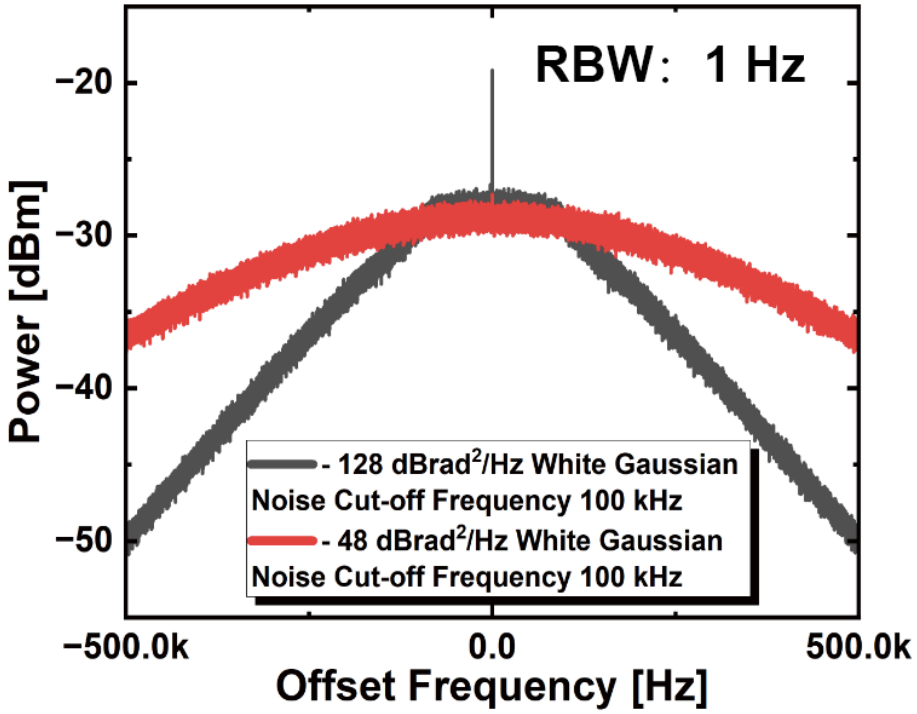

Figure 2.5: Simulation results on the laser spectrum of different power with same cutoff frequency.

carrier frequency of the laser spectrum can not to be modulated. A thorough investigation of the effects of an unbounded random walk, in contrast to its bounded counterpart, can clearly know the reason for the unmodulation, which necessitated conducting complex simulations that required high-performance computing, facilitated by Amazon Web Services.

The results of these simulations are presented in Figures 2.7 and 2.8. The parameters were carefully adjusted to a step length of 0.01 V and a time interval of 0.1 ns. As illustrated in Figure 2.8, the laser linewidth ranged up to 40 MHz,

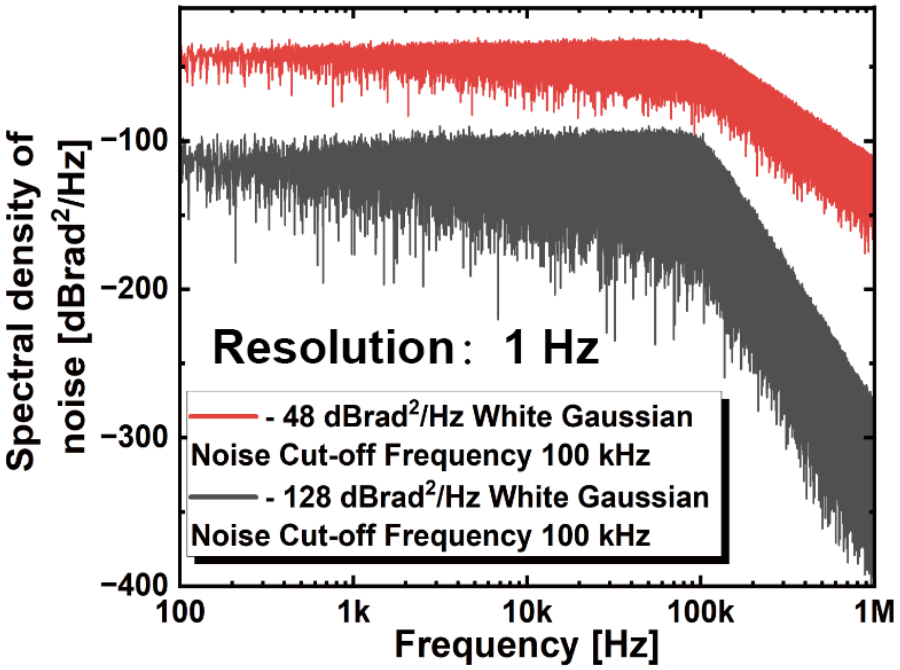

Figure 2.6: The respective noise PSD of different power with the same cutoff frequency.

with a RBW of 1 kHz. The brown curve represents the unbounded random walk, suggesting a theoretical laser linewidth of 159.154 kHz, while the actual measured value was 155.927 kHz. A noticeable difference between theoretical predictions and experimental results is observed, attributed to the incorporation of random walk noise. This noise, derived from pseudorandom sequences generated by the PC, introduces a degree of inconsistency. Furthermore, the unrestrained nature of the random walk, progressing with incremental steps, results in high-voltage noise in the time domain, exceeding the power capacity of the PM.

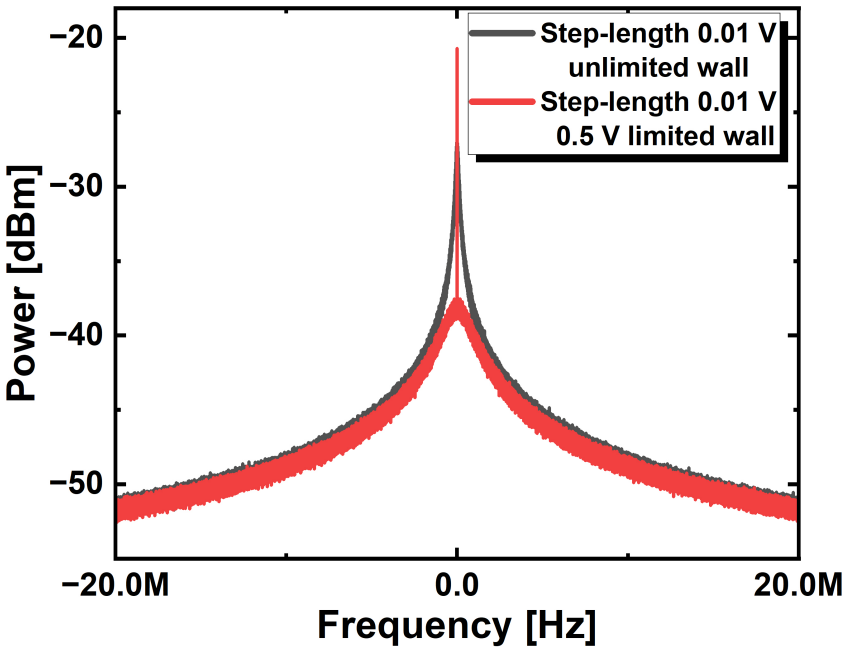

Figure 2.7: Simulation results on the laser spectrum of the random walk without a limited wall and with a limited wall.

A ’mirror technique’ was developed to confine the boundary of the random walk to overcome the limitation. In the simulation, a boundary of 0.5 V was established, as depicted by the red curve. Spectral analysis revealed an unmodulated central portion of the laser linewidth, indicating a distinct carrier frequency. Further examination of the noise PSD in Figure 2.8 showed that the low-frequency segment of the constrained noise was dominated by low PSD white noise. This level of noise was insufficient to modulate the laser carrier frequency, resulting in a linewidth that extended into the central region.

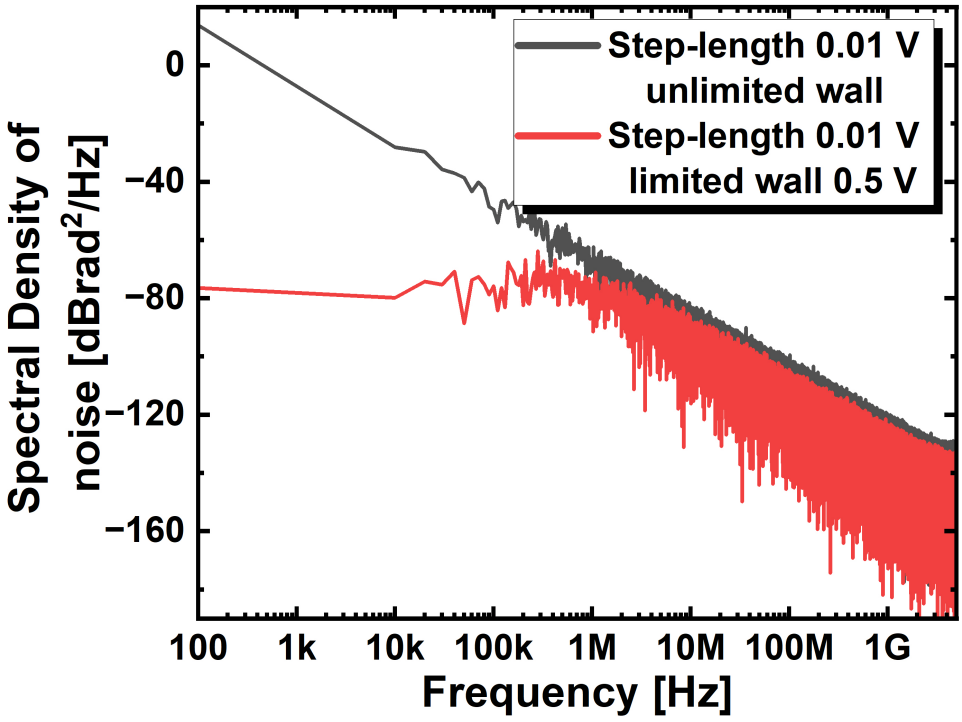

Figure 2.8: The respective noise PSD of the random walk without a limited wall and with a limited wall.

2.4.2 Experimental results of the variable linewidth laser

Figure 2.9 illustrates the impact of the modulation signal on the half-wave voltage of the PM, where an acousto-optic (AO) effect was notably induced within the 10−100 MHz frequency range. However, the combined influence of the AO and electro-optic (EO) effects led to unforeseen interference, resulting in abnormal fluctuations in the PM half-wave voltage within this specified range [66]. This phenomenon is supported by the findings in reference [66].

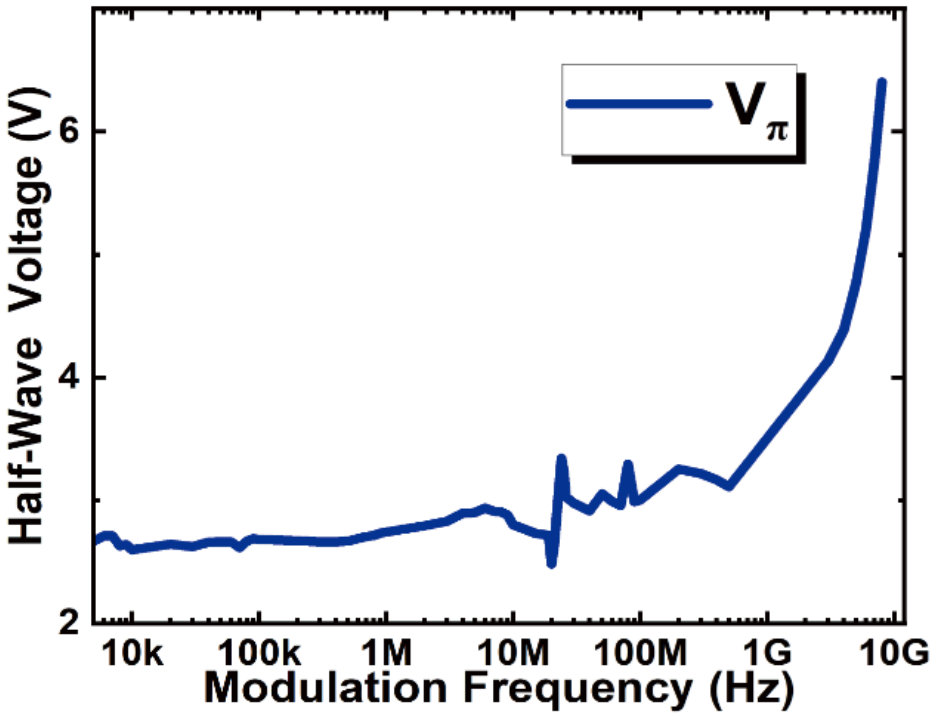

Figure 2.9: Results of the half-wave voltage of the phase modulator.

Figure 2.10 provides insights into the effects of white Gaussian noise on the laser linewidth. A thorough investigation involving the application of various levels of white Gaussian noise power to the laser system revealed significant results. Notably, increasing the white Gaussian noise power to 28 dBm led to the complete modulation of the laser linewidth carrier line, indicating a phase shift of 3.6 π. Conversely, reducing the noise power resulted in the carrier line remaining largely unmodulated. This lack of modulation became more pronounced at lower power levels.

To achieve modulation within the central laser spectrum linewidth, an

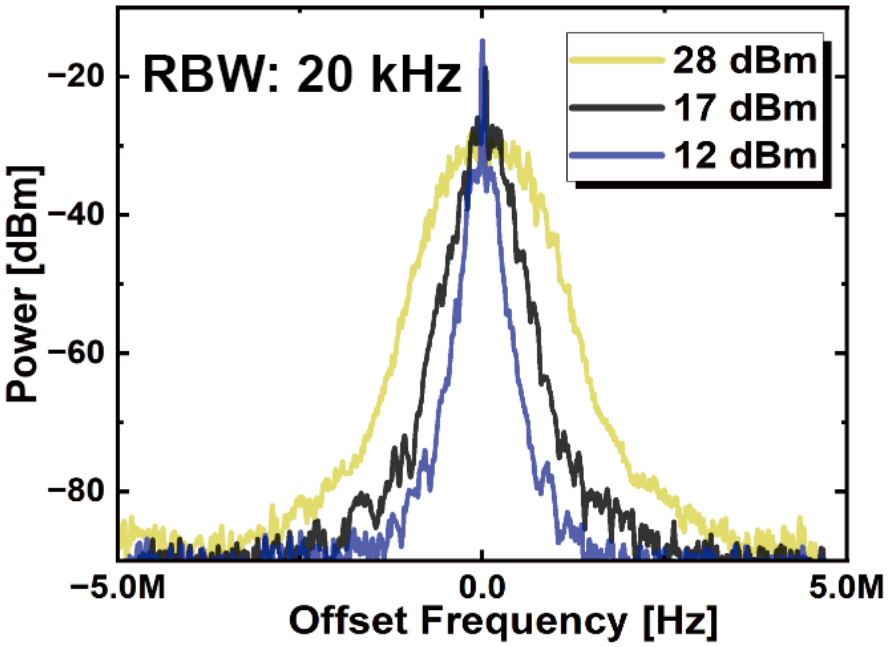

Figure 2.10: Results of laser spectrum for the different powers of white Gaussian noises.

optimal white noise power, intricately linked to the half-wave voltage of the PM, is imperative. This intricate dynamic is further underscored by Figure 2.11, which underscores the pivotal role of varied cutoff frequencies of the white Gaussian noise in shaping the laser spectrum linewidth. Notably, with a constant noise power set at 26 dBm, a surge in the cutoff frequency from 100 kHz to 300 kHz manifested in a substantial amplification of the laser linewidth, leaping from 222 kHz to a staggering 1443 kHz.

In the effort to accurately define the central section of the laser spectrum linewidth, it is essential to carefully balance the appropriate level of white

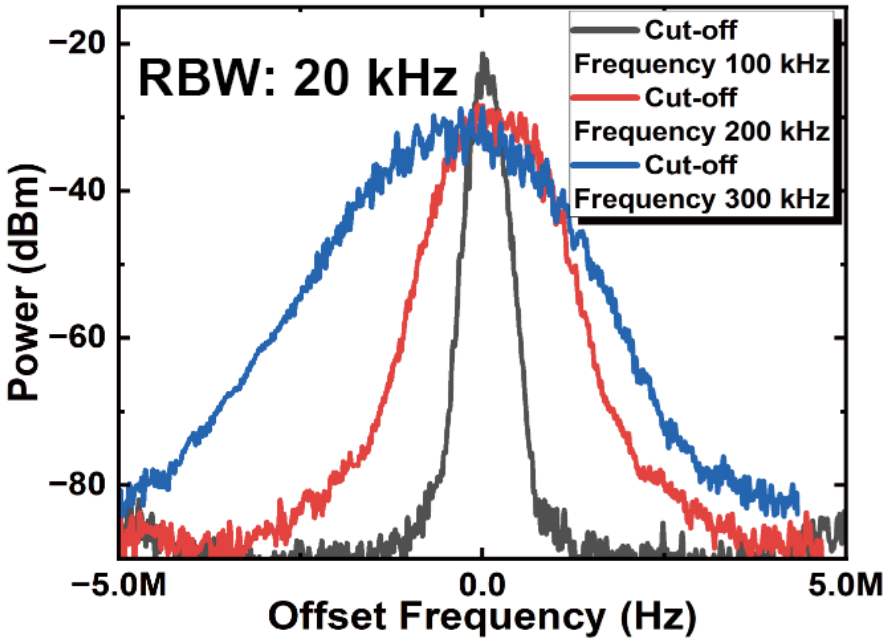

Figure 2.11: Results of laser spectrum for the different cutoff frequencies of white Gaussian noises.

Gaussian noise power with the half-wave voltage of the noise. Figure 2.12 illustrates the power spectrum of white noise prior to its amplification. The graph clearly shows the cutoff frequency of the noise ranging from 100 kHz to 300 kHz. Notably, the power level is maintained at about -5 dBm, a precautionary step to protect the RSA from possible damage caused by high-power, low-frequency noise. Therefore, the noise is measured before amplification and is then consistently amplified to 26 dBm for further analysis. The horizontal axis of the graph employs a logarithmic scale to improve the visibility of the noise cutoff frequency.These points highlight subtle variations within the

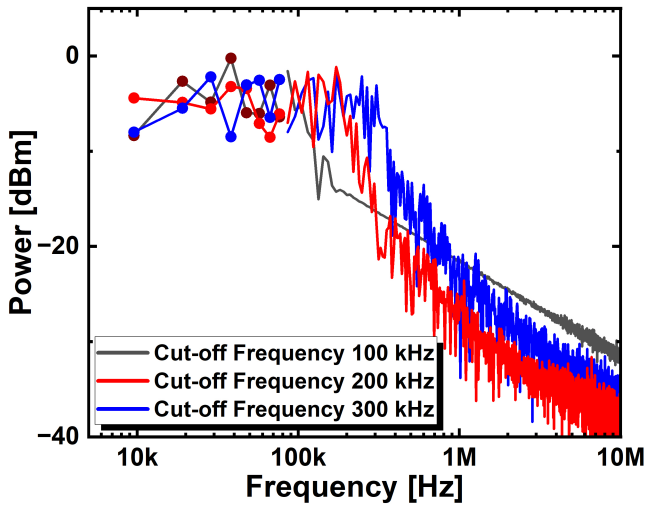

Figure 2.12: Spectrum results of laser for the noise of different cutoff frequencies.

low-frequency range, making these minor fluctuations more noticeable and analyzable. This careful representation aids in a more detailed understanding of the noise characteristics in the lower frequency domain. Interestingly, the cutoff frequency of the white Gaussian noise proves to be a factor affecting the laser linewidth, a conclusion that aligns well with the simulation results. From these results, the white Gaussian noise makes the lineshape of the laser into Gaussian lineshape.

Further exploration focused on the effects of combining random walk noise with white Gaussian noise on the laser spectrum linewidth. This complex interaction is illustrated in Figure 2.13, where the white Gaussian noise is set with a cutoff frequency of 200 kHz.

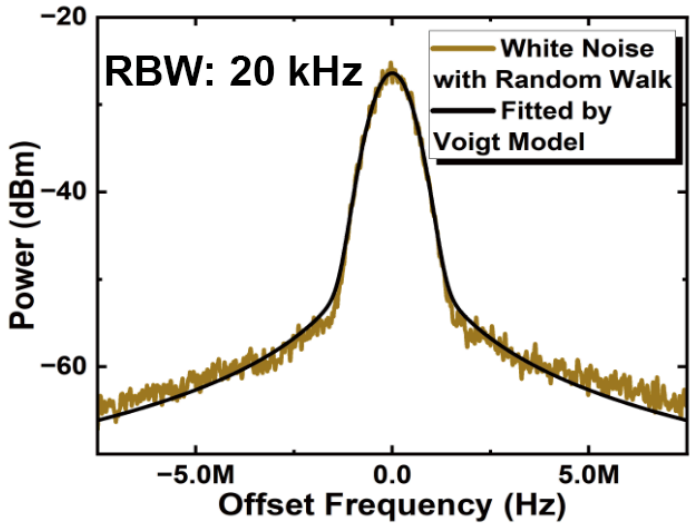

Figure 2.13: Laser spectrum of the white Gaussian noise compensation.

The Voigt fit model was employed to accurately analyze laser linewidth and know the different noise effects on the line shape of the laser, the Voigt fit model was employed. The analysis resulted in a precise Voigt lineshape for the linewidth, measured at 898 kHz.

Figure 2.14 reveals the noise spectrum of the noise before amplification, which contributes to the 898 kHz laser linewidth observed with a fine resolution of 10 kHz. This hybrid noise profile, marked by a significant low-frequency component, ultimately led to a distinct Voigt lineshape when analyzed using the Voigt fit model.

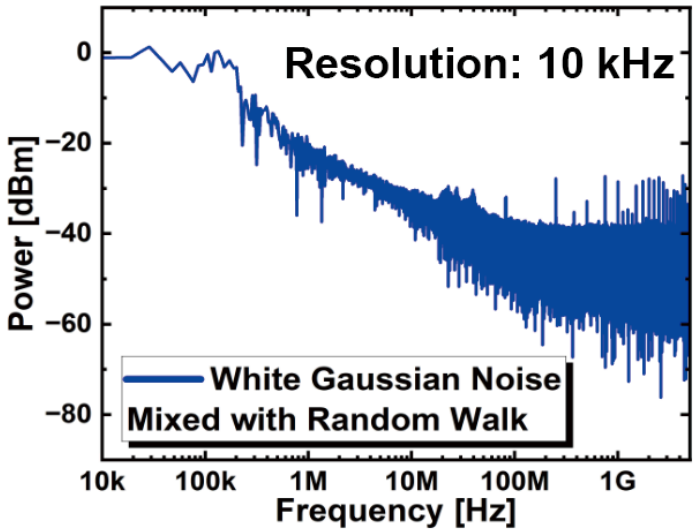

Figure 2.14: The noise spectrum of the mixed noise.

2.4.3 Simulation results of the variable line shape laser

In an endeavor to delve into the intricacies of random walk noise dynamics—characterized by a step length precisely calibrated at 0.015 Vpp and constrained by a stringent wall threshold of 0.5 Vpp, coupled with a temporally defined interval of 0.1 ns—the said noise was subjected to amplification via a meticulously selected amplifier. Concurrently, the spectral properties of white Gaussian noise underwent rigorous modulation, both in the realm of its cutoff frequency (spanning a range from 100 kHz to 220 kHz) and power magnitude (oscillating between 25 dBm to 28 dBm).

Drawing inspiration from these empirical undertakings, simulations of the laser linewidth and line shapes were meticulously crafted, anchoring their foundational logic on the findings harvested from the laser with mutable linewidth characteristics. Augmenting this narrative, the amplified random walk, circumscribed by its limiting wall, was synergistically amalgamated with white Gaussian noise in the numerical simulation. This noise exhibited a dynamic spectrum, pivoting on a variable cutoff frequency domain ranging from 80 kHz to 450 kHz and a power spectrum delineated between 25 dBm and 28 dBm.

In the numerical simulations, depicted comprehensively in Figure 2.15, nuanced interplays were observed between the power and cutoff frequency of white Gaussian noise and their subsequent impact on the Lorentzian components. The findings delineate a pronounced hyperbolic trend, with the predominance of the cutoff frequency exerting a salient influence on the Lorentzian constituents.

The underpinnings of this phenomenon can be attributed to the inherent Gaussian distribution of the white Gaussian noise and the linear traits of PM. As a corollary, post-modulation, the linewidth transmutes into a Gaussian distribution, discernibly manifesting as a Gaussian contour in the laser spectrum linewidth. Additionally, the input power of the PM is subject to specific limitations. Therefore, in the simulations, the maximum power setting was aligned with the actual input power limit of the Power Meter (PM), which is 26 dBm. This approach ensures that the simulated conditions accurately reflect the real-world constraints and capabilities of the PM.

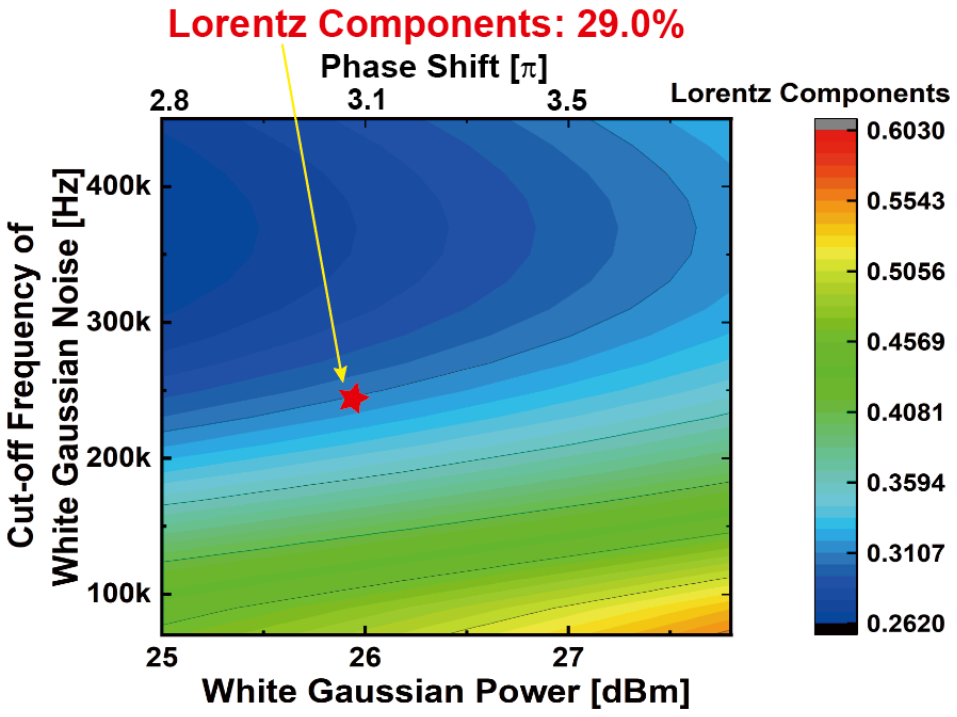

Figure 2.15: Simulation results of different white Gaussian noise power and cutoff frequency on the Lorentz components.

2.4.4 Experimental results of the variable lineshape laser

Figures 2.16 and 2.17 present the data illustrating the laser spectrum linewidth. A key observation was made when the cutoff frequency was set at 220 kHz and the white noise power was adjusted to 26 dBm.

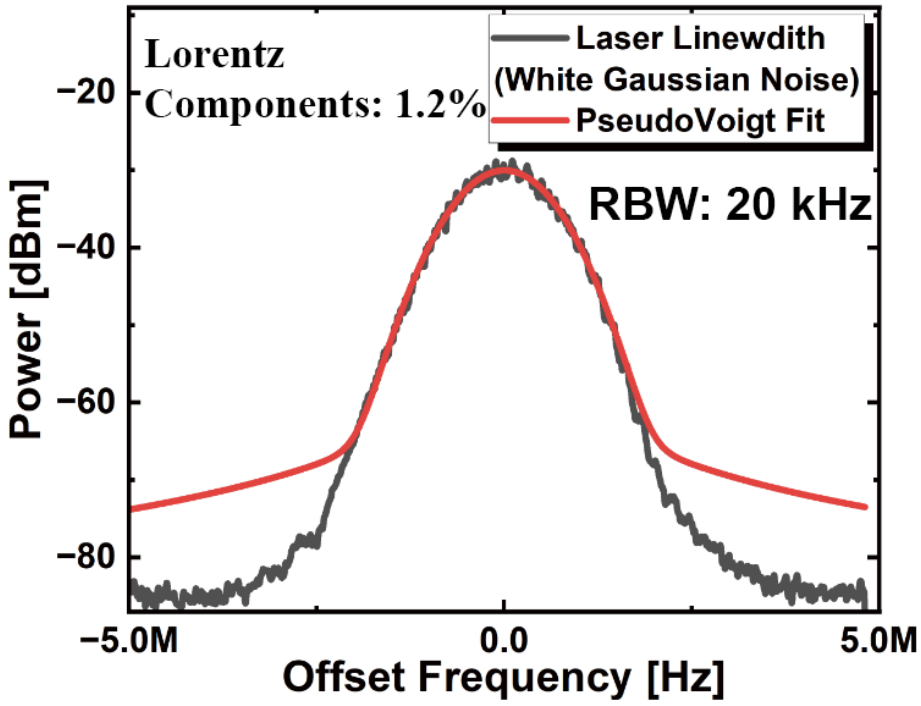

Figure 2.16: Laser spectrum of only white Gaussian noise.

Under these conditions, the resulting laser linewidth was measured to be 1.078 MHz, with a Lorentzian contribution of only 1.2% (0.012). It was noted that the central region of the linewidth closely matched the fitted curve. However, a significant difference was observed in the wings of the spectrum, as shown in Figure 2.16. Although the line shape of the laser is expected to be 100 %

following the Voigt model. However, these errors of the wing parts can be attributed to the behavior of the amplifier (NF 3628), which tended to amplify low-frequency signals, filtering more effectively. Consequently, there was a noticeable difference between the wings of the spectrum linewidth and the theoretical fit, highlighting the impact of the amplifier on the spectral properties of the laser.

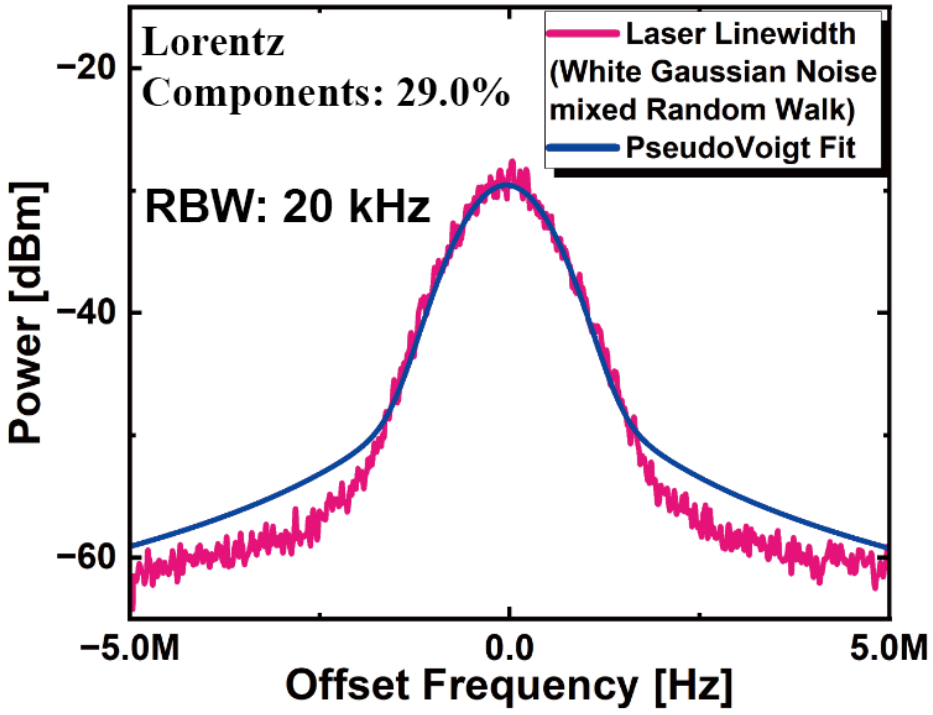

Figure 2.17: Laser spectrum of white Gaussian noise mixed random walk noise.

In a more detailed examination, Figure 2.17 showcases the laser spectrum linewidth resulting from a combination of white Gaussian noise—specified by a cutoff frequency of 210 kHz and power of 26 dBm—and random walk noise,

which was subjected to a 23 dB amplification. The measured linewidth was 1.017 MHz, with a significant Lorentzian component accounting for 29% (0.29) of the spectrum. Closer inspection revealed that the central part of the linewidth closely matched the theoretical fit. However, differences were again observed in the wings of the spectrum linewidth. This variation can be attributed to the diminished power of the white Gaussian noise used in the experiment at higher frequencies, in contrast to its theoretical model. Furthermore, the high-frequency mixed noise in the experimental setup deviated from its idealized profile. These complexities highlight the challenges encountered in achieving an accurate fit with the PseudoVoigt model, particularly for the wings of the spectrum linewidth.

2.5 Summary

This chapter focuses on the theoretical foundations, simulation results, and experiments referring to the development of lasers with adjustable linewidth and lineshape. First of this discussion is an exploration of the control mechanisms for these laser parameters. This is achieved by applying white Gaussian noise and random walk noise within defined boundary conditions coupled with the use of an external LN phase modulator. The laser linewidth increases with the increase of the cutoff frequency of the white noise; it is also affected by the power of the white noise, and the carrier frequency of the laser linewidth is affected by the mirror method of the random walk. Such an approach allows for the precise manipulation of the laser linewidth, enabling adjustments within a range of 400 kHz to 1 MHz and facilitating the incorporation of Lorentzian components up to 29%. However, the maximum Lorentzian component achievable is 29% because of limitations in input power, falling short of a pure Lorentzian shape. Future explorations should consider other low-frequency adjustments to attain a pure Lorentzian shape, enhancing the understanding of its effects in coherent systems.

The analytical review and discussion presented in this chapter mark a substantial contribution to the field of laser technology, especially regarding the variability of linewidth and lineshape. Importantly, the extensive research, findings, and academic discourse detailed in this chapter have earned acknowledgment and recognition through their publication in the journal Optics Continuum,volume 2, in 2023, entitled ”Effects of a variable linewidth laser and

variable linewidth shape laser on coherent FMCW LiDAR" [61] (Section 2.2-2.4).

Chapter 3 FPGA-based variable linewidth and lineshape laser

3.1 Introduction

In the pursuit of enhancing optical communication systems, the need for lasers with variable linewidth is evident[67]. Traditional methods require exchanging laser diodes to achieve different linewidths; however this can lead to inconsistencies in optical power and wavelength, potentially causing errors [29]. An advanced solution is utilizing an external LN phase modulator, which allows for the modulation of random walk noise within certain bounds, thus supporting the creation of lasers with tunable linewidths [61]. However, the mirror method typically used for laser linewidth control is poor in low-frequency components, resulting in inadequate modulation of the central part of the laser spectrum linewidth.

A low-frequency compensation technique that utilizes white Gaussian noise generated from an FG has been developed to address this issue [65]. Regrettably, this method depends on pre-recorded noise, which contrasts sharply with the dynamic noise produced by thermal fluctuations within the laser diode [36, 37, 38, 39]. The difference between FG-derived noise and actual laser noise hinders the accurate simulation of laser behavior.

The investigation focuses on the synthesis of real-time white Gaussian noise, moving away from the conventional FG noise, to assess its impact on the laser spectrum linewidth. The laser linewidth sensitivity to the cutoff frequency of the white Gaussian noise is a significant challenge, as small alterations can lead to considerable changes in linewidth, complicating the achievement of precise control [61]. This study explores the variation of white Gaussian noise parameters, including standard deviations (STDs) and mean values [68]. This novel approach seeks to shed light on the influence of noise characteristics on the laser spectrum linewidth and may reveal new methods for precise linewidth regulation.

The current limitations of instruments like FG and analog noise sources, which block easy modulation of noise parameters, highlight the need for new mechanisms that can generate real-time white Gaussian noise with adjustable parameters [69]. Field Programmable Gate Arrays (FPGAs), equipped with digital-to-analog converters (DACs), offer a promising solution. They enable the production of real-time noise, encompassing a range of white Gaussian noise

parameters, allowing for a more detailed examination of how noise characteristics affect the laser spectrum linewidth.

The success of this research could lead to the identification of lasers that not only emulate the behavior of actual lasers but also reduce the costs associated with such sophisticated systems. The implications of this research could make high-precision variable linewidth lasers more accessible, thereby advancing the field of optical communications toward greater affordability and technical refinement.

3.2 White Gaussian noise for variable linewidth laser in FPGA

3.2.1 The principle of white Gaussian noise generation in FPGA

Figure 3.1 illustrates the complex process for generating white Gaussian noise using the Look-Up Table (LUT) method [41, 42]. This critical advancement in noise generation starts with the creation of a pseudo-random sequence [32, 34], using the highly regarded linear feedback shift register (LFSR) method [35]. The LFSR is noted for its computational efficiency and robustness, skillfully producing 16-bit pseudo-random sequences with unmatched precision [40, 43].

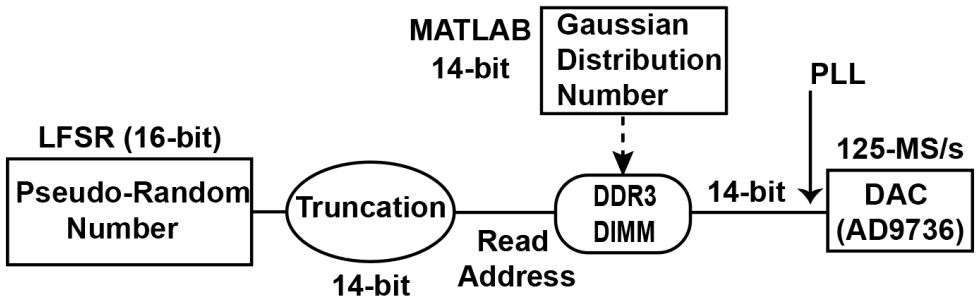

Figure 3.1: Principle of the programmable white Gaussian noise using the FPGA with DACs.

These carefully sequences serve two primary purposes. Primarily, they act as reference points within the double-data-rate3 (DDR3) dual inline memory module (DIMM), an essential component for noise generation. The LFSR

method is admirable in producing pseudo-random sequences; however, it faces challenges like periodic repetition and bit-number limitations, which are particularly problematic when aligned with Gaussian numbers, affecting real-time efficiency.

This study introduces a novel truncation technique to deal with these issues. This method effectively mitigates the effects of periodic repetition by discarding the top two bits from the LFSR pseudo-random sequence, enhancing system efficiency and keeping the integrity of real-time operations.. Utilization a 16-bit LFSR is a deliberate choice, given the importance of timing in real-time systems. The next stage focuses on quantization, where Gaussian distribution numbers with mean values of 1 V and 0.9 V are converted into a 14-bit format using MATLAB (R2022a). These quantized numbers are precisely associated with the LFSR-generated pseudo-random sequences and stored within the FPGA DIMM for subsequent noise generation.

This procedure allows for the adjustment of key parameters such as STDs and means, enabling the dynamic creation of random white Gaussian distribution sequences. On the hardware front, the FPGA board, specifically the Xilinx Artix 7 evaluation board AC 701, connects with high-capacity 600-MSamples/s DACs (Analog Device AD 9736) via a 14-bit double data rate (DDR) low-voltage differential signaling (LVDS) channel, ensuring synchronized and accurate analog noise generation [44]. The DACs, configured to produce a signal strength of 1 Vpp (V), modulate the output to achieve mean values of 0.125 V and 0.113 V

STD. A phase-locked loop (PLL) is used to enhance the output and improve low-frequency dynamics, converting the sampling rate of DACs to 125-MSamples/s. Finally, an analog noise filter is integrated, exceeding its digital FPGA equivalent in stability and precision for bandwidth control of the generated white Gaussian noise.

3.2.2 Experimental setup

In the advanced field of optical experimentation, Figure 3.2 illustrates a carefully engineered setup designed for the detailed modulation and measurement of laser linewidth spectra. This method employs the principle of coherent interference, utilizing the precision of two narrow fiber laser diodes (LD, NKT photonics Koheras BASIK) with slightly different wavelengths: 1550.075 nm and 1550.090 nm. Optical attenuators (Anritsu MN 935A2) are integral to the system, managing the power distribution between the paths. This arrangement creates a clear distinction between the reference path and the path used for modifying the laser linewidth.

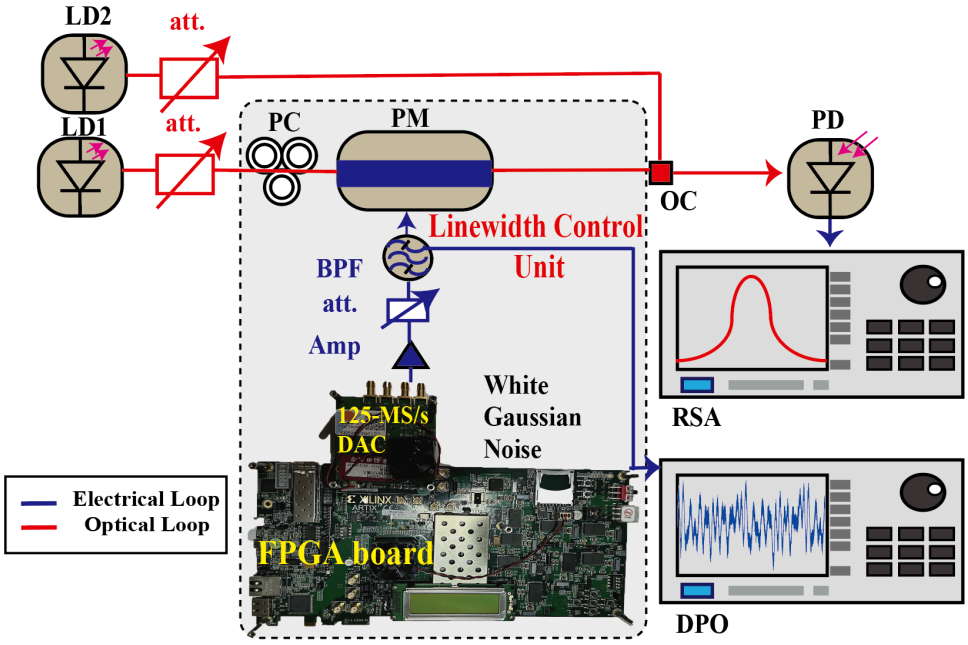

Figure 3.2: Principle of generating white Gaussian noise using the FPGA with DACs.

Central to this experimental configuration is the polarization controller (PCs, Alnair Labs MLC15 QHN SMFS), which thoroughly adjusts the polarization of light within the control path. This path is then modulated by an LN phase modulator (PM, Sumitomo Osaka Cement T.PMH1.55 S), noted for its half-wave voltage of 2.7 V at an operational frequency of 1 MHz. To generate noise, the system integrates an FPGA board connected to DACs operating at 125-MS/s. This combination, further enhanced by electrical amplifiers (Amp, NF BA4805, and FEMTO DHPVA-101), electrical attenuators (att., Fairview microwave SA 4090), and a low-frequency variable bandpass filter (BPF, NF 3628), grants exceptional control over the noise power and bandwidth.

After thorough noise filtration, the path of the white Gaussian noise is carefully examined using a DPO (Agilent DSO81204B). The phase noise, modulated by the FPGA-generated white Gaussian noise parameters, is then applied to the laser spectrum linewidth within the control path. An OC merges the two optical paths, resulting in coherent interference. The interference is detected by a photodetector (PD, Sevensix Inc 12.5Gb/s Optical Receiver) that captures a wavelength difference of 0.015 nm. The system utilizes a real-time spectrum analyzer (RSA, Tektronix RSA 3308A) to analyze the electrical signal from the PD and deduce the laser spectrum linewidth. This component signifies the synthesis of accuracy and innovation in this experimental setup.

3.2.3 Results and discussions

Figure 3.3 illustrates the spectrum of white Gaussian noise, as precisely measured by the DPO. The DPO successfully captures the noise, characterizing it with a low-frequency bandwidth of 200 kHz, and STDs of 0.125 V and 0.113 V. Further analysis through FFT enhances these observations. With an RBW set to 250 Hz, the blue and red lines on the spectrum distinctly indicate the noise spectra for the 0.125 V and 0.113 V STDs, respectively. Notably, both lines show a clear cutoff frequency at 200 kHz despite the different STD values. This characteristic cutoff frequency underlines the Gaussian nature, presenting with equal intensity across all frequencies beneath this cutoff point. This feature explains the Gaussian distribution fundamental attribute—its consistent intensity across the spectrum up to its defined limit.

The measurement of noise power is estimated at -20 dBm. This figure may show slight variances, which are more likely due to natural fluctuations in signal voltage rather than inaccuracies in the analysis. This level of detailed examination demonstrates the effectiveness of producing white Gaussian noise with predetermined STDs of 0.125 V and 0.113 V, over a bandwidth of 200 kHz.

Figure 3.4 offers a comparative look at the laser spectrum linewidth, highlighting the effects of changes in Gaussian noise STDs. The spectrum with a 0.113 V STD noise, represented by the red line, results in a linewidth of 659 kHz over a 4-MHz frequency span with an RBW of 20 kHz. A Gaussian model applied to this data produces a black line that verifies the initial observations and shows

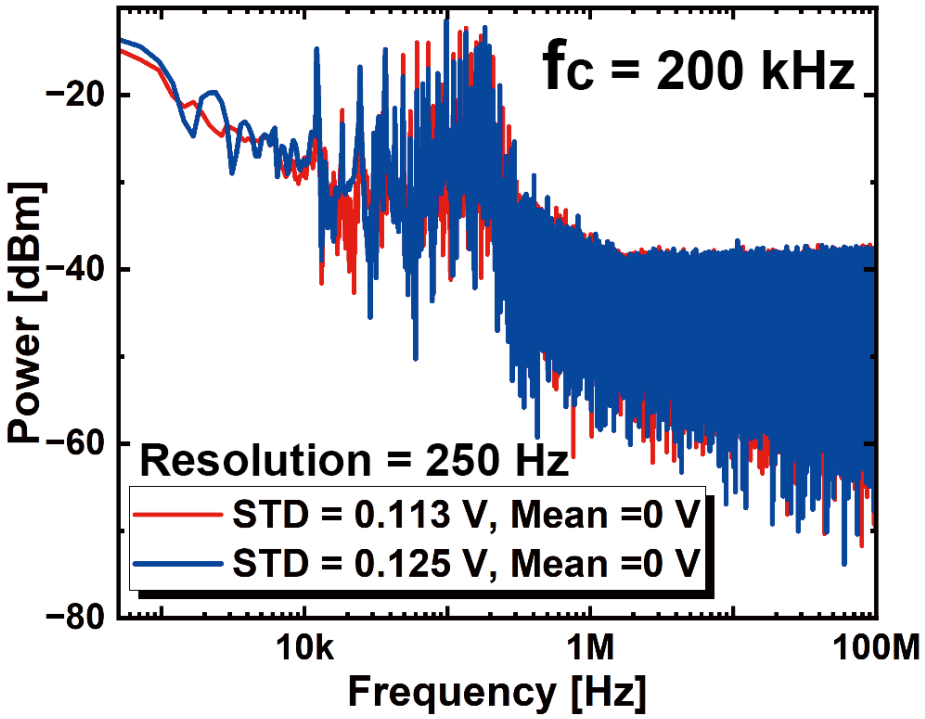

Figure 3.3: Spectrum of white Gaussian noise with a 200 kHz cutoff frequency and varying standard deviations.

the expected Gaussian shape, further evidenced by a peak power at -30 dBm. Conversely, the noise with a 0.125 V STD, shown by the blue line, produces a slightly wider linewidth of 743 kHz. The Gaussian fit, indicated by the yellow line, confirms the bell-shaped curve of the spectrum, though it appears flatter compared to the 0.113 V STD case. The noted peak power at -36 dBm and a linewidth disparity of 84 kHz between the two spectra reveal the delicate effects that even small variations in STD can have on the spectral characteristics.

Figure 3.5 uses a normal distribution graph to illustrate each noise

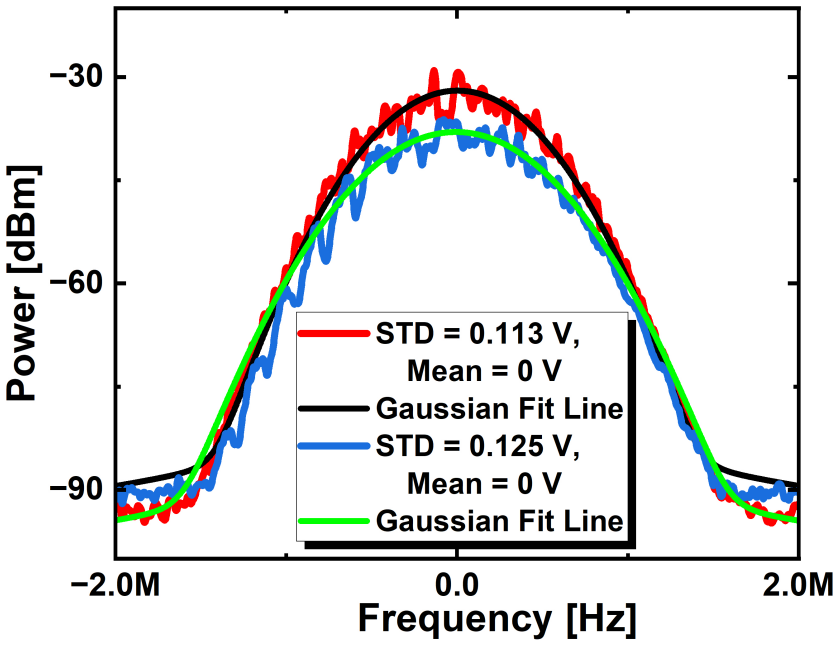

Figure 3.4: Laser spectrum linewidth under different standard deviations of white Gaussian noise.

distribution. This graphical representation aids in highlighting the slight, yet significant, differences in the laser spectrum linewidth that arise due to the varying STDs of the Gaussian noise.

Figure 3.6 provides a detailed comparison of the probability density functions (PDFs) of two different white Gaussian noises, completely plotted against their respective deviations from a standardized mean value of 0 V. In this graphical representation, the Gaussian noise with a STD of 0.125 V is marked by a blue curve. Conversely, the Gaussian noise possessing a slightly lower STD

of 0.113 V is depicted by a red curve. This side-by-side illustration in the graph effectively demonstrates the variations in the PDFs of these two noises, offering a clear visual understanding of how changes in the STD value impact the overall distribution of the noise.

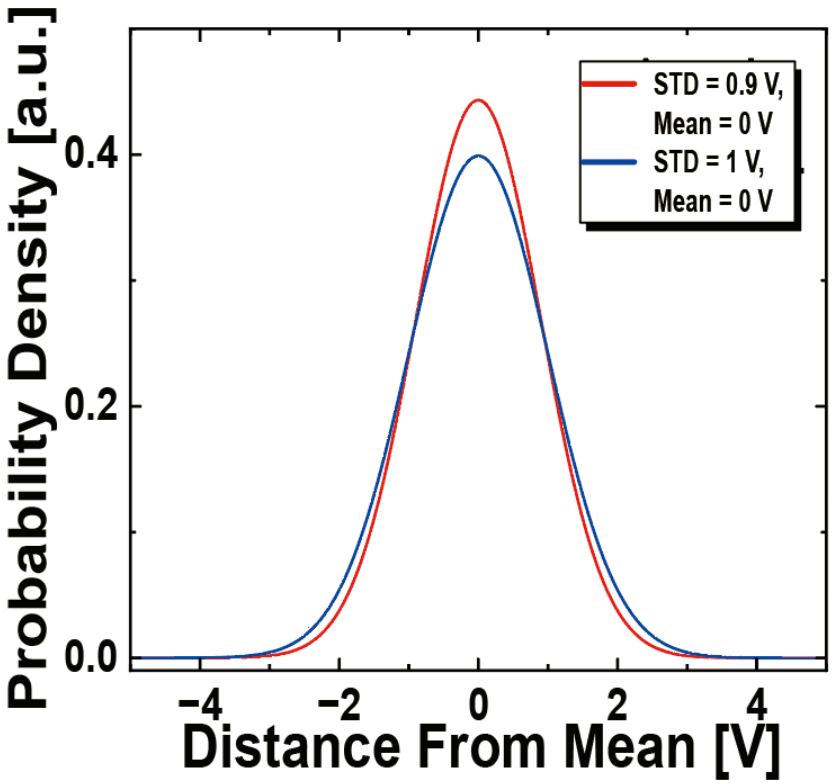

Figure 3.5: Spectrum of the original normal distribution of white Gaussian noise with different standard deviations.

These results have proved that the different power makes the laser linewidth different, as discussed in section 2.

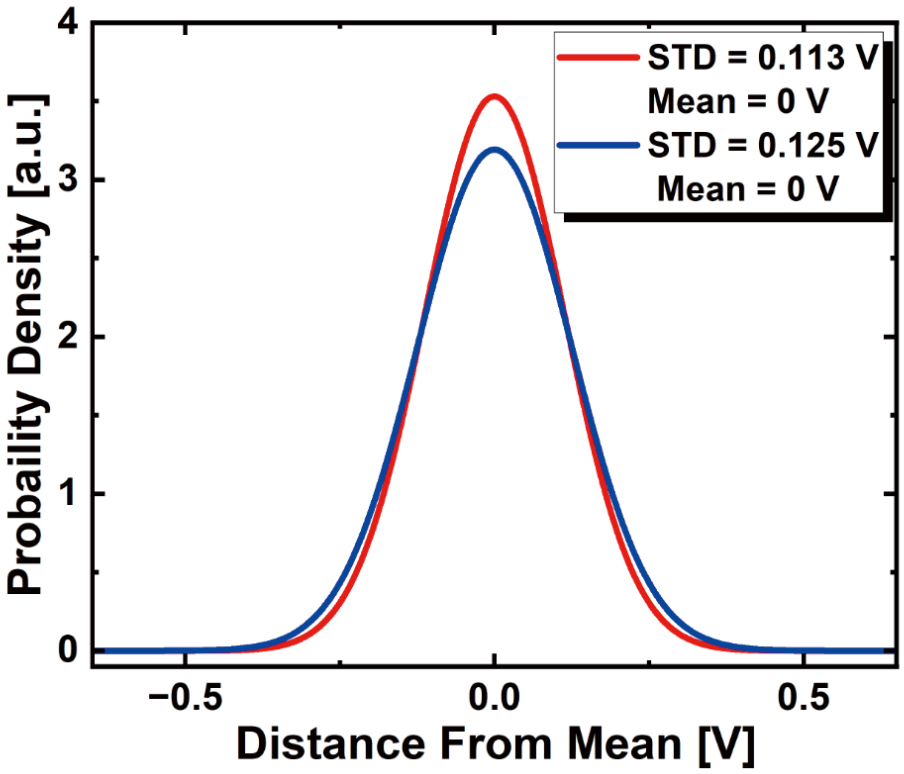

Figure 3.6: Spectrum of normal distribution of white Gaussian noise with different standard deviations.

3.3 Random walk noise for variable linewidth laser in FPGA

3.3.1 The principle of the random walk noise generation in FPGA

Figure 3.7 depicts the advanced method for generating random walk noise within specified boundaries using an FPGA. The process starts with the LFSR technique [40, 43], well-known for its ability to quickly generate non-sequential number sequences through a combination of right-shift and exclusive-OR gate (XOR) operations. This technique efficiently produces 16-bit pseudo-random numbers. However, inherent limitations of the LFSR method, such as the time intervals required to complete a period and then repeat it, bring challenges to real-time functionality. Additionally, generating long pseudo-random number sequences can slow down the real-time performance of the system. A truncation strategy was implemented to overcome these challenges, removing the uppermost two bits from the LFSR-generated pseudo-random numbers, thereby mitigating issues related to time interval differences. Choosing a 16-bit LFSR was a deliberate decision to aid in balancing the generation of pseudo-random numbers with the requirements of real-time system operations. The procedure then monitors the lowest bit of the sequence. If this bit equals 1, the walk path increases; otherwise, it decreases, ensuring an equal 50% probability of either outcome at each step. The walk is then modified by a predetermined step length

(SL), which is compared against a boundary set at ± 0.5 V. Crossing this limit indicates an overshoot, leading to a reversal in the walk direction. Given the specific characteristics of the AD 9736, with a 1 Vpp output voltage and 14-bit output data [44], the relationship between the SL in the FPGA (WSL) and the actual output SL (WSLout) is defined by the following equation:

$$W_{SLout} = \frac{W_{SL}}{2^{14}} \times 1\ V_{pp} \tag{3.1}$$

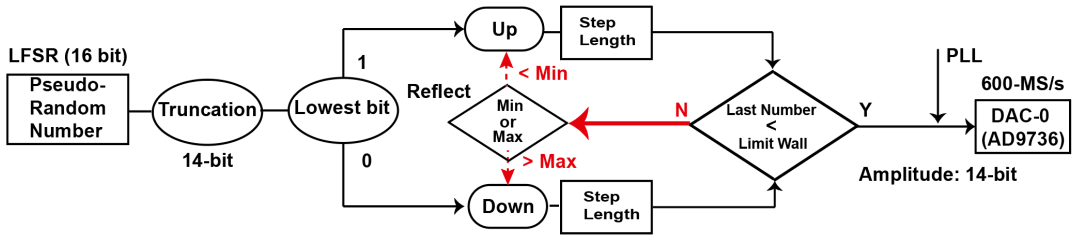

Figure 3.7: Principle of generating random walk noise with a limit wall using the FPGA with DACs.

The FPGA board used in this setup, the Xilinx Artix 7 evaluation board AC 701, was carefully integrated to ensure optimal performance. It was connected to the DACs (Analog Device AD 9736), which are notable for their high sampling rate of 600 MSamples/s. A key feature of the AD 9736 is the inserted PLL mechanism, which plays a role in adjusting the sampling rate (SR) to the desired level. A 14-bit DDR3 LVDS interface was employed to transfer efficiently the generated data to the DACs. This thoughtful integration not only secures the integrity of data transmission but also ensures the real-time generation of analog

noise, reflecting the advanced design and effectiveness of the system.

3.3.2 Experimental setup

The experimental setup, as illustrated in Figure 3.8, was developed to examine the laser spectrum linewidth using an advanced coherent interference method.

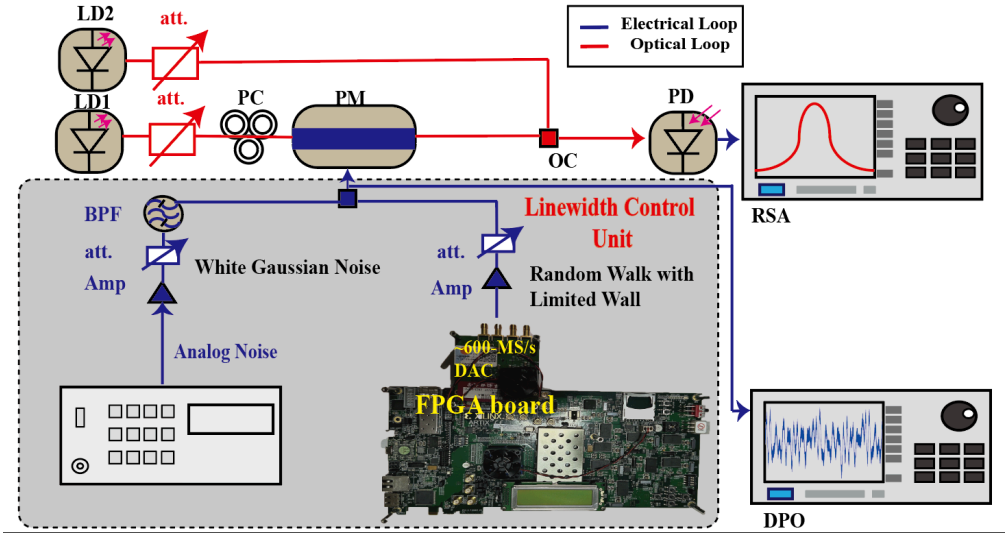

Figure 3.8: Experimental scheme of the variable linewidth laser and laser linewidth measurement.

An analog noise source (Noisecom UFX 7107), designated as WGN, was integrated into the setup. The FPGA board, capable of a remarkable 600 MS/s, generated limit-wall random-walk noise. The noise power was effectively managed by an amplifier and electrical attenuators, amplifying it by 7 dB.

3.3.3 Results and discussions

Figure 3.9 illustrates a detailed spectral analysis of the unique random walk noise generation with a limit wall, operating at a notable 10 kHz RBW. The blue curve in the figure represents a step SL of 0.09 V and a peak SR of 600 MHz. Considering the PM's inherent V_π and its interaction with the amplifier's gain profile, an optical phase shift of approximately 0.075 rad is observed over a 1.67 ns time frame. Notably, the presence of limit-wall reflections transforms the traditional low-frequency domain into an attenuated white noise profile, while the high-frequency spectrum maintains a consistent noise gradient.

The red curve in Figure 3.9 provides insight into a different result, where the SL is set at its lowest value of 0.01 V and operates in conjunction with the lowest SR at 50-MHz intervals. This setup results in a noticeable phase shift, quantified at 0.0083 radians, but over a longer duration of 20 ns. The precision of the PLL in controlling the SR, even at these finer 50-MHz increments, is particularly noteworthy. This capability allows for the finely adjustable production of an SL, with a precision down to 0.01 V. A decrease in the SL leads to a reduction in reflections, resulting in a more pronounced gradient and a frequency cutoff around the 100 MHz mark.

The essence of random-walk noise, marked by its variable SR and SL, presents an interesting contrast to low-frequency compensation typically seen in analog noise systems, especially when confined by a limit wall. This complex noise structure, with its cutoff frequency largely determined by filter constraints

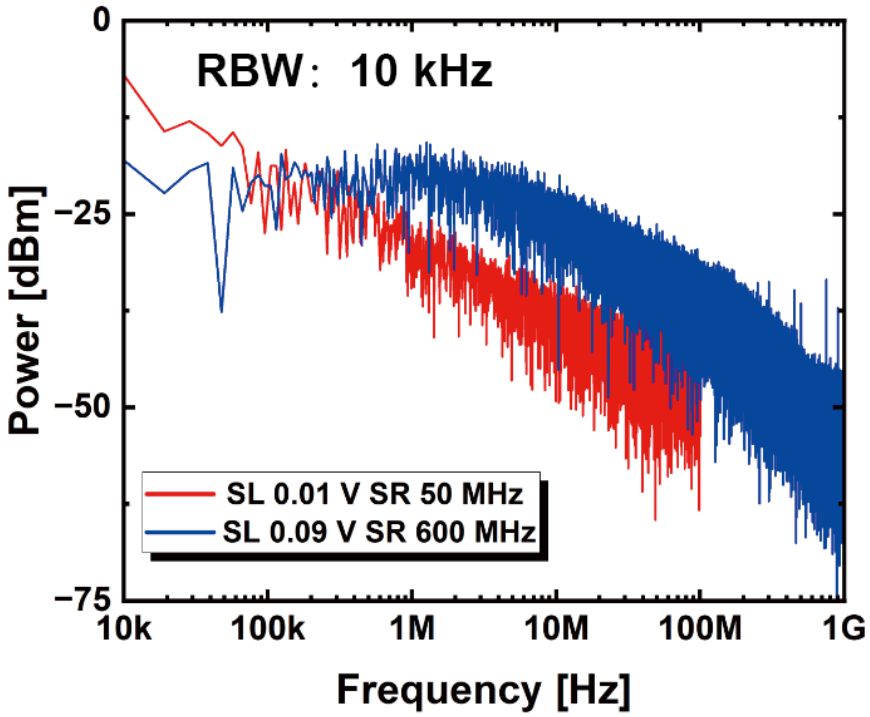

Figure 3.9: Random walk noise in the frequency domain: 0.09 V SL with 600 MHz SR and 0.01 V SL with 50 MHz SR.

and the extremities of SR and SL, oscillates within a range from 120 kHz to an upper boundary of 170 kHz. Initially, the cutoff frequency for the analog noise varies between 120 kHz and 140 kHz. This frequency is then paired with an SL of 0.07 V at an SR of 500 MHz, followed by an SL of 0.08 V at 400 MHz, and finally, an SL of 0.07 V operating at 600 MHz. These variations underscore the interplay between SL, SR, and the resultant spectral characteristics within the framework of random-walk noise generation.

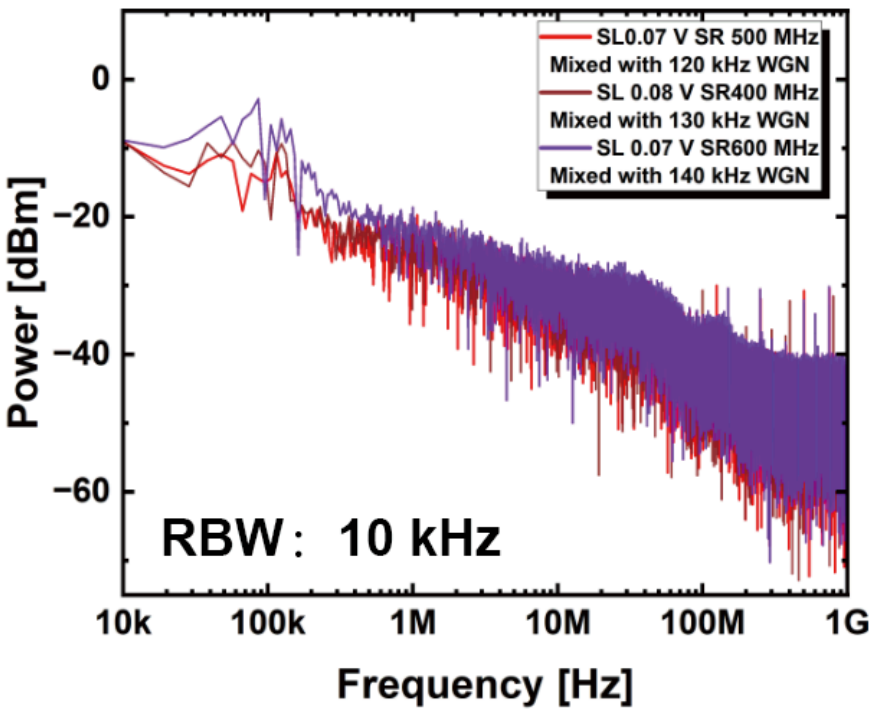

Figure 3.10: Spectrum of random walk noises mixed with WGN of 120-140 kHz.

Figure 3.10 offers a spectral view of the resulting hybrid noise, consistently analyzed at a 10 kHz RBW. A key finding is the balance achieved between all forms of random walk noise and the elements of the low-frequency spectrum. The rise in the cutoff frequency evens out the gradient of the hybrid noise, indicating an interaction between different noise components. Extending this analysis, Figure 3.11 (a) displays the laser spectrum linewidth modulated by these noise variants, and the details are displayed in Figure 3.11 (b), (c), and (d). Remarkably, the laser linewidth spans a range of 6 MHz, analyzed at a

20 kHz RBW. This spectral profile highlights a clear correlation: as the laser linewidth increases, it parallels the flattening gradient observed in the noise frequency domain. In quantitative terms, the laser linewidth experiences a sequence of amplification, starting from 251 kHz, increasing to 297 kHz, and reaching 313 kHz. These changes in the spectral characteristics are attributed to the low-frequency compensation inherent in the noise and the distinct temporal features of the random walk noise, which together influence the carrier frequency. Upon thorough examination, the resulting laser spectrum linewidth reveals a perfect pseudo-Voigt profile, showing both its central core and outer edges. This demonstrates a complex interplay between the spectral characteristics of the noise and their impact on the laser linewidth, providing valuable insights into the mechanisms governing these interactions.

In recognizing the complex, dual nature of noise, the pseudo-Voigt model is strategically employed for its capability to accurately represent composite phenomena. Figure 3.12 reveals the detailed behavior of WGN across a frequency domain ranging from 150 kHz to 170 kHz. This representation effectively contrasts the noise behavior at SL of 0.08 V and 0.09 V, with SR set at 600 MHz and 500 MHz, respectively, and each analyzed with a 10 kHz RBW. The data presented in this figure illustrates how the WGN makes the low-frequency components, resulting in a seamless integration with the random walk noise. A noticeable trend observed in the data is the progressive attenuation of the noise gradient. This attenuation evolves in conjunction with increases

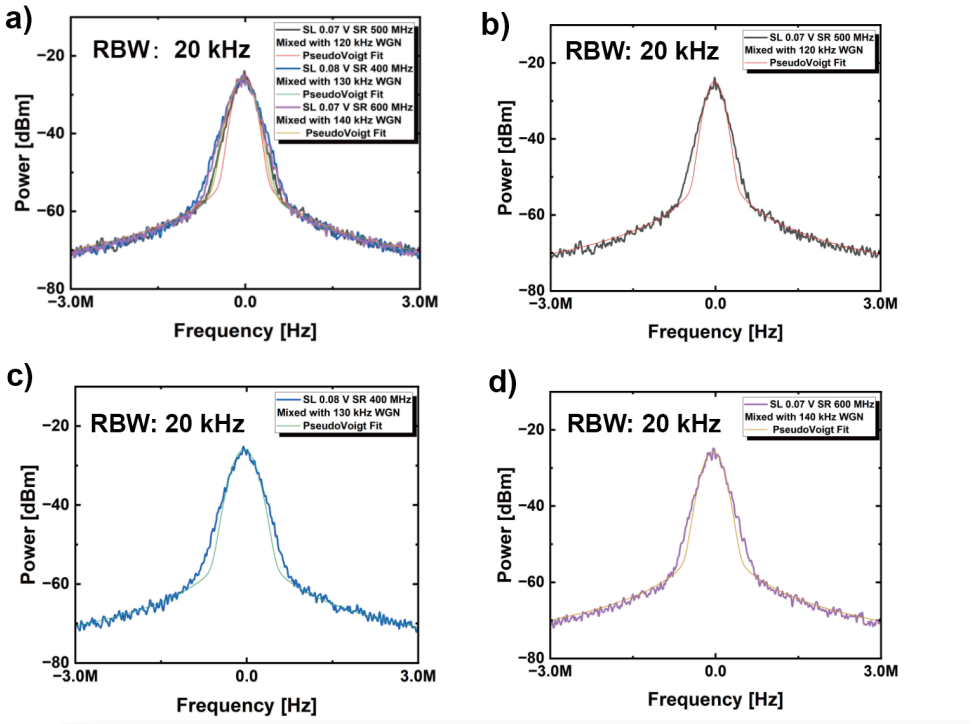

Figure 3.11: Laser spectrum linewidth affected by random walk noises mixed with WGN of 120-140 kHz.

in the cutoff frequency, SL, and SR, suggesting a dynamic interplay between these parameters. The graphical representation in Figure 3.12 thus provides insightful revelations about how different noise parameters influence the overall noise spectrum, underscoring the utility of the pseudo-Voigt model in analyzing complex noise structures.

Figure 3.13 (a) provides a detailed visualization of the laser spectrum linewidth, spanning an 8 MHz range with an RBW of 20 kHz, Figure 3.13 (b),(c), and (d) provide the details of them. This extensive display is crucial

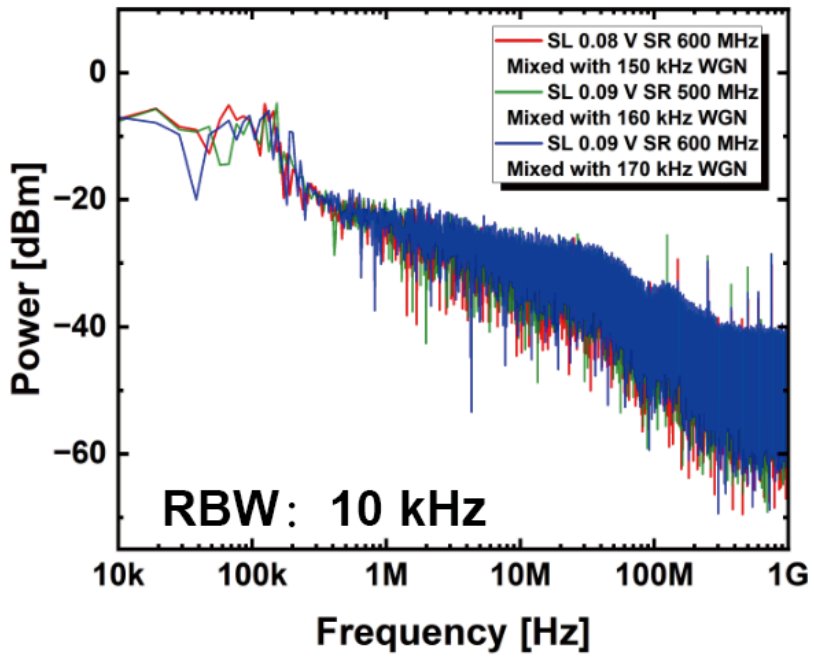

Figure 3.12: Spectrum of random walk noises mixed with WGN of 150-170 kHz.

for capturing the linewidth wings, particularly as the linewidth progresses from an initial value of 394 kHz, rises to 470 kHz, and ultimately peaks at 611 kHz. These variations in the linewidth are indicative of exceptional performance across both the central and peripheral areas of the spectrum, aligning well with the predictions of the pseudo-Voigt model. The accuracy and consistency seen in these measurements reflect the effective interplay between the immediate noise dynamics and the low-frequency compensation methods employed. The broad range of the spectrum covered and the precision of the measurements underscore the efficacy of the experimental setup in capturing the intricate details of the

laser linewidth behavior. This detailed representation in Figure 3.13 not only validates the theoretical model but also highlights the relationship between noise characteristics and their impact on the laser linewidth, offering valuable insights into the underlying processes governing these phenomena.

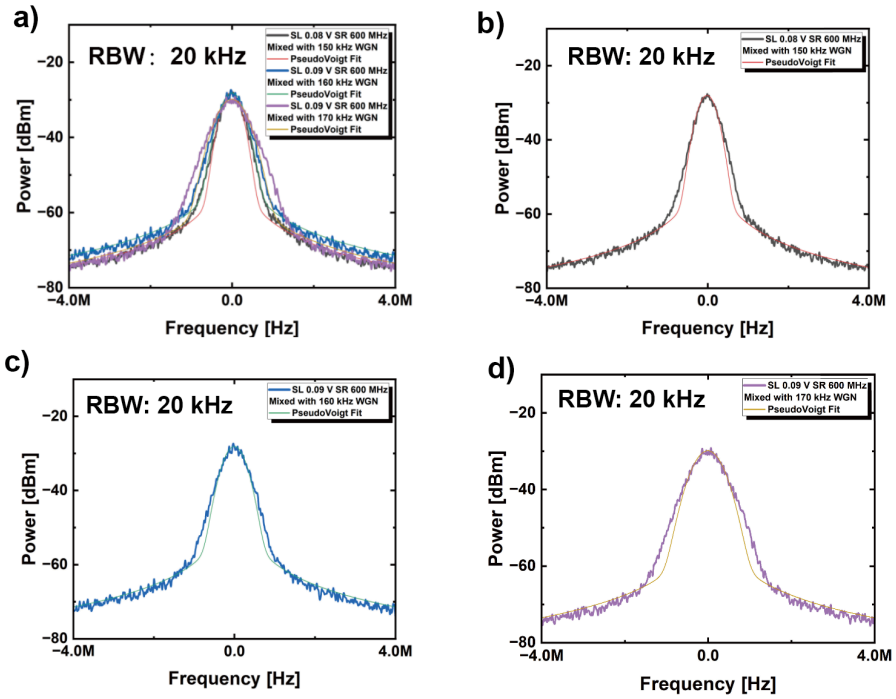

Figure 3.13: Laser spectrum linewidth affected by the random walk noises mixed with WGN of 150-170 kHz.

Table 3.1 provides a detailed comparison between theoretically predicted and experimental measured laser linewidths. The theoretical predictions, which are closely aligned with the cutoff frequency and the characteristics of the random walk noise, range from 268 kHz to a maximum of 588 kHz. In contrast, the

Cutoff frequency of WGN	The condition of the random walk noise	Theoretical linewidth	Actual linewidth
120kHz	SL 0.07 V SR 500MHz	268kHz	251kHz
130kHz	SL 0.08 V SR 400MHz	280kHz	297kHz
140kHz	SL 0.07 VSR600MHz	321kHz	313kHz
150kHz	SL 0.08 VSR600MHz	420kHz	394kHz
160kHz	SL 0.09 VSR500MHz	444kHz	470kHz
170kHz	SL 0.09 VSR600MHz	588kHz	611kHz

Table 3.1: Dependence of theoretical and actual laser linewidths on the random walk SL and WGN.

measured linewidths vary from 251 kHz to 611 kHz. The differences observed, ranging from 8 to 26 kHz, can likely be attributed to a combination of factors like losses, reflections inherent in the noise integration process, and inaccuracies in SR and SL. An interesting observation is that the use of an AWG could potentially reduce the maximum error margin to around 21 kHz. However, the FPGA-based approach for noise generation proves to be notably more effective with its capability for real-time modulation, particularly in terms of enhanced performance in the wing spectrum of the linewidth. Moreover, when compared with the relatively minor difference of 5 kHz associated with the AWG, the FPGA-centric method stands out not only for its precision but also for its cost-effectiveness and flexibility. This makes the FPGA-based approach a more ideal choice for controlling the tunable laser linewidth, especially in applications requiring a high degree of precision and adaptability. The comparative data in Table 3.1 demonstrates the strengths and limitations of each method, highlighting the superiority of FPGA in terms of overall performance and operational benefits.

3.4 Varibale linewidth and line shape laser based on two FPGAs

In the study, the primary method for random number generation utilizes the xorshift 128 algorithm within the FPGA framework [43] and has the better randomness than the LFSR method before This algorithm offers fast generation speeds and simplicity in implementation. However, a significant limitation of the xorshift 128 method is its inherent periodicity, which can impact the randomness of the output. The integration of an analog noise source for random number generation was undertaken to improve the system's randomness. However, a thorough analysis revealed that the analog noise source typically follows a Gaussian distribution. This distribution tends to be narrower at the edges, leading to a shortage of random numbers at these extremes. Since actual laser noise exhibits true randomness, the limitations of both the xorshift 128 method and the analog noise source must be carefully considered.

To address these issues, the current focus is on combining these two methods. The goal is to overcome the strengths of each while minimizing their respective weaknesses. This hybrid approach aims to provide a more effective solution for random number generation. As part of this effort, Figure 3.14 demonstrates how the analog noise source is integrated with ADCs. These ADCs, limited to a 14-bit resolution, convert the analog noise signals into digital random numbers [33]. However, the 14-bit limitation of the ADCs restricts the range of

output random numbers from the analog noise source. In addition, the Gaussian distribution of the analog noise source, with its reduction at the ends, results in a lack of random numbers at the boundaries. Consequently, the analog noise source primarily serves as a generator of low-bit random numbers. This innovative strategy of combining an analog noise source with the digital capabilities of FPGA-based generation offers a promising direction for producing more diverse and random number sequences.

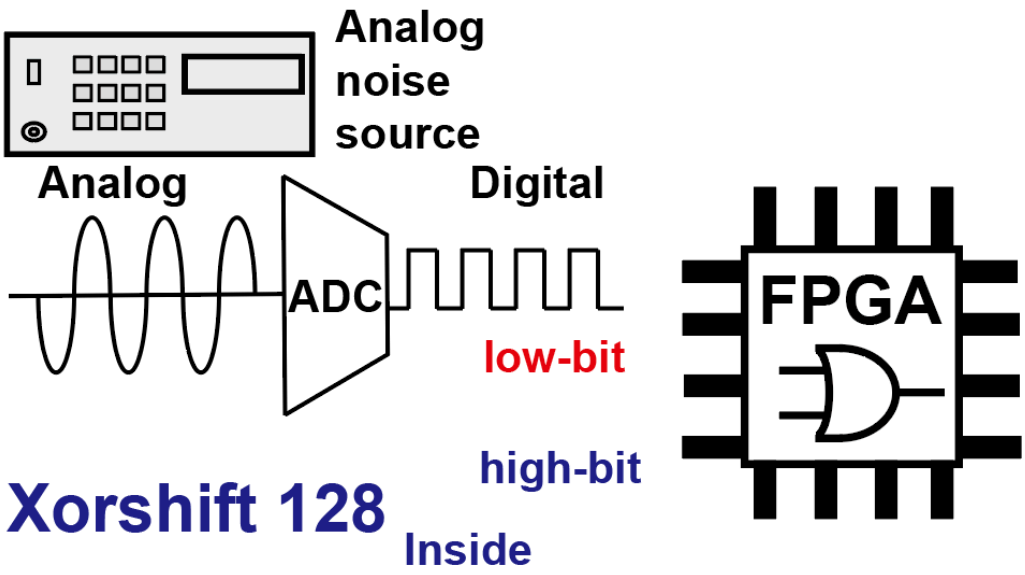

Figure 3.14: Principle of the new random number generation method.

The xorshift 128 algorithm, central to this approach, generates random numbers with a relatively uniform distribution. However, it has its limitations, notably a compromise in achieving true randomness and a tendency towards periodicity. These characteristics, though seen as drawbacks, interestingly

position the xorshift 128 as a complementary method to the analog noise source. The xorshift 128 algorithm excels in providing high-bit random numbers, a segment where the analog source falls short due to its Gaussian distribution focus on lower-bit numbers. The xorshift 128 method is combined with the analog noise source in this innovative fusion within the FPGA framework. This combination represents a significant pace forward in random number generation technology. The innovative approach leverages the strengths of both the xorshift 128 algorithm and the analog noise source. By doing so, it addresses the periodicity issue inherent in the xorshift 128 and compensates for the Gaussian distribution effect at the extremes, seen in the analog source. This combination ensures a more balanced distribution of random numbers across the entire spectrum, enhancing the overall effectiveness and reliability of the random number generation process.

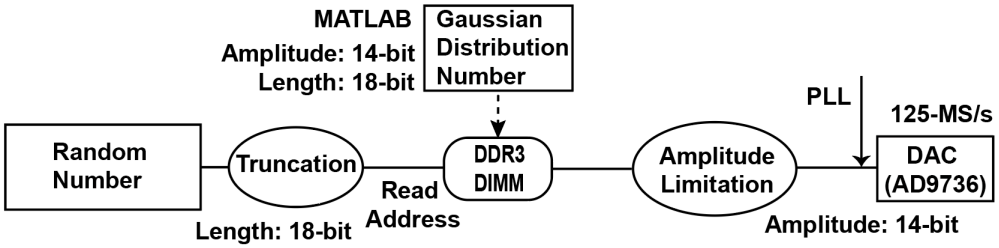

Figure 3.15: Principle of generating white Gaussian noise using the FPGA with DACs with novel random number generating method.

Figure 3.15 illustrates the method for generating white Gaussian noise using the LUT approach. The process begins with the creation of random numbers

through a novel fusion of the xorshift 128 technique and an analog noise source. This combination has been shown to exceed the randomness typically achieved by conventional 14-bit LFSRs, as supported by the findings in [68]. For maximum effectiveness, the bit length of these generated random numbers is carefully calibrated. After truncation, these bit lengths are fine-tuned to match the storage capabilities of the DIMM. The next step involves the precise quantization of STD Gaussian distribution numbers, ranging from 1 V to 1.62 V. This transformation converts these values into 14-bit amplitude and 18-bit length representations, a process managed by MATLAB (R2022a), considering the limitations of the semiconductor intellectual property (IP) core. Once quantified, these numbers are stored in the FPGA's DIMM, where the pseudo-random figures are used as memory addresses for efficient recovery. The hardware selected for this task, the Xilinx Artix 7 evaluation board AC 701, is integrated with 125-MSamples/s DACs (Analog Device AD 9736). These DACs utilize a PLL for precise sampling rate adjustment. The transfer of data to the DACs is conducted through a 14-bit DDR LVDS interface, ensuring the real-time generation of analog noise. This systematic approach to noise generation combines complex hardware with intelligent software algorithms, enabling the production of high-quality white Gaussian noise suitable for various advanced applications.

In Figure 3.16, the method for precisely adjusting random walk noise within specific limits is detailed. This approach, which replies to the fundamental random number generation strategy, requires a 10-bit random number length to

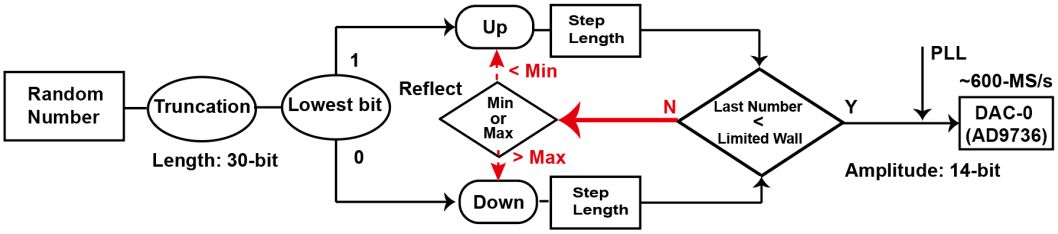

Figure 3.16: Principle of generating random walk noise with limited wall using the FPGA with DACs with new random number generating method.

maintain randomness effectively. A novel system is implemented to analyze the least significant bit of each random number. If this bit is 1, the path of the noise increases; if not, it decreases. This binary appliance guarantees a 50% chance of either outcome at each step, ensuring a balanced probability. The next phase of the process involves monitoring whether the step stays within the set bounds. Exceeding these limits leads to a reversal in direction while remaining within them enables a direct link to the DACs. Despite potential time delays in processing noise that breaches the boundary conditions, the speed of the FPGA, in conjunction with the DDR LVDS data transmission method, enables the real-time generation of noise. By combining bounded random walk noise with white Gaussian noise, a unique profile for the variable spectrum linewidth is created.

3.4.1 Experimental Setup

Figure 3.17 presents the elaborate experimental setup designed to precisely modulate and measure the laser spectrum linewidth using coherent interference.

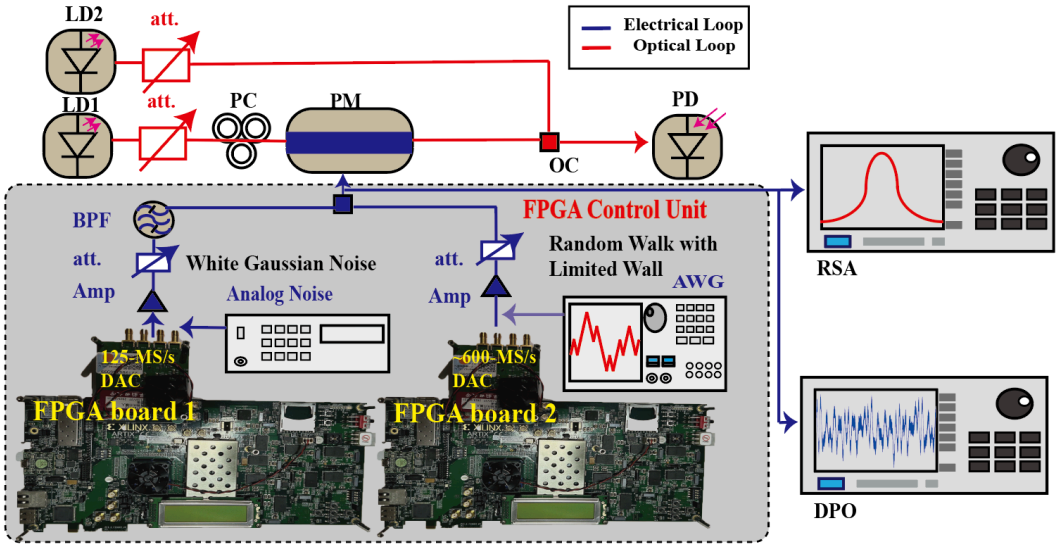

Figure 3.17: Experimental scheme of the variable linewidth laser and laser linewidth measurement with FPGA system.

The setup incorporates two key FPGA boards, each with specific roles. The first FPGA board is equipped with 125 MS/s DACs, responsible for generating white Gaussian noise. Analog noise (Noisecom UFX 7107) unit is converted into digital random numbers via 125 MS/s ADCs for input into the FPGA.

Another critical component is a second FPGA board, operating at a remarkable 600 MS/s. This board generates limited wall random walk noise. To address the sampling rate limitations of this FPGA, an AWG (Tektronix

AWG7102) is used for high-frequency compensation.

3.4.2 Random numbers for noise generation

Figure 3.18 showcases a computational simulation and visualization of the distribution of random numbers for white Gaussian noise. The graph illustrates the Gaussian probability density function, emphasizing the concentration of values around the mean and forming a typical bell curve. However, the tails of the distribution show fewer values, indicating the limitation of analog noise sources in generating random numbers at the distribution extremes. This feature is a crucial consideration in achieving a uniform random number distribution, particularly at the boundaries.

A strategic truncation technique has been implemented to overcome the limitations inherent in traditional random number generation methods. The random numbers generated from the Gaussian-distributed analog source are truncated to a 10-bit representation. These truncated values are then combined with higher-bit-range numbers from the xorshift 128 algorithm. This innovative amalgamation method effectively compensates for the shortcomings of each individual approach.

The mixed random number generation strategy, illustrated in Figure 3.19, shows improved randomness across the entire value spectrum, including the previously edge regions. The expanded bit depth, reaching up to 2^{20}, is evident in the uniform distribution of randomness throughout the graph. This hybrid approach successfully combines genuine randomness while ensuring a wide range of random values is covered.

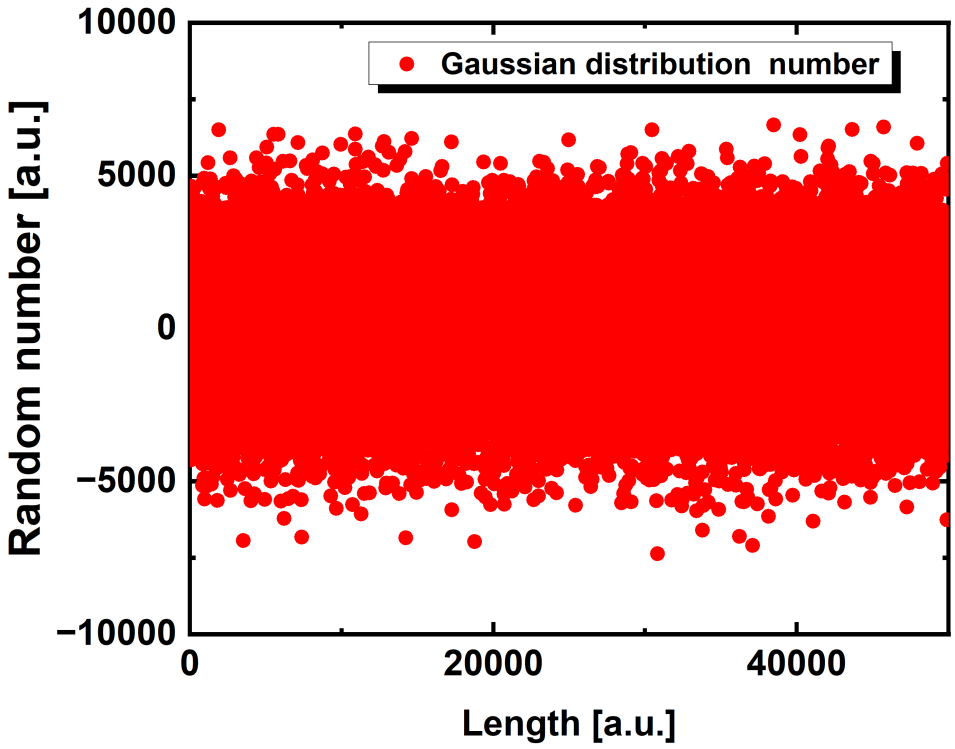

Figure 3.18: The simulation results of the white Gaussian distribution.

This method enhances the random number generation process by incorporating true random behavior and extending the uniform randomness across the entire distribution. It represents a complex blend of the strengths of both digital and analog random number generation techniques, creating a more effective framework for random number generation. This approach is particularly valuable in applications that demand high accuracy and diversity in random number generation.

In Figure 3.20, data from the ADCs show a 14-bit random number output.

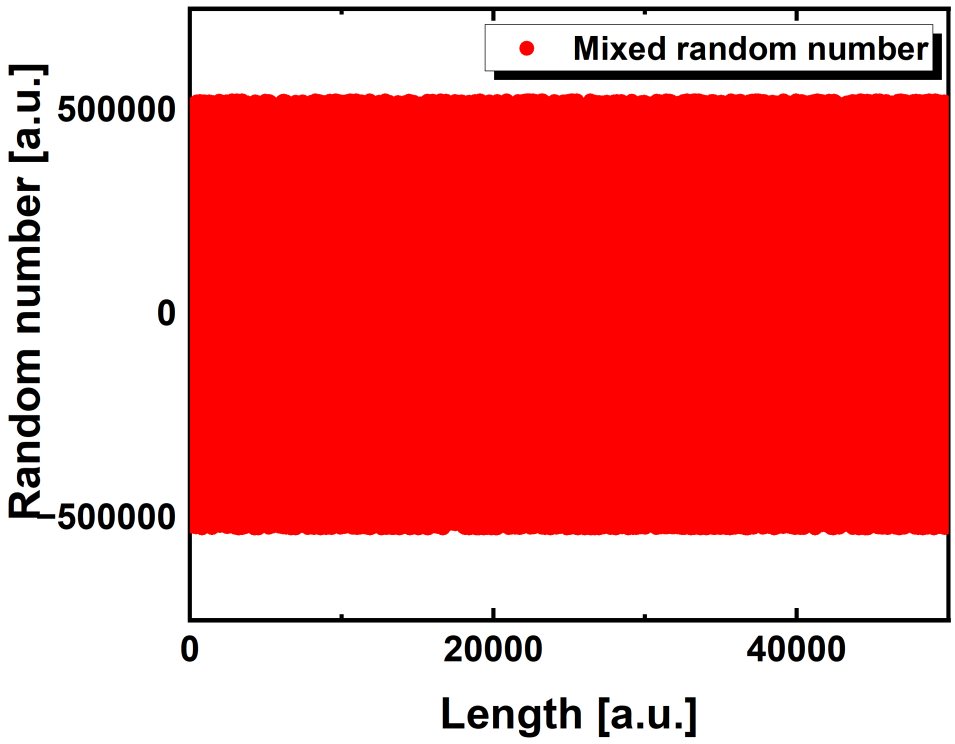

Figure 3.19: The simulation results of the white Gaussian distribution number mixed with pseudorandom number.

A closer analysis of this data confirms a concentration of values around the central region, in line with simulated predictions. However, this visualization also highlights a notable shortage in random number generation at the edges of the distribution, a common limitation of analog noise sources. This characteristic strengthens the need for a hybrid approach, which seeks to balance and expand the randomness across the entire spectrum of the distribution.

To address the uneven distribution of random numbers and achieve a more

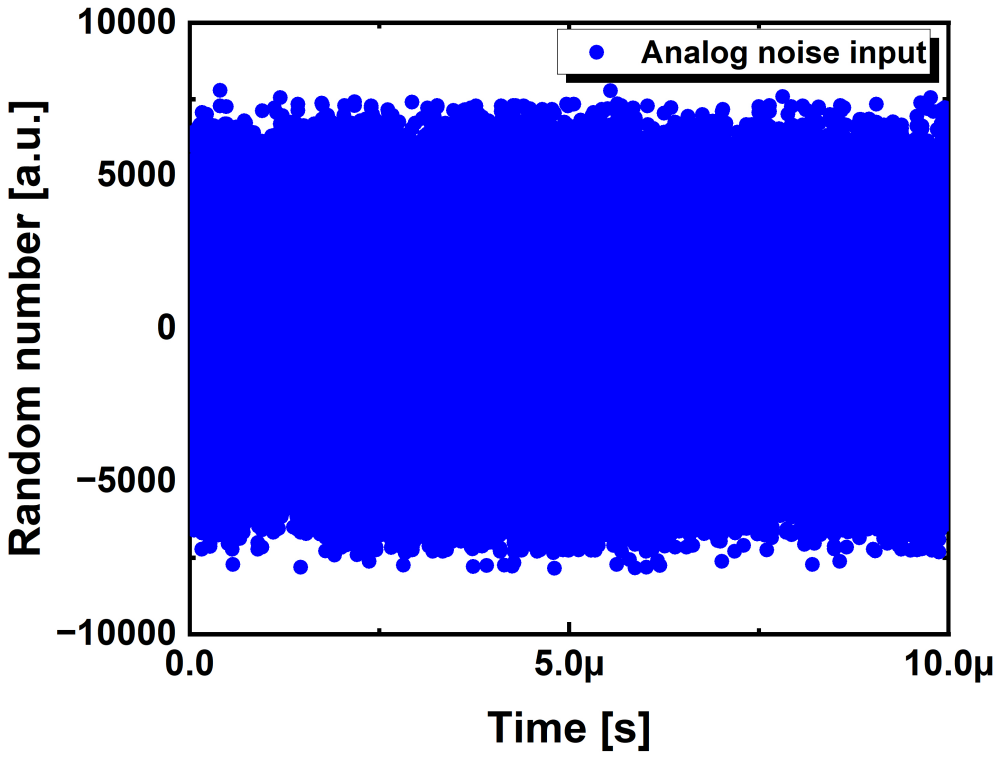

Figure 3.20: The random number results of the analog noise from ADCs.

uniform spread, an additional 13-bit random number sequence, generated using the xorshift 128 algorithm, has been incorporated. This enhancement is illustrated in Figure 3.21, where the resulting data set vividly displays a random number distribution that not only fully spans the 2^{20} bit domain but also maintains the randomness inherent to the analog noise source.

This strategy is both careful and systematic. It significantly improves the random number generation process by combining the random properties of analog noise with the broad coverage provided by digital algorithms. This careful

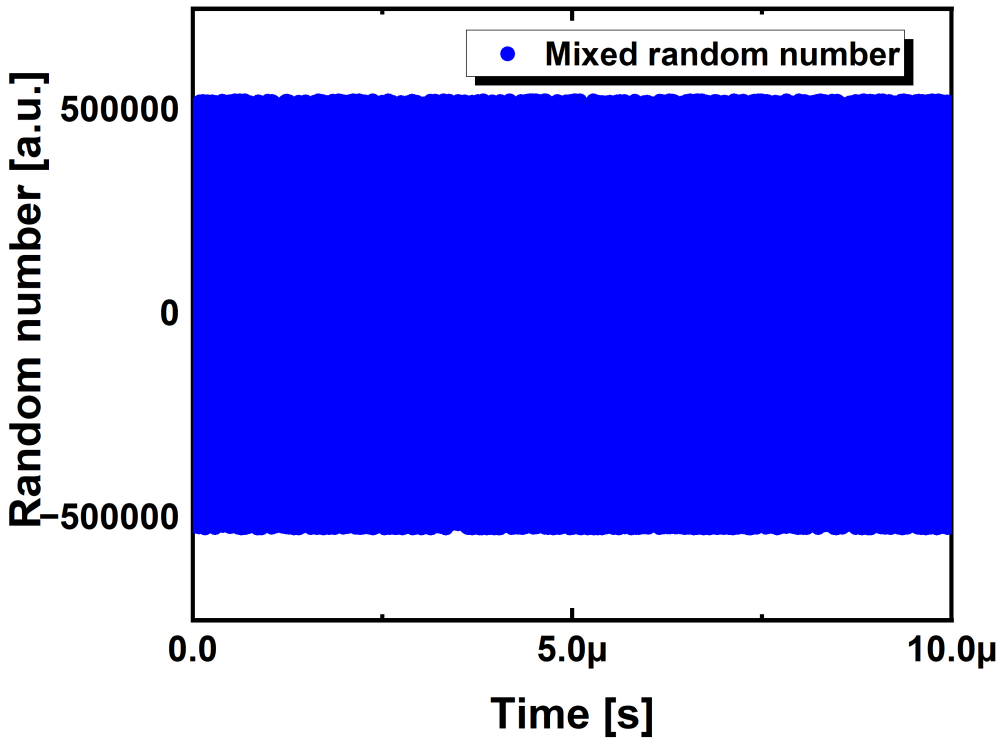

Figure 3.21: The results of the mixed random number from analog noise and pseudorandom number.

combination results in a random number generation system, capable of simulating truly random sequences free from any observable patterns or predictability. The integration of digital and analog methods in this manner produces an advanced random number generation system. This system exhibits superior coverage, making it especially suitable for complex computational simulations and high-level encryption agreements where the quality of randomness is critical. By effectively bridging the gap between the two methods, a level

of randomness and distribution is achieved that neither method could attain independently, illustrating the potential of hybrid approaches in technical and scientific applications.

3.4.3 Results and discussions

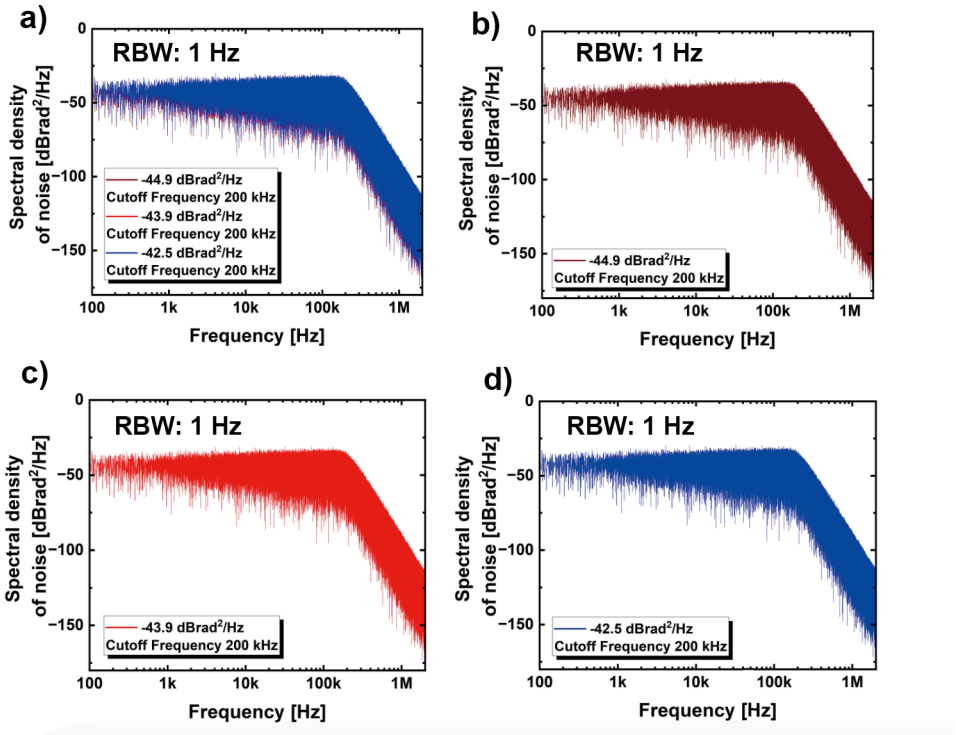

Figure 3.22: Noise power density spectrum of white Gaussian noise with different STDs.

A detailed simulation study was undertaken to investigate the effects of increasing the STD on the phase modulation characteristics of an optical system. For the purposes of this study, the half-wave voltage (V_π) of the phase modulator was set to 1 Volt to simplify the computations. The simulation monitored the effect of a linear increase in the STD of white Gaussian noise from 1.6 to 2.1 arbitrary units (a.u.), corresponding to a phase shift range from 2.6 to 3.1 π.

Initial results, illustrated in Figure 3.22 (a), show a notable increase in the

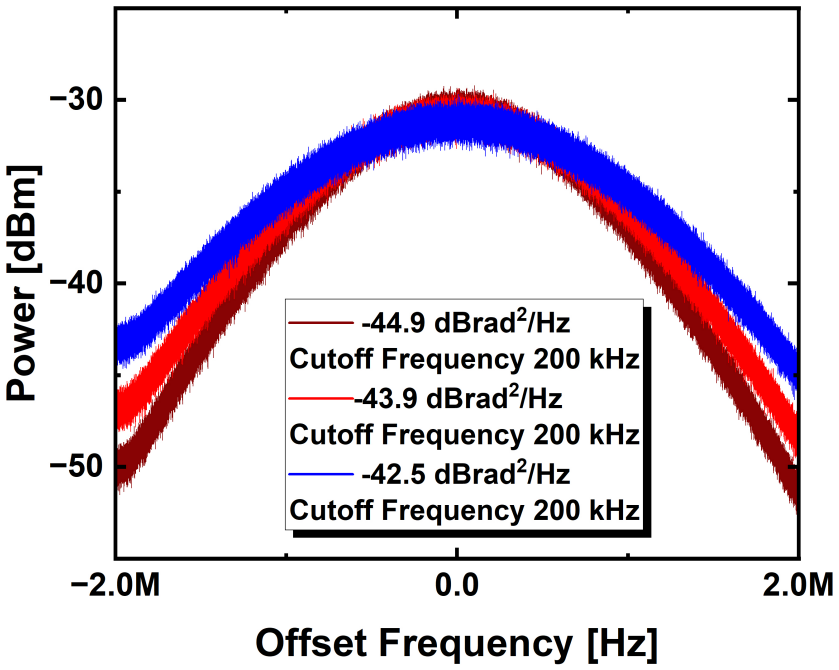

Figure 3.23: Laser spectrum of white Gaussian noise with different STDs.

Power Spectral Density (PSD) of the noise, climbing from -44.932 to -42.5703 $dBrad^2/Hz$, and the details are shown in Figure 3.22 (b),(c),and (d). This increase follows a linear trend, with the cutoff frequency of 200 kHz clearly observable. As depicted in the Figure 3.23 further examination reveals how variations in the laser spectrum linewidth are affected by these rising STD values. As the STD gradually increases from 1.6 to 2.1 a.u.—equivalent to an optical phase shift from 2.6 to 3.1 π—the laser linewidth correspondingly expands from 910 kHz to 1.128 MHz.

The precise nature of these changes is further emphasized in Figure 3.24,

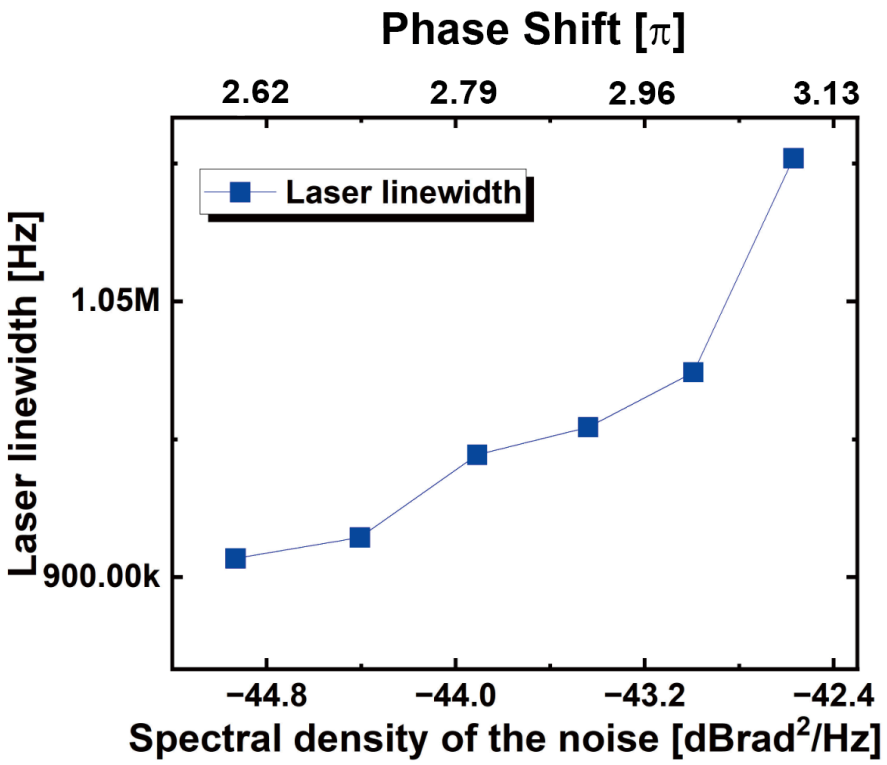

Figure 3.24: Relationship of laser spectrum and white Gaussian noise with different STDs.

where each 0.1 a.u. increase in STD results in a corresponding 0.1 π phase shift, leading to a 20 kHz increase in linewidth. These observed patterns confirm the ability to utilize linear modulation of the STD as a method for precise control over the laser spectrum linewidth. This method proposes a new approach for accurately adjusting laser linewidths, with significant potential applications in optical communication and laser modulation technologies.

The comparative results of three different methods are presented in Figure

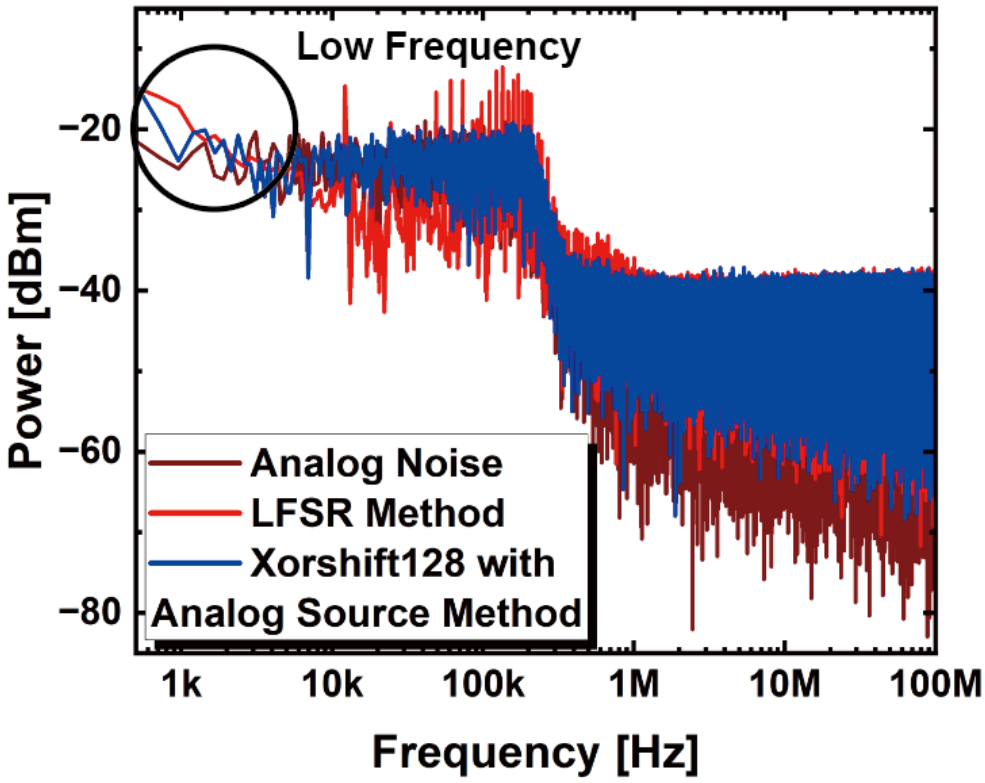

Figure 3.25: Spectrum of white Gaussian noise with a 200 kHz cutoff frequency and different generation methods.

3.25. This figure highlighted the combination of the xorshift 128 algorithm with an analog noise source, particularly its performance in the low-frequency domain, as indicated by the marked circle. This method demonstrates a noise profile that closely resembles an analog noise source, exhibiting an average vibration pattern. Conversely, the LFSR method does not display this average vibration and instead shows some atypical vibrations.

In the experimental setup, the STDs were carefully calibrated using

MATLAB to match the dynamic range and resolution of the DACs within the FPGA framework. This calibration was essential to ensure that the STDs remained accurate within the operational limits of the DACs. Figure 3.26 illustrates data showing how the original STD values were adjusted across a range from 1 to 1.6218 volts.

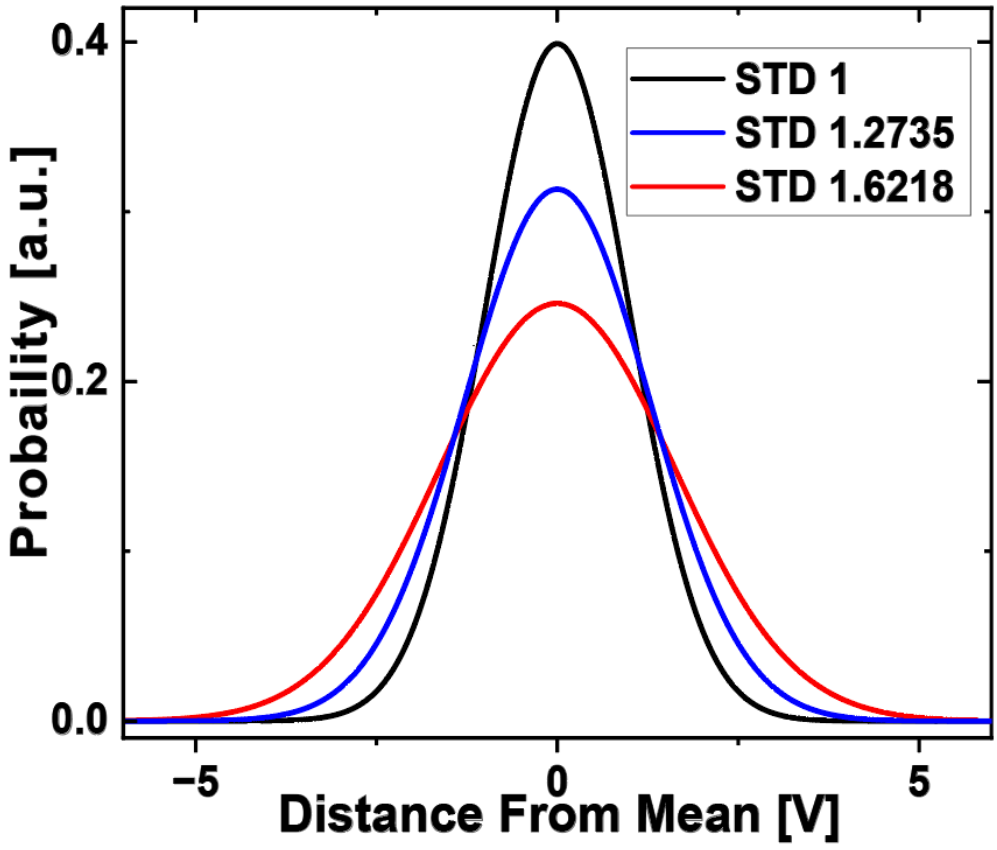

Figure 3.26: Spectrum of normal distribution of white Gaussian noise with different STDs of the original one.

Figure 3.27 displays the STD values, which were found to vary between

0.1248 volts and 0.2027 volts. This range illustrates a noticeable flattening of the Gaussian distribution bell curve, indicating a change in the signal amplitude. Such variations in amplitude are critical for the creation and analysis of white Gaussian noise in signal processing applications. The calibration and presentation of these STDs are crucial not only for validating experimental methods but also for enhancing the precision of noise simulations in practical cases.

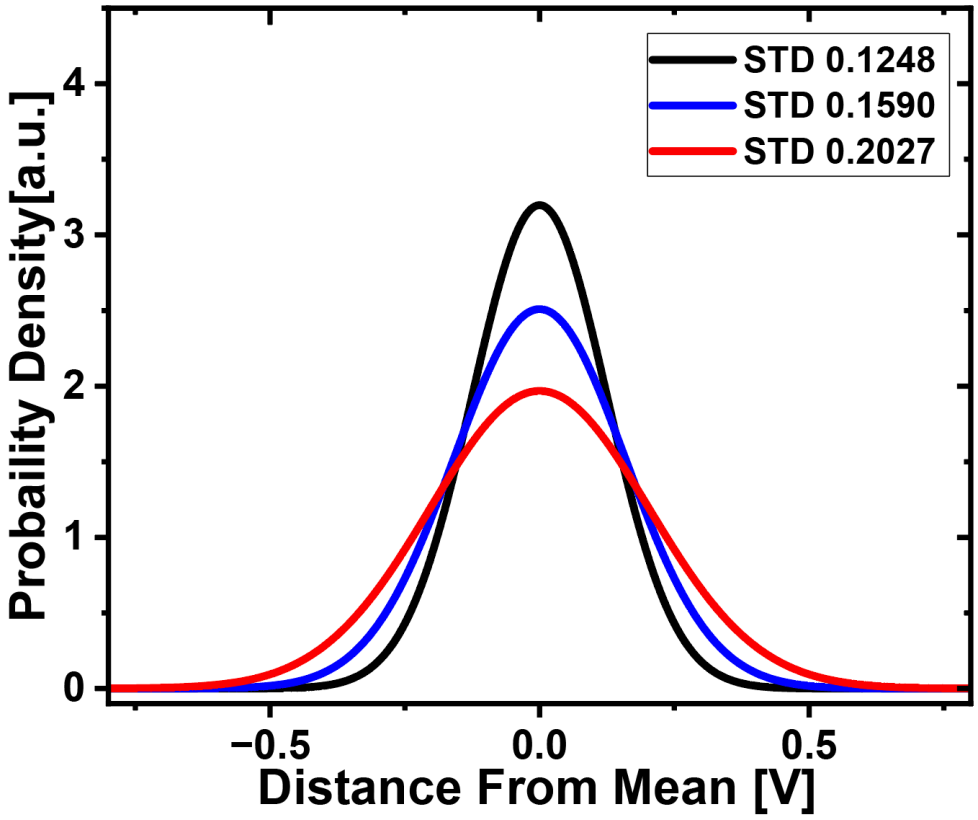

Figure 3.27: Spectrum of normal distribution of white Gaussian noise with different STDs of the actual one.

In Figure 3.28, the noise spectrum is shown with a fixed 200 kHz cutoff frequency and an RBW of 250 Hz. This spectrum reveals a direct relationship between the magnitude of the STDs and the spectral power, where an increase in STDs uniformly boosts the low-frequency components within the noise spectrum. Furthermore, the established cutoff frequency for each portion of the spectrum is clearly visible, allowing for straightforward comparisons across different STD levels. The slight increase in STDs results in a corresponding rise in power, demonstrating the proportional effect of STD variations on the noise spectrum. This observation is instrumental for understanding how changes in noise characteristics can impact the overall performance of optical systems, particularly in terms of signal processing and modulation.

Figure 3.29 provides a detailed quantification of the effects of increasing STDs on the laser spectrum linewidth. For this analysis, a narrower RBW of 20 kHz is used to enhance spectral resolution. As the STDs of the generated white Gaussian noise increase, there is a noticeable change not only in the power level but also in the spectral characteristics of the laser. A rise in STDs results in a more pronounced flattening of the Gaussian bell curve, accompanied by an increase in power. This, in turn, leads to an expansion of the laser linewidth, with an observed increase from 580 kHz to 604 kHz, and eventually to 706 kHz. The laser linewidth shows progressive enlargement in direct proportion to the STDs. This effect can be attributed to the linear response of the PM, which linearly impacts the spectrum linewidth, with different noise parameters leading to distinct linewidth variations.

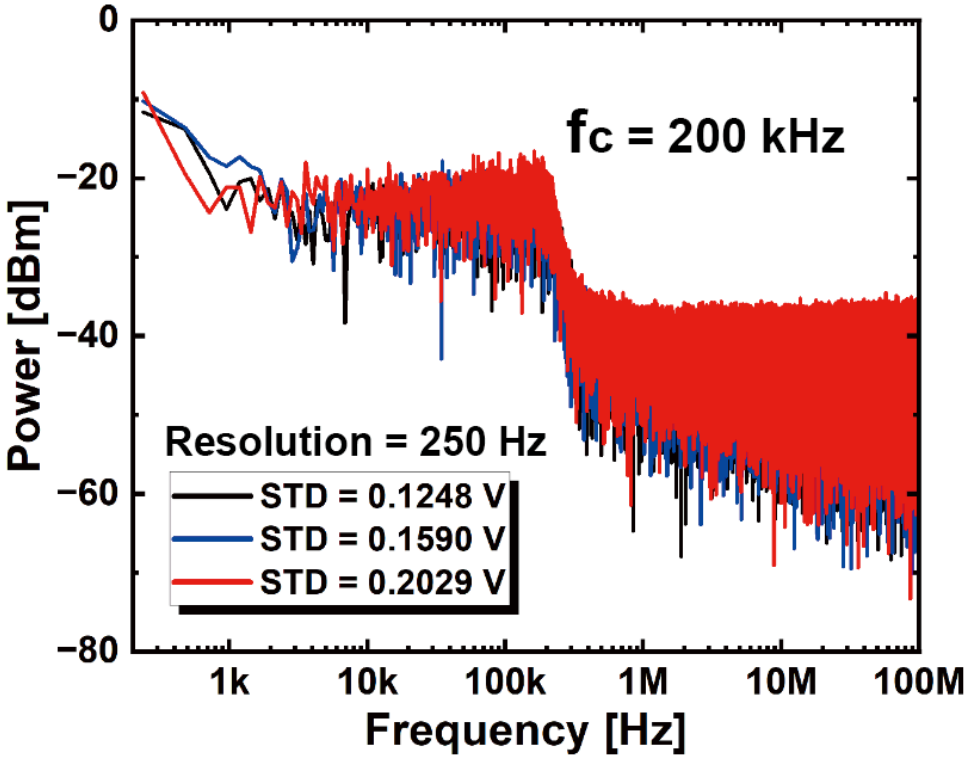

Figure 3.28: Spectrum of white Gaussian noise with different STDs and a 200 kHz cutoff frequency.

The linear relationship between noise parameters and linewidth results in a Gaussian-shaped laser spectrum linewidth. However, it is noteworthy that the amplifier within the filter mainly amplifies low-frequency components. This leads to a Gaussian contour in the central part of the spectrum while introducing deviations in the spectral wings. These differences are crucial, especially when considering the impact of the cutoff frequency on the laser spectrum linewidth. The analysis underlines the complex relationship between noise characteristics

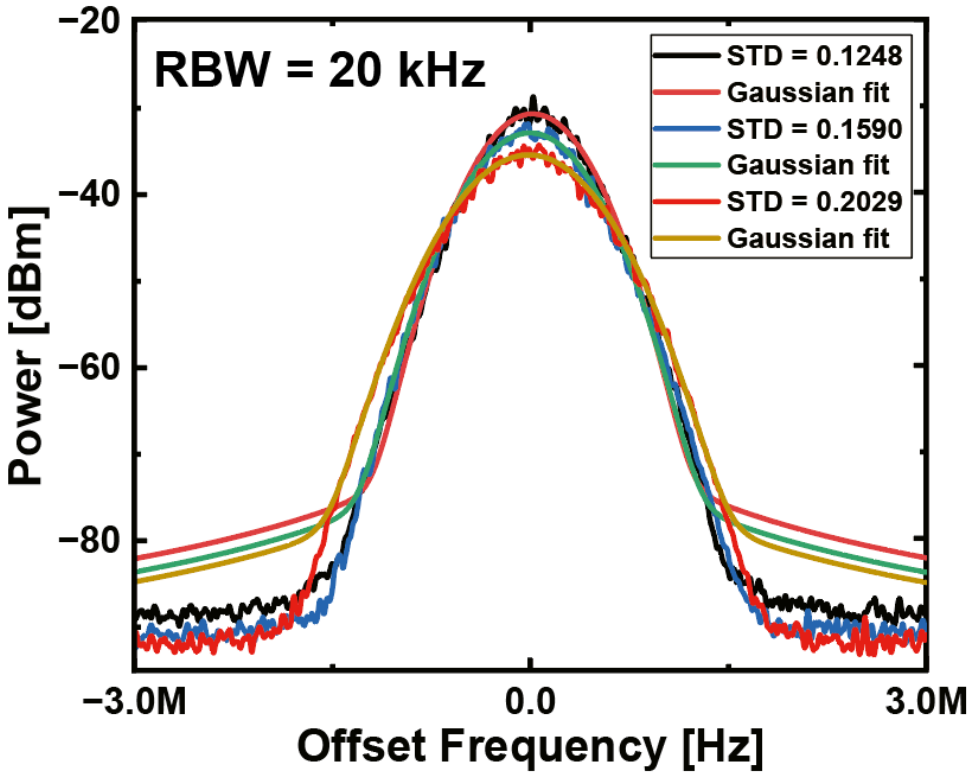

Figure 3.29: The laser spectrum linewidth of with white noise having different STDs.

and their effects on the spectral properties of laser systems.

In Figure 3.30, the STD is maintained consistently at 0.2027 V, while the cutoff frequency is varied to distinct values of 110 kHz, 180 kHz, and 250 kHz. The analysis, conducted with an RBW of 250 Hz, clearly standardizes the cutoff frequencies in the frequency domain. This allows for a thorough exploration of how bandwidth limitations affect the noise profile. The shifts in the frequency

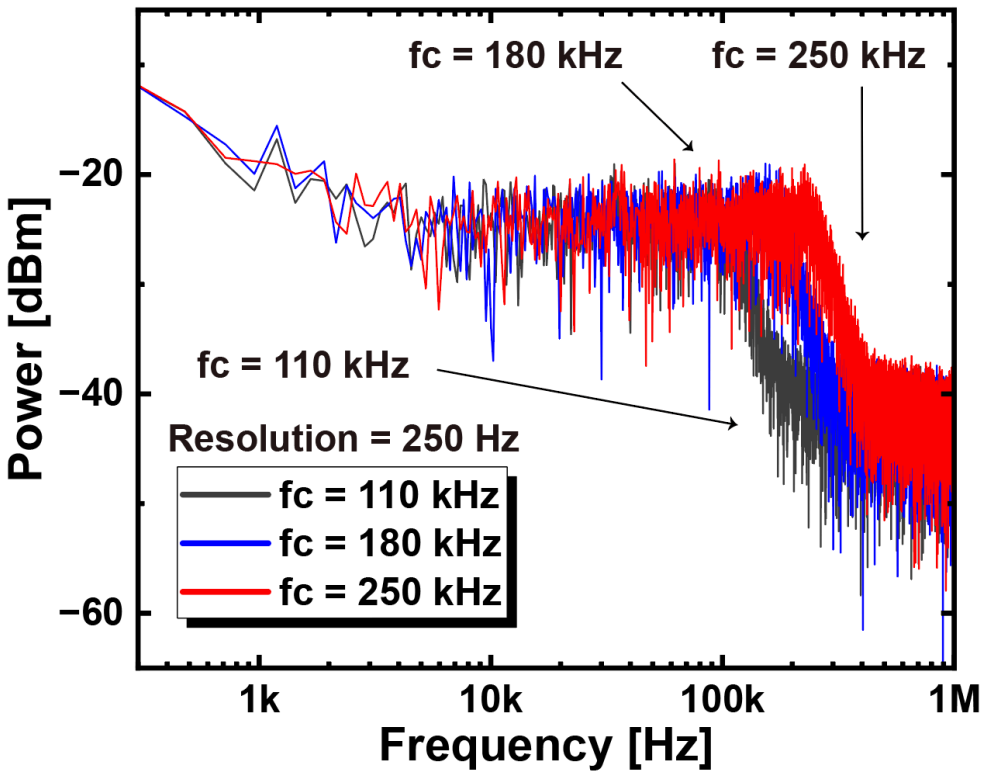

Figure 3.30: Spectrum of the 0.2029 V STD white Gaussian noise with different cutoff frequencies.

domain with different cutoff thresholds provide key insights into the dynamic response of the system noise profile and facilitate a deeper understanding of the spectral behavior under various conditions.

Figure 3.31 illustrates the spectral dynamics of the laser system, where the laser linewidth is seen to expand substantially from 219 kHz through 588 kHz to 1025 kHz. This significant growth is directly linked to the increased white Gaussian noise introduced into the PM, highlighting a strong correlation between

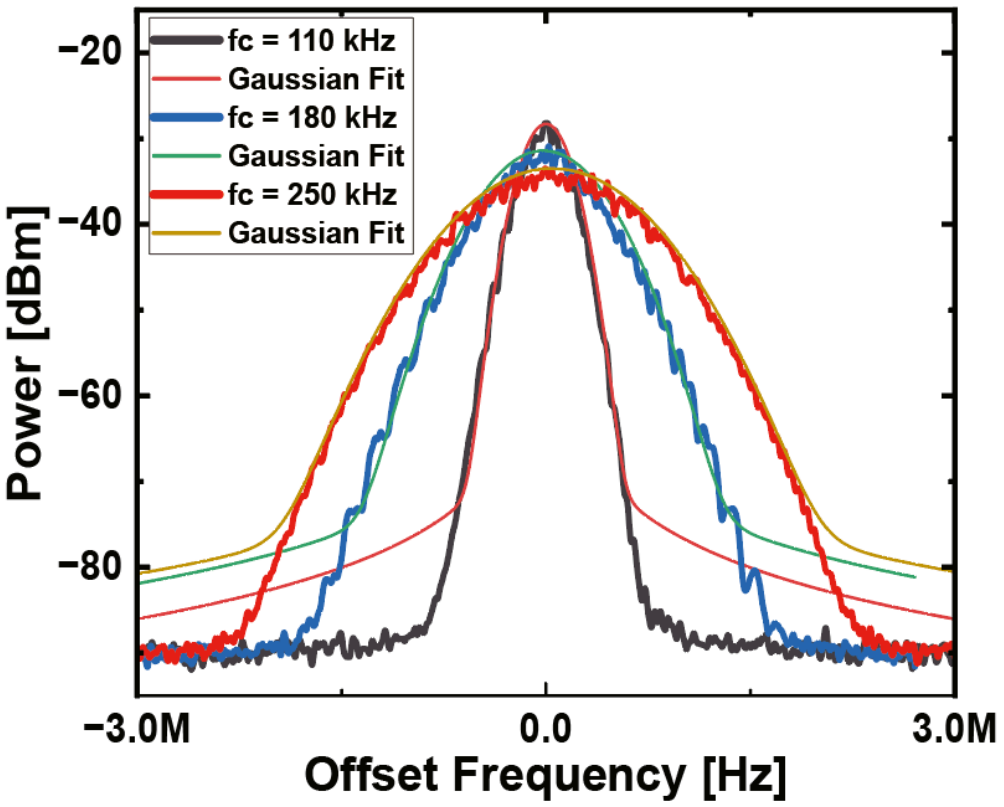

Figure 3.31: The laser spectrum linewidth of the 0.2029 V STD white Gaussian noise with different cutoff frequency.

the amount of noise and the expansion of the laser linewidth. This relationship is fundamental for understanding and controlling the performance characteristics of laser systems in various applications.

Figure 3.32 demonstrates how precise handling of the laser linewidth can be achieved by combining minor adjustments via STD increments and major

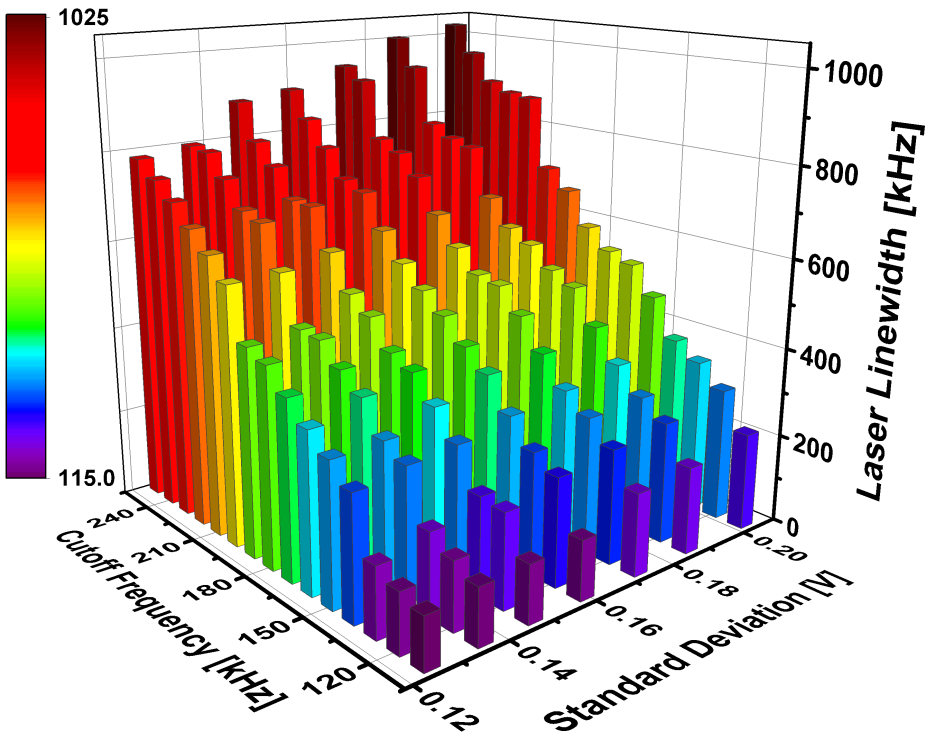

Figure 3.32: Measured linewidth results with different STDs having different cutoff frequencies of the white Gaussian noise.

modulations through cutoff frequency changes. Incremental increases in STD, in the range of 0.0106 V from 0.1248 V to 0.2027 V, lead to modest variations in the linewidth. In contrast, significant spectral range adjustments are realized by altering the cutoff frequency, enabling the laser spectrum linewidth to span from 115 kHz to 1025 kHz. The noise used in this method is only the Gaussian noise, which makes the line shape become the Gaussian line shape. This data suggests the feasibility of creating a cost-effective, highly precise, and adaptable narrow

linewidth laser system using a comprehensive noise control strategy.

The noise generated through this method closely mimics analog noise characteristics, verifying the validity of this approach in simulating a wide array of real-world laser noise profiles with enhanced accuracy. Moreover, the integration of random walk noise within a bounded limit imparts a pseudo-Voigt profile to the laser spectrum linewidth. This profile allows for a detailed breakdown of noise components using Lorentzian component analysis. The random walk noise, which dominates in the spectral wings, is efficiently produced by an FPGA paired with DACs characterized by a flexible sampling rate. This combination of advanced technologies ensures a faithful replication of laser noise spectra, crucial for many applications that demand noise performance standards.

For precise control over the laser line shape, the Pseudovoigt model is skillfully applied. This control is achieved through two distinct methodologies: a dual FPGA setup and a hybrid FPGA with an AWG configuration. The operational frequency limit of 600 MHz for the FPGA sets its boundary for controlling the linewidth lineshape, especially at frequencies above 500 kHz. In situations where higher frequencies are involved, the AWG plays a vital role, serving as a key tool for high-frequency modulation. This dual approach of using FPGA and AWG offers an adaptable solution for managing the laser line shape of the laser linewidth, catering to a wide range of frequencies and ensuring high-precision modulation in optical systems.

Figure 3.33 provides an analytical view of the noise spectrum, highlighting

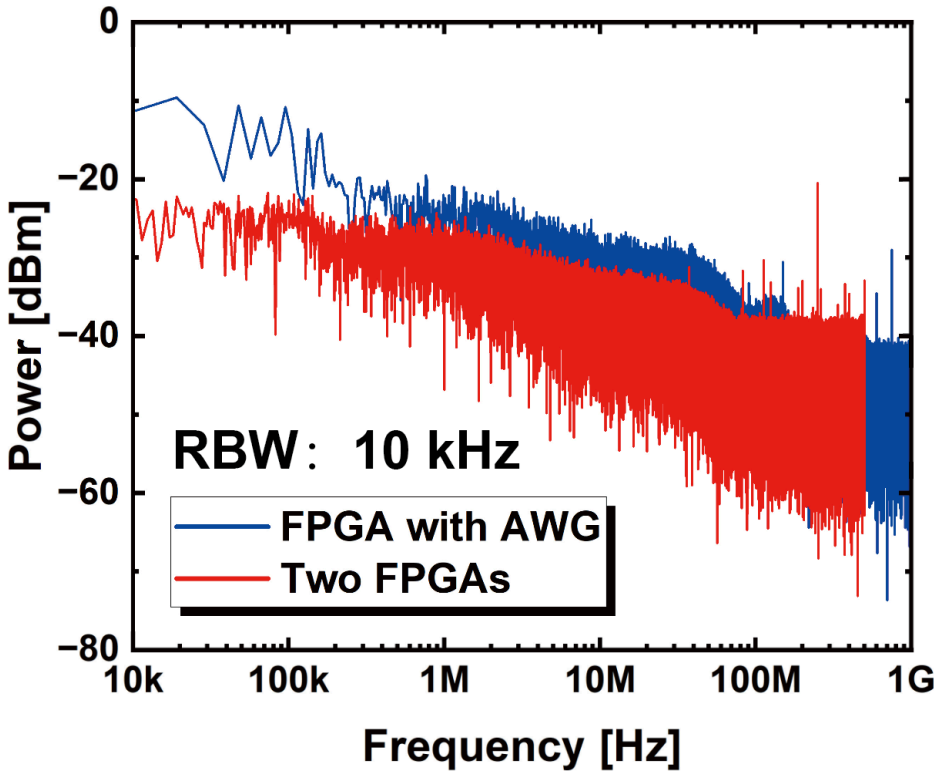

Figure 3.33: The noise spectrum of the two FPGA methods and FPGA with AWG method.

the performance of different methods in managing low-frequency noise domains. The graphical data show that both the dual FPGA and the FPGA-AWG hybrid methods perform effectively in low-frequency noise control. However, a notable distinction is observed in the high-frequency domain. The red line in the figure, representing the dual FPGA method, displays anomalies characterized by red lines, likely due to the FPGA instability at higher frequencies. In contrast, the blue line, indicating the FPGA-AWG hybrid approach, exhibits superior

control over high-frequency noise. This method not only corrects the slope differences seen with the dual FPGA setup but also demonstrates robust high-frequency noise suppression, leading to improved spectral performance. This dual strategy enhances the system flexibility and allows for precise control of the laser linewidth across an extensive frequency range, making it suitable for advanced applications requiring strict noise control.

Figure 3.34 offers a detailed representation of the laser spectrum linewidth. The red line shows the performance of the dual FPGA method, achieving a peak linewidth of 420 kHz, with the Lorentzian component constituting 10% of the spectral composition. This data emphasizes the ability of the method to achieve a moderate level of lineshape precision.

Alternatively, the blue line represents the results from the FPGA-AWG hybrid method. This approach faces the limitations of the FPGA in low-frequency ranges, resulting in a maximum linewidth and lineshape of 1021 kHz and a Lorentzian fraction of 9.3%. The slight difference in the Lorentzian components between the two methods suggests minor differences, likely due to the integration of two different noise profiles. Nonetheless, the combined approach of FPGA and AWG manages to maintain precise control over the Lorentzian components, demonstrating its effectiveness in achieving high accuracy in linewidth control. This level of precision is critical for applications where precise lineshape handling and noise control are important. However, the percentage of the Lorentzian components should be improved to make the line shape like the actual laser line

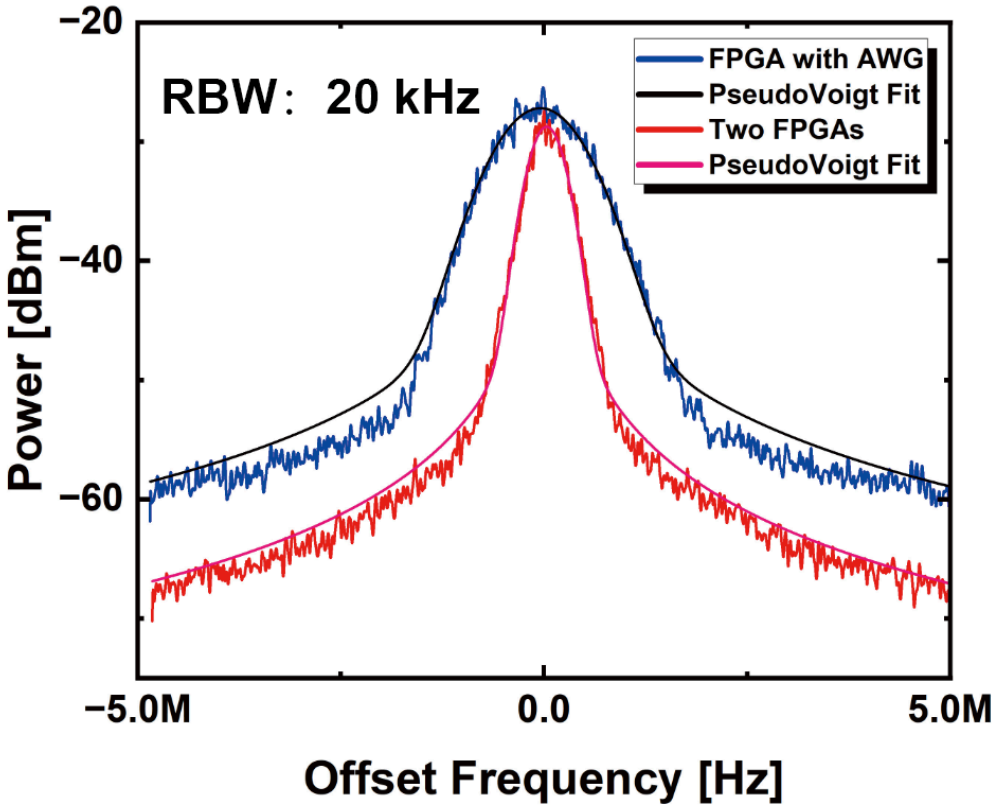

Figure 3.34: The laser spectrum linewidth using the two FPGA method and FPGA with AWG method.

shape; for example, using high precision digital filter to make low-frequency noise have a good performance.

3.5 Summary

This chapter introduces a cutting-edge approach to controlling laser linewidth and lineshape, using FPGAs to generate both low-frequency white Gaussian noise and high-frequency random walk noise. The capability of these FPGAs, reaching up to 600 MHz, allows for precise modulation of the noise spectrum. This method significantly enhances the randomness in the noise generation process, a factor for achieving high-precision laser control.

Incorporating AWG with FPGA-based methods results in a comprehensive system that can accurately control laser linewidth across a broad range, from 115 kHz to 1 MHz. This integrated approach not only ensures fine-tuned adjustments of the laser linewidth but also allows for the considerate modulation of the Lorentzian component of the lineshape within the spectrum. The devotion of this modulation can be achieved by up to 10% Lorentzian components, demonstrating the capability of the system in precision lineshape management.

Looking ahead, plans are in place to deploy these FPGA-controlled lasers with variable linewidth and line shape in optical systems such as coherent FMCW LiDAR. This will involve comparative analyses with systems utilizing analog noise sources and FG. Simultaneously, to make the laser line shape more near the pure Lorentzian line shape also should be improved. Additionally, the implementation of high-frequency sampling rate ADCs is expected to generate lasers with a wide range of variable linewidths and line shapes.

The findings and discussions presented in this chapter, including the

innovative methodologies and their implications for laser technology, have earned recognition with their publication in the letter IEICE Electronics Express, volume advpub, in 2023, entitled ”FPGA-driven random walk noise generation for tunable laser linewidth control” [69] (Section 3.3); and 2023 Opto-Electronics and CommunicationsConference (OECC), entitled ”Effects of the Programmable Real-Time White Gaussian Noise Generated by FPGA on the Laser Linewidth Spectrum” [68] (Section 3.2).

Chapter 4 Exploring the Impact of Laser Linewidth on FMCW LiDAR

4.1 Introduction

The rise of autonomous vehicles has encouraged a need for advanced sensors, especially FMCW LiDAR systems. These systems are crucial for vehicle safety, offering vital velocity and distance measurements. However, they bring complexities like signal aliasing within the FMCW LiDAR framework. Newer LiDAR designs using phase-diversity coherent receivers have been suggested to overcome these issues [53]. This marks a significant advancement in LiDAR technology, enhancing its role in autonomous driving.

However, another problem is that the laser phase noise directly affects LiDAR performance [65], being a key factor in their efficiency. Traditionally, narrow linewidth lasers are used for best results, but they are expensive [53].

Shifting to lasers with precisely controlled linewidth and shape could significantly help understand the effects of phase noise on LiDAR, making it more accessible and practical.

Most research on laser linewidth and signal quality has focused on lasers with fixed linewidths, leaving gaps in the understanding of how linewidth variations impact LiDAR performance. A thorough, quantitative analysis of LiDAR's tolerance to linewidth changes is essential for optimal system design. A variable linewidth laser, using a mirror method, becomes a valuable tool for this purpose [65]. It allows for easy modulation of laser linewidths, for studying LiDAR systems' tolerance to laser phase noise, and for optimizing LiDAR setups for better accuracy and cost-effectiveness in autonomous navigation.

In improving FMCW LiDAR systems, understanding the mathematical relationships between distance and velocity signals and phase noise is vital.

For the distance signal I_D, a key equation representing the system's low-frequency behavior is established. This relationship is expressed as follows [53, 65]:

$$I_D = J_2(\beta)^2 \cos\left(2\pi f_R t + \phi\right) \tag{4.1}$$

The 2nd-order Bessel function is represented by $J_2(\beta)^2$. The frequency shift caused by distance, f_R, is further detailed in Eq. 4.2. The term ϕ relates to the physical distance, corresponding to the fiber length; however its impact on the overall equation is minimal and can be considered negligible.

$$f_R = \frac{8kR}{2}\pi c \tag{4.2}$$

The variable k signifies the rate of exponential change in the frequency of the chirp signal. R stands for the single mode fiber length, which is also the measure of distance. The symbol c denotes the speed of light in a vacuum. Importantly, this formula shows that the distance signal is unaffected by phase noise disruptions, suggesting that variations in laser linewidth do not significantly alter the accuracy of distance measurements.

Conversely, the velocity signal [65] involves:

$$I_V = \frac{1}{2}\sin\left[2\omega_d t + 2\left(\varphi_{PO}(t) - \varphi_{LO}(t)\right)\right] \tag{4.3}$$

The angular frequency of the Doppler frequency shift (DFS) is denoted by ω_d. The terms $\varphi_{PO}(t)$ and $\varphi_{LO}(t)$ represent the phase noise components in the local optical (LO) and the probed optical (PO) paths, respectively. This equation indicates a significant sensitivity of the velocity signal to the laser linewidth, as the linewidth directly affects the phase noise in the system and, consequently, the accuracy of the velocity signal.

These derivations highlight the role of laser linewidth in determining the accuracy and reliability of velocity measurements in FMCW LiDAR systems. They underscore the necessity of precise control over laser linewidth to ensure the integrity of velocity data.

In addition, digital noise, known for its effective low-frequency

performance, has a notable drawback in that it is periodic, which can limit its application in certain scenarios. Conversely, analog noise closely resembles actual noise conditions but presents challenges in terms of control and often lacks significant low-frequency components. Therefore, this research aims to explore and combine these two types of noise, leveraging their respective strengths.

4.2 Experimental setup

4.2.1 Low-frequency compensation using digital noise source

The experimental setup, as shown in Figure 4.1, consists of two main components: the laser linewidth control unit and the FMCW LiDAR unit.

A high-power white Gaussian noise generator (FG, Keysight, 33600A) is used to compensate for the central part of the laser spectrum linewidth. This allows for low-frequency compensation by this method. The noise spectra from both the FG and the AWG are shown in Figure 4.1.

The combined noise spectrum is also illustrated in Figure 4.1.

For the FMCW LiDAR part, light modulation is carefully carried out by the mach-zehnder modulator (MZM, Sumitomo Osaka Cement, T. MZH1.5-10PD-ADC-101) using the linearly frequency modulated (LFM) signal, covering 0.1 to 4.1 GHz, follows the equation $\omega = \omega_0 + 2$kt, with k representing the rate of frequency change. The starting frequency, ω_0, is set at 2 GHz, and k is calculated to be $3.183{\times}10^{11}$ from another AWG (Tektronix AWG7102B). The MZM is set at its null bias for optimal modulation. An Erbium-Doped Fiber Amplifier (EDFA, FITEL, ErFA1215) and an Optical Band-Pass Filter (OBPF, Optoquest, TFA-1550-S/F) are used to maintain the right power levels and reduce amplified spontaneous emission (ASE). The optical signal is split by an optical coupler (OC) into local optical (LO) and probed optical (PO) paths. The LO path

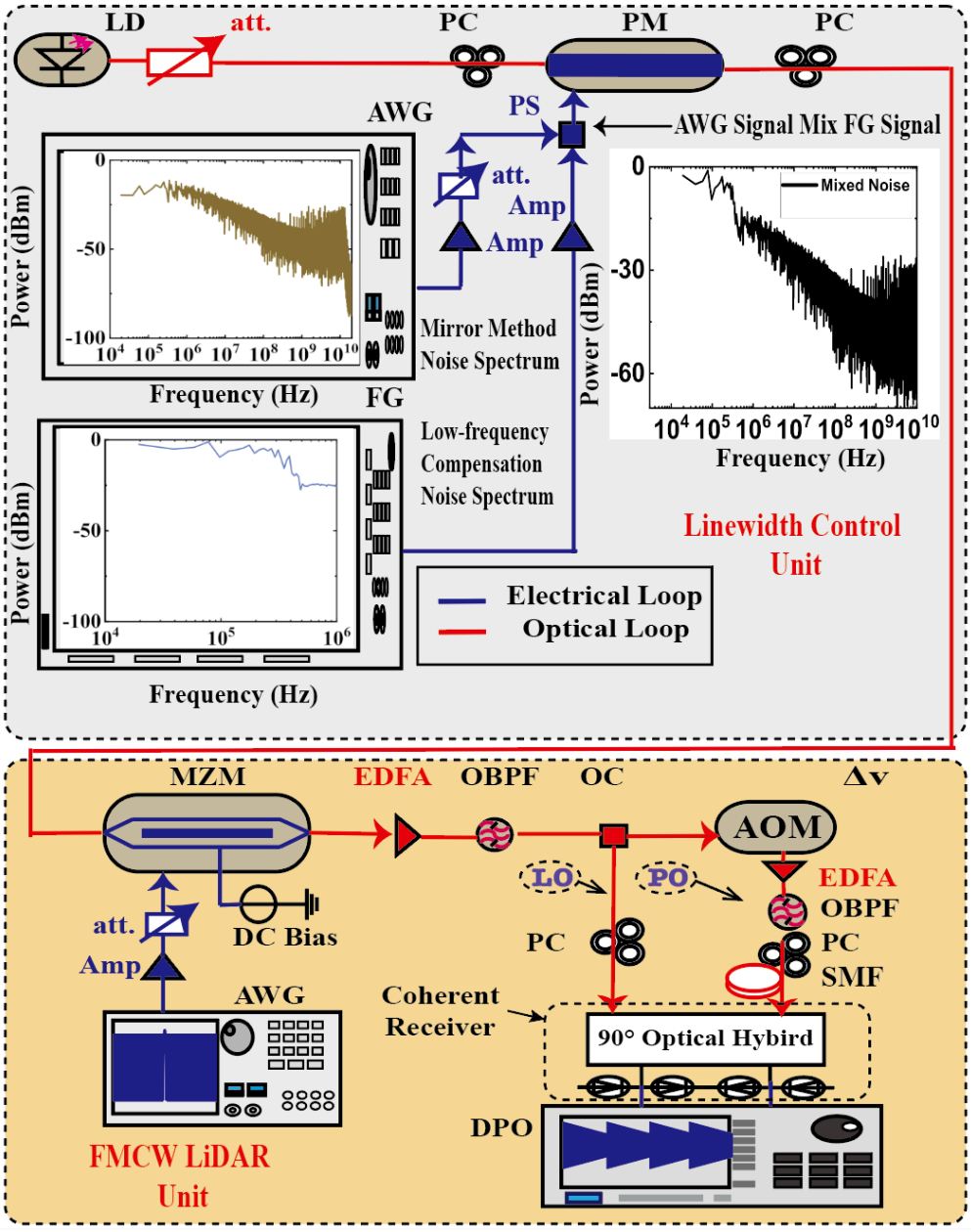

Figure 4.1: The experimental scheme of a phase-diversity coherent FMCW LiDAR using variable laser linewidth.

connects to the coherent receiver (Pure Photonics ECO-031837), while the PO path includes an acousto-optic modulator (AOM, Gooch & Housego T-M110-0.2C2J-3-F2S) to mimic Doppler frequency shifts (DFSs), achieving a shift of 110 MHz that corresponds to a real-world velocity of 85.525 m/s. The PC (Optoquest, PCMA-15-S/F), EDFA (FITEL, ErFA11021B), and OBPF (Optoquest, TFA-1550-S/F) in this path are carefully calibrated for polarization, amplification, and ASE reduction, respectively.

Finally, a single-mode optical fiber (SMF) of 431 meters in length is used to simulate a real spatial distance. The coherent receiver, equipped with a 90-degree hybrid and dual balanced photodetectors (BPDs), is strategically placed to receive signals from both the LO and PO paths. The resulting photocurrents are then analyzed using a digital oscilloscope (DPO Agilent DSO81204B).

4.2.2 Low-frequency compensation using an analog noise source

In the expanded setup shown in Figure 4.2, an FMCW LiDAR system is combined with a linewidth control unit. The analog noise source (Noisecom UFX 7107) plays the role of low-frequency compensation.

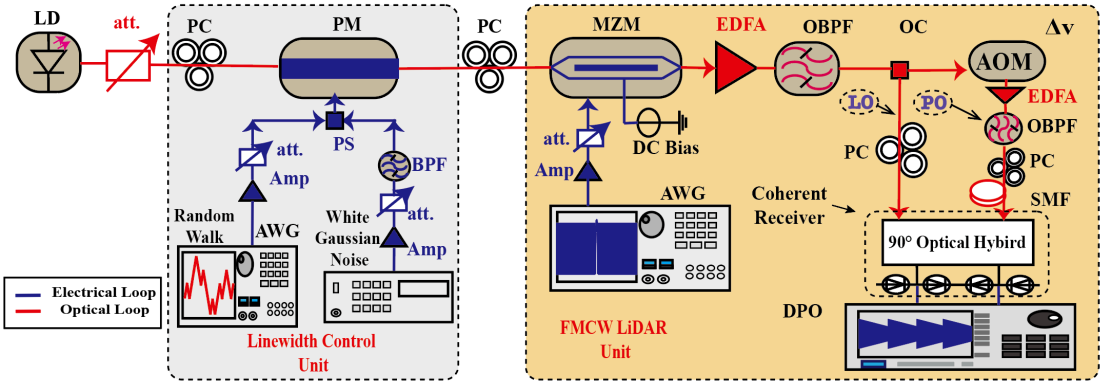

Figure 4.2: Experimental scheme of phase-diversity coherent FMCW LiDAR using variable linewidth and variable line shapes laser.

4.3 Results and discussions

4.3.1 Results of digtial noise

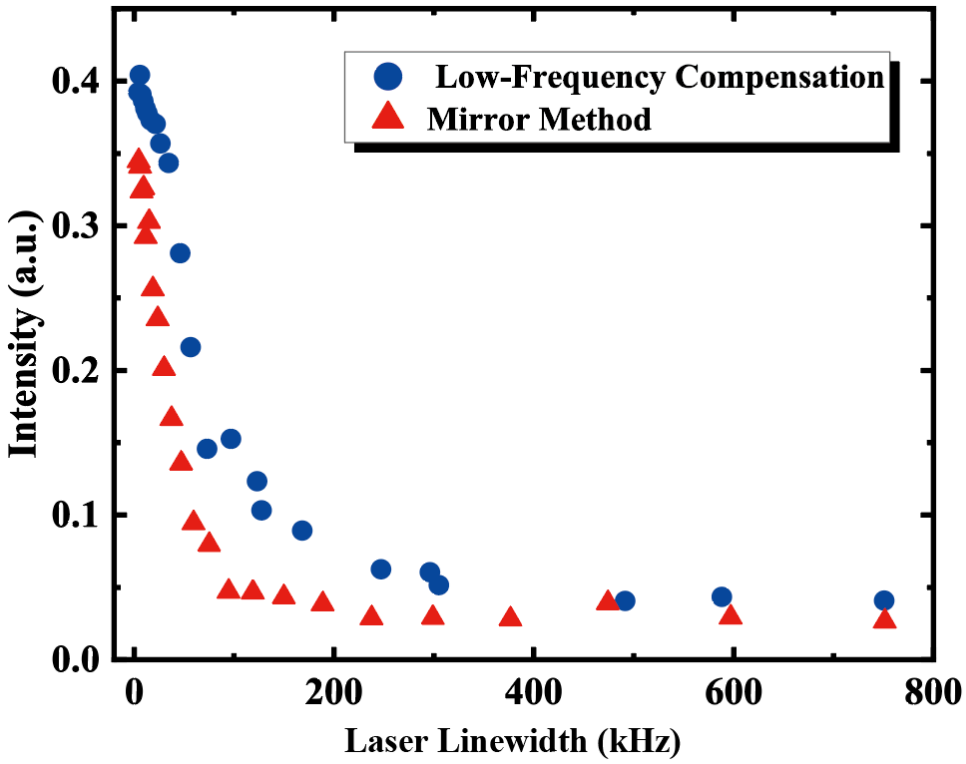

Figure 4.3: The relationship between the laser linewidth and the intensity of the velocity signal.

A significant change was made by adjusting the laser's linewidth from an initial value of 6 kHz to an expanded 752 kHz. This was primarily accomplished by controlling the gain of the amplifier. According to the specifications in equation 4.3, it became clear that increasing the laser linewidth negatively impacted the intensity of the velocity signal. This increase made the signal more

likely to noise interference, leading to a reduction in its strength. However, relying exclusively on this equation was insufficient for a detailed analysis of the effects of phase noise. This realization highlighted the need for empirical investigations to understand the implications of phase noise on the experimental outcomes. Such investigations would provide a deeper insight into how the laser linewidth and other factors influence the performance and accuracy of the system under study.

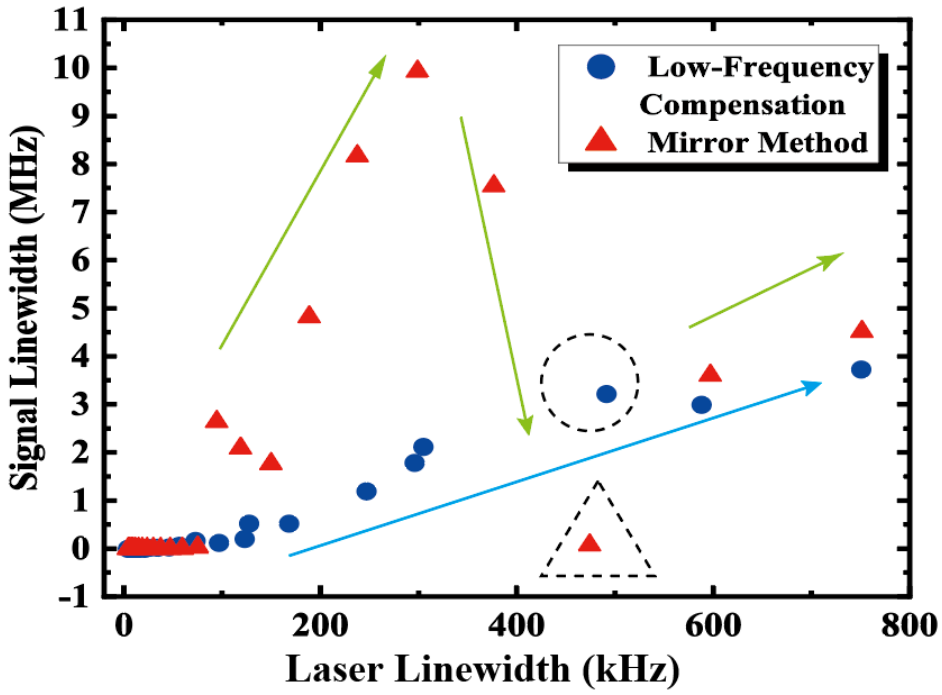

Figure 4.4: The relationship between the laser linewidth and the linewidth of the velocity signal.

This experimental research is divided into two distinct approaches: the mirror technique and the low-frequency compensation method. These methods

were applied to understand the relationship between the laser linewidth and various aspects of the signal. Figure 4.3 illustrates how the intensity of the velocity signal changes with the laser linewidth. Employing the mirror method (triangles) revealed that increasing the laser linewidth from 6 kHz to 752 kHz resulted in a decrease in the velocity signal intensity, dropping from 0.35 to 0.03. Similarly, the low-frequency compensation approach (circles) showed a comparable trend.

In Figure 4.4, the relationship between the signal linewidth and the laser linewidth is explored. Data from the mirror method (triangles) showed that increasing the laser linewidth to 299 kHz caused the velocity signal linewidth to increase to 9.9 MHz. Interestingly, further increasing the laser linewidth to between 299 kHz and 474 kHz resulted in a decrease in the velocity signal linewidth, from 9.9 MHz to 0.07 MHz. However, raising the laser linewidth further to 751 kHz caused the velocity signal linewidth to rise again to 4.5 MHz. Contrastingly, results from the low-frequency compensation method (circles) indicated a linear relationship between the laser linewidth and the velocity signal linewidth.

The mirror method involves a boundary mechanism that limits and reflects any excessive random walk, when dealing with large numbers of walks. In practice, such frequent reflections are unusual. These reflections accidentally suppressed the low-frequency components of the laser, causing fluctuations in the laser linewidth within certain frequency bands. Notably, this effect reduced

beyond the 299 kHz threshold, a phenomenon not observed with the low-frequency compensation method.

Figure 4.5 details the complex relationship between the signal position frequency and the laser linewidth. According to Equation 3.3, the DFS is twice the frequency shifted by the AOM, which is 110 MHz. The mirror method results (triangular markers) showed that the peak frequency deviated from the theoretical value of 220 MHz when the laser linewidth was around 95 kHz. This method's results were closer to theoretical predictions in the range of 150 kHz to 238 kHz. Beyond this range, further deviations occurred, with the vibration range of the velocity signal in the mirror method limited to 1 MHz. In contrast, the low-frequency compensation method (circular markers) started showing frequency vibration when the laser linewidth exceeded 156 kHz. Past this point, the velocity signal consistently deviated from theoretical values, fluctuating with the increasing laser linewidth. This approach exhibited a wider vibration range for the velocity signal, measured at 1.9 MHz.

The experimental data revealed a notable difference between the mirror method and the low-frequency compensation approach, particularly when the laser linewidth was around 470 kHz. It is essential to compare the laser spectrum linewidth with the velocity signal spectrum to understand and validate these observations. This comparison can shed light on the reasons behind the observed differences between the two methods.

In Figure 4.6, the laser spectrum linewidth obtained using the low-frequency

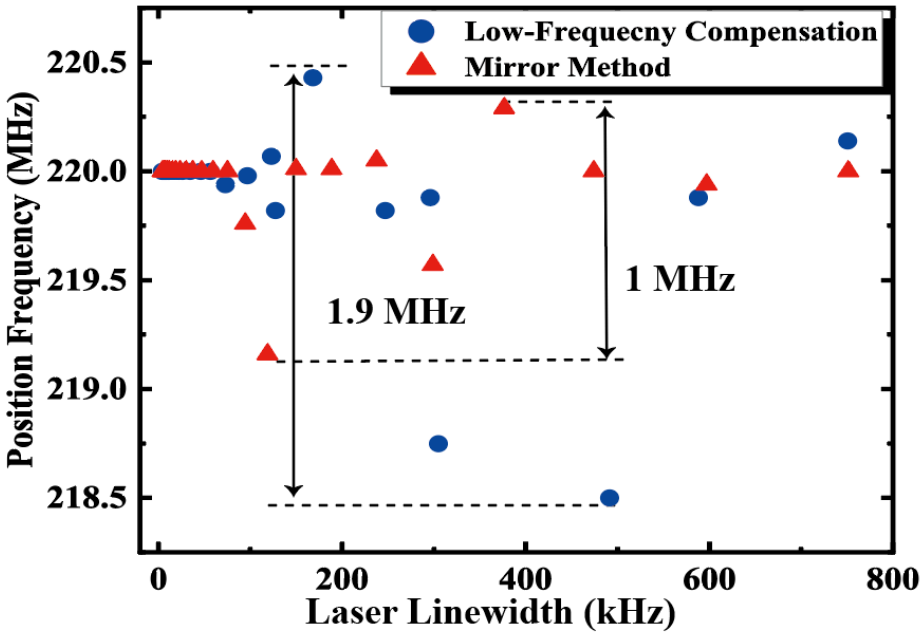

Figure 4.5: The relationship between the laser linewidth and the position of the velocity signal.

compensation method is displayed in detail. A Lorentzian curve fit, shown with a black line, indicates a linewidth of 492.248 kHz. This contrasts with the actual laser spectrum, depicted by the blue line. Notably, the central part of the actual laser spectrum exhibits a degree of modulation.

An interesting observation arises when comparing the actual laser spectrum to the fitted Lorentzian curve. The central part of the actual laser spectrum closely aligns with the fitted curve. This close alignment is significant and suggests that while there is modulation in the actual laser spectrum, its central part largely attaches to the expected Lorentzian profile. This finding is crucial

for understanding the behavior of the laser linewidth under different modulation conditions and how it affects the overall performance of the system, particularly in terms of the velocity signal's linewidth.

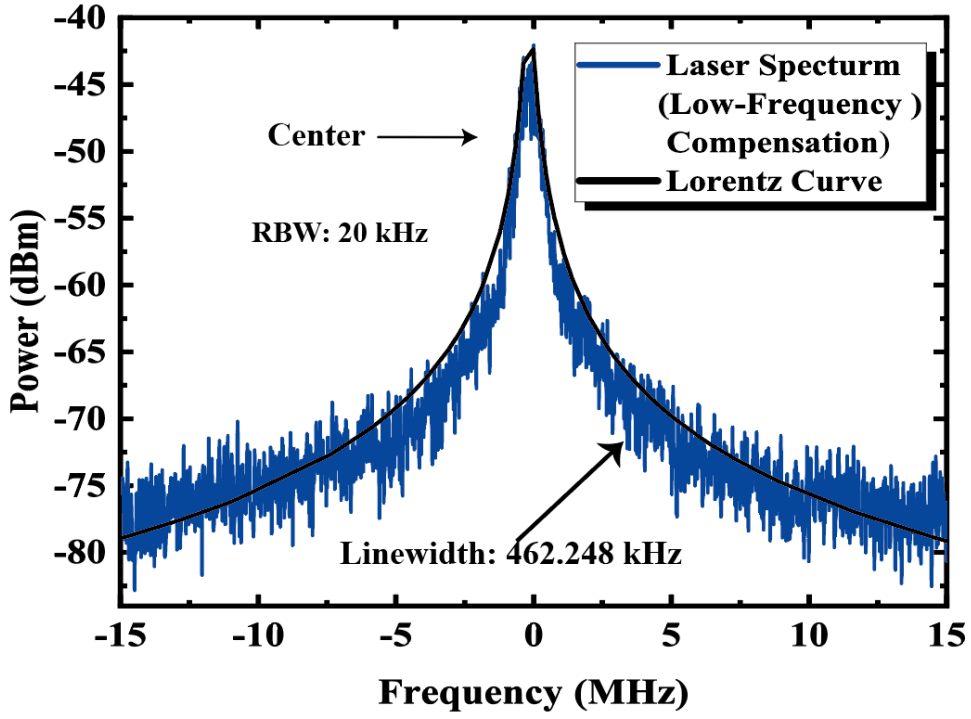

Figure 4.6: The laser spectrum of the low-frequency compensation method.

Figure 4.7 presents a contrasting assumption with the laser spectrum obtained using the mirror method. In this representation, the black line illustrates the fitted Lorentzian curve, which shows a linewidth of 474.219 kHz. The actual laser spectrum, depicted by the red line, reveals an unmodulated central section of the laser linewidth, significantly deviating from the fitted Lorentzian curve. It is because the digital noise has a good performance of the low-frequency

components, and the digital filter in it can help it have a good combination with the random walk to have this line shape. This lack of modulation in the central part of the laser spectrum, as seen in the mirror method, marks a clear departure from the observations made in the low-frequency compensation method. The absence of modulation indicates that the central part of the laser linewidth remains more stable and consistent compared to the low-frequency compensated spectrum. The difference in modulation within the central part of the laser spectrum between the two methods can be attributed to the effect of low-frequency compensation. The low-frequency compensation method involves adding white noise, which affects the laser spectrum, particularly in its central part. This addition of white noise is responsible for the modulation observed in the central section of the laser spectrum in the low-frequency compensation method. In contrast, the mirror method, which lacks this compensation, shows a more consistent and unmodulated laser linewidth, as evidenced by the closer alignment of the actual laser spectrum to the fitted Lorentzian curve. These observations emphasize the impact of different noise compensation techniques on the laser spectrum linewidth. Understanding these effects is crucial for optimizing laser performance in various applications, especially those requiring precise control over the linewidth, such as in optical communication systems.

The analysis of the velocity signal spectrum associated with the low-frequency compensation method, as shown in Figure 4.8, reveals significant findings. Specifically, it is observed that the central frequency region, which is

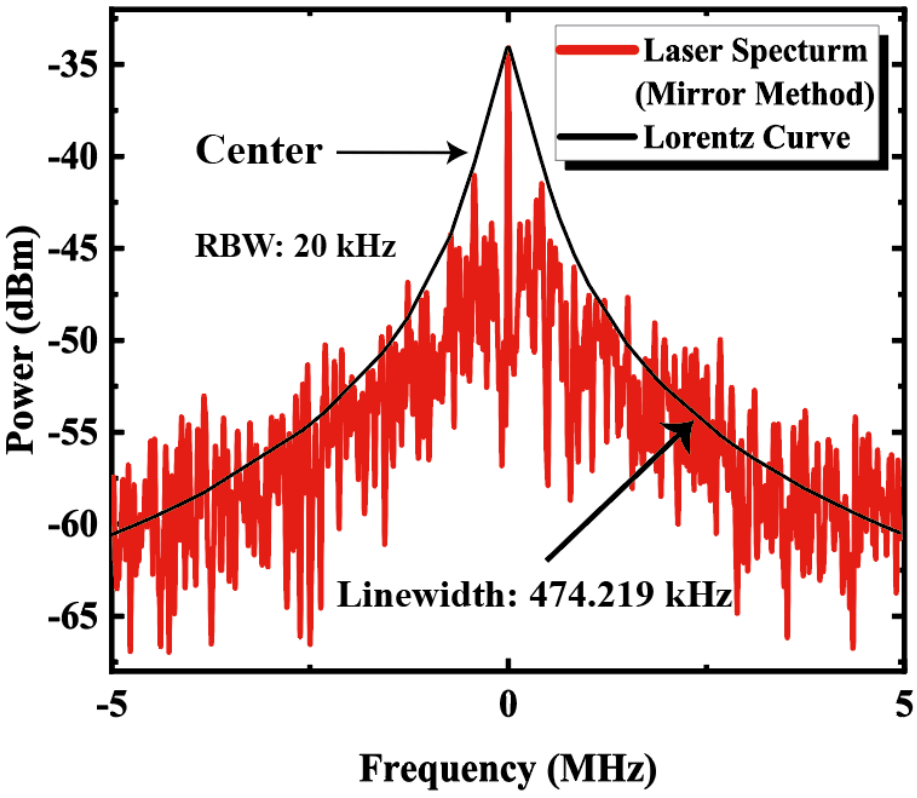

Figure 4.7: The laser spectrum of the mirror method.

around 220 MHz, exhibits noticeable modulation. This modulation in the velocity signal spectrum is a key aspect of the experiment's outcomes. The modulation of the central frequency region can be understood by combining insights from Equation 2.13 and applying Fourier transformation techniques. These analytical methods help to separate the complex connections within the signal spectrum. The key consequence of this modulation, as indicated by the analysis, is the absence of a distinct peak in the central part of the velocity signal spectrum. This lack of a distinct central peak is attributed to the spectral modulation of the

laser linewidth. In other words, the variations and fluctuations within the laser spectrum linewidth, particularly when low-frequency compensation is employed, lead to a modulation in the velocity signal spectrum. This modulation effectively masks or blurs the central peak that would otherwise be expected in the velocity signal.

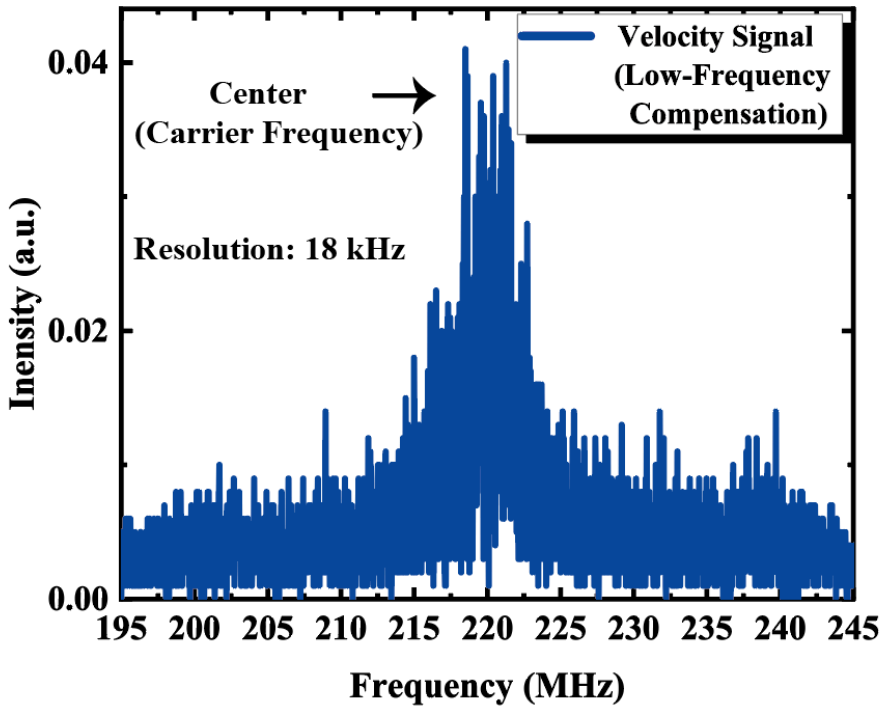

Figure 4.8: The velocity signal spectrum of the low-frequency compensation method.

In contrast to the low-frequency compensation method, the velocity signal spectrum obtained using the mirror method, as indicated by the red line in Figure 4.9, offers a different viewpoint. Here, a clear peak is observable at 220

MHz within the central frequency region. This is a remarkable aspect of the mirror method's results. The being of a distinct peak in the central frequency domain signifies that the core part of the velocity signal spectrum remains largely unaffected by noise. Interestingly, the impact of noise is primarily confined to the marginal regions of the spectrum, leaving the central part intact and well-defined. This phenomenon can be attributed to the lack of low-frequency components in the phase noise of the laser when using the mirror method. The absence of these low-frequency components in the laser's phase noise directly influences the composition of the velocity signal spectrum. Specifically, it leads to a shortage of low-frequency elements in the central part of the velocity signal. This effect, in turn, results in the observed narrowing of the velocity signal's linewidth at certain frequencies. Another is when the effects of the mirror method overlay the phase noise, it will make the laser linewidth bigger than the actual one, which will not provide a valuable reference. The implications of this observation are significant. It highlights how the characteristics of the laser's phase noise, particularly its low-frequency components, play a role in shaping the velocity signal's spectrum. In systems where a clear and unmodulated central peak is essential, such as in certain precision measurement applications, the mirror method's ability to preserve the central peak with minimal low-frequency interference becomes highly advantageous. Understanding and operating these spectral characteristics is key to optimizing the performance of optical systems, especially those relying on precise signal analysis and interpretation.

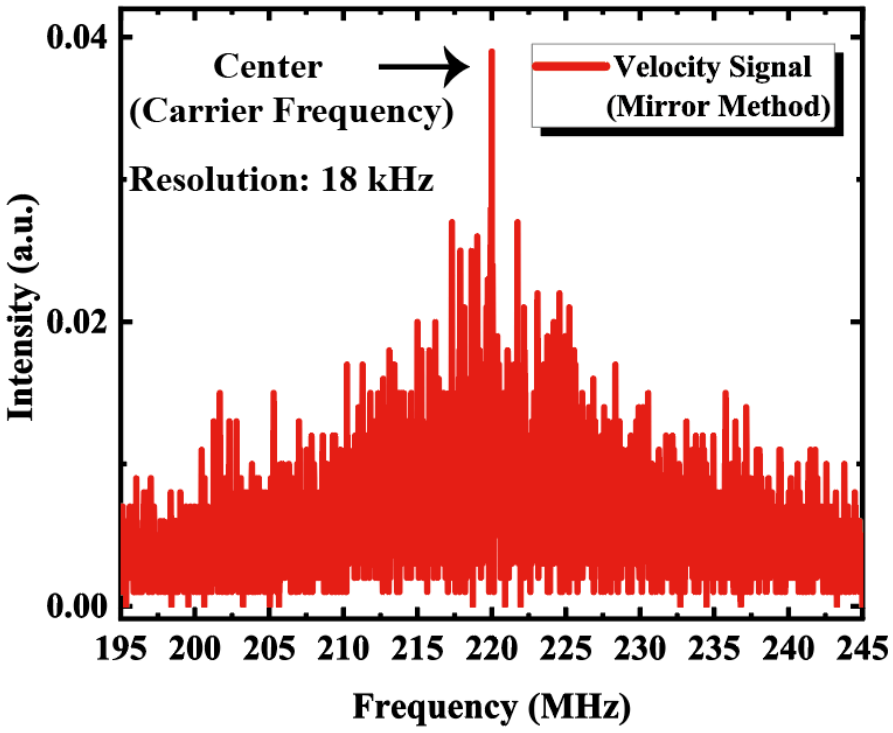

Figure 4.9: The velocity signal spectrum of the mirror method.

4.3.2 Results of analog noise

The study focused on the modulation of laser linewidths, a critical area in the optical field due to its significant impact on various applications. The investigation explored linewidth modulation within the range of 400 kHz to 1 MHz, employing two different noise configurations: independent white Gaussian noise and a combination of white Gaussian noise with random walk noise.

Figure 4.10 illustrates the outcomes of this modulation process. It provides a detailed view of the different Lorentzian components resulting from these two noise types. To analyze these variations, the PseudoVoigt model, known for its accuracy, was used over a spectrum of 10 MHz with a carefully selected 20 kHz resolution bandwidth (RBW). One key finding from the initial observations was that when the modulation was limited to only white Gaussian noise, the resulting Lorentzian components were relatively weak, with a contribution of about 1.4%. This presents a challenge for those seeking to enhance these Lorentzian components in their applications. To achieve this, precise calibration of the cutoff frequency and power of the white Gaussian noise is necessary. Additionally, this calibration must be seamlessly integrated with the random walk noise for optimal results.

However, the study faced inherent limitations. One major limitation was the precision of the filters and the limitations of the electrical attenuators used. These factors set a definitive upper limit on the attainable Lorentzian components, which could not overtake 25%. This limitation illustrates the challenges

and boundaries within which researchers must operate when modulating laser linewidths, especially when aiming to maximize the contribution of Lorentzian components for specific optical applications.

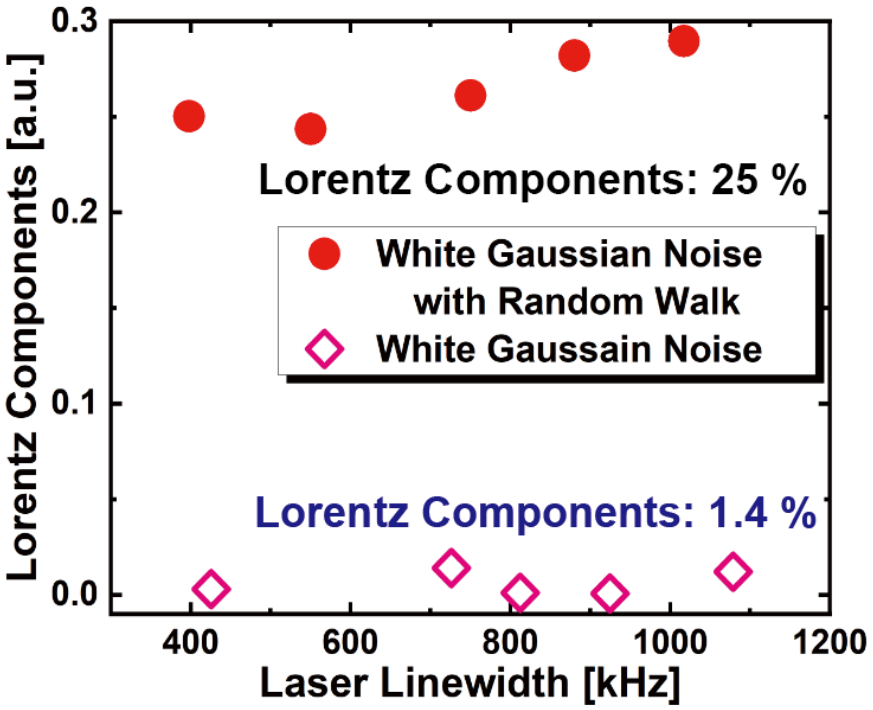

Figure 4.10: Relationship between laser linewidth and laser line shape.

The study then focused on its primary objective: understanding the impact of these modulations on the velocity signal. The velocity signal in this context is defined as the Doppler-shifted target signal, especially after undergoing fast Fourier transform (FFT) processing on the current output from the coherent receiver. Figure 4.11 is a reference for this aspect of the study. It graphically illustrates how the intensity of the velocity signal changes as the laser linewidth

is modulated. A clear pattern is observed, consistent across linewidths with 25% and 1.4% Lorentz components. However, while the trend is the same, the degree of intensity reduction varies between the different linewidth changes. Each change exhibits a reduction of signal intensity. The velocity signal intensity of Gaussian shape is higher than the Lorentz one is because the inherent power fluctuations of the detected electrical signals. These fluctuations play a significant role in determining the intensity of the velocity signal. Understanding how laser linewidth modulation affects the velocity signal is crucial for applications where Doppler-shifted signals are used, such as in radar and LiDAR systems. The findings from this investigation provide valuable insights into optimizing these systems for better performance and accuracy.

A significant aspect of the study also focused on the behavior of the DFSs. For clarity, DFSs can be defined as the central spectral domain of the velocity signal, specifically centered around 220 MHz. Figure 4.12 plays a role in this part of the study. This figure is used to understand how changes in the laser linewidth affect the central frequency domain of the velocity signal. DFSs are a key component in accurately determining the velocity of a target in Doppler-based systems, such as in radar and LiDAR.

For a comprehensive analysis, the study further explored detailed spectral examination, as shown in Figures 4.13 and 4.14.

These figures reveal two different velocity signal spectra of the center part. The first, which came from pure white Gaussian noise, displays a clear

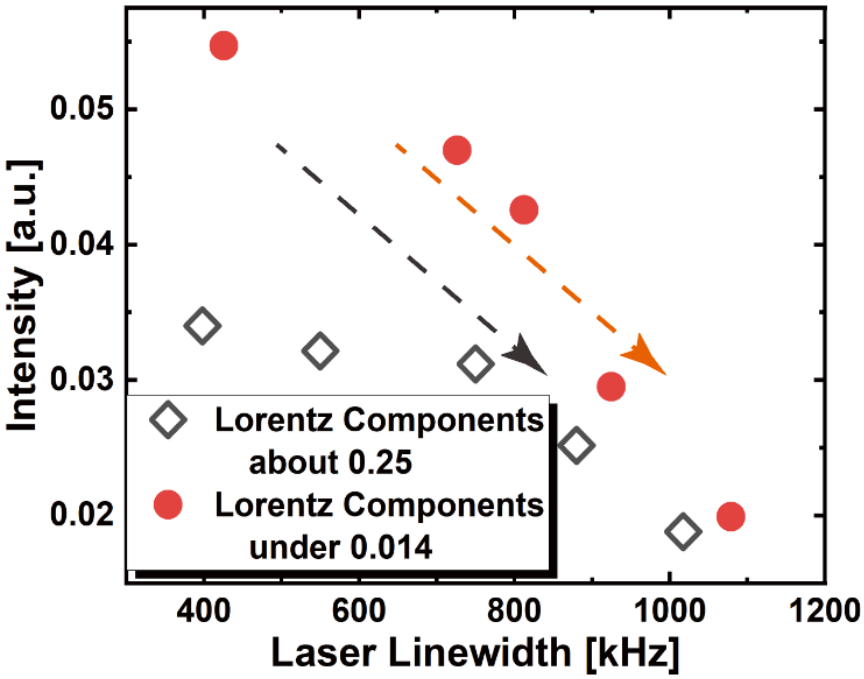

Figure 4.11: Relationship between laser linewidth, laser line shape, and velocity signal intensity.

Gaussian-shaped velocity signal. On the other hand, the spectrum produced by the mixed noise contains a more complex pattern, combining elements of both Lorentzian and Gaussian shapes. With increasing noise levels, the DFSs exhibit greater fluctuations. An important finding is noted: Gaussian spectra, typically recognized by their flat-center appearance, are more affected by these fluctuations. In conclusion, Figure 4.15 illustrates a critical point: a linewidth rich in Lorentzian components is more resistant to DFS variations, significantly exceeding the performance of a spectrum dominated by Gaussian features.

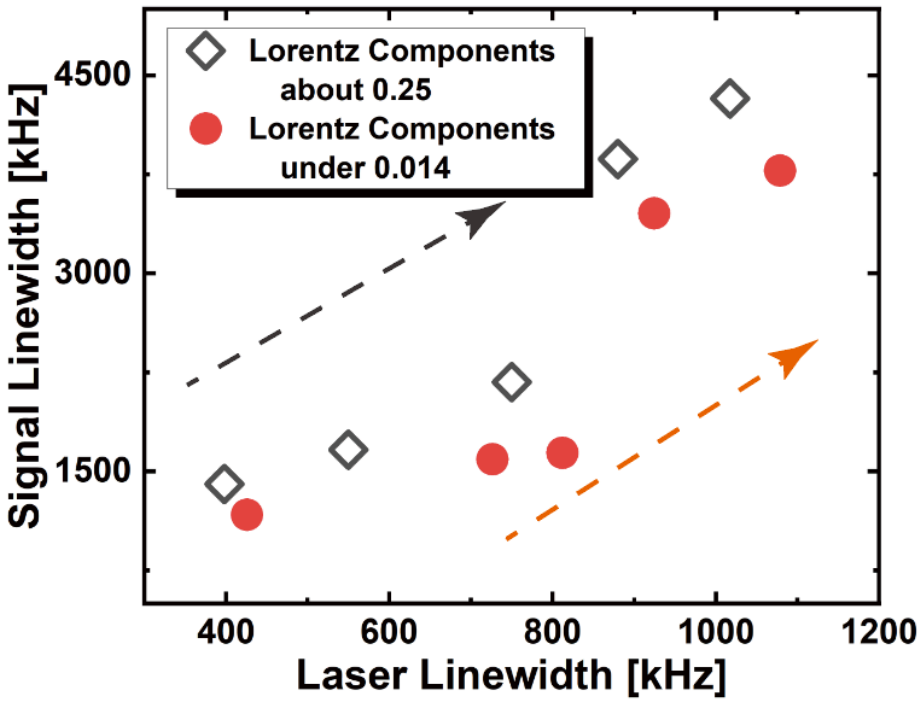

Figure 4.12: Relationship between laser linewidth, laser line shape, and velocity signal linewidth.

The Lorentz line shape has less vibration of the Doppler frequency position when the distance is 431 m than the Gaussian line shape, it will have less error and is preferred in the LiDAR application. The phase modulator input power limits have set a maximum of 28% for the Lorentzian component within the laser line shape. Looking forward, the creation of a laser with a purely Lorentzian linewidth is expected. Nevertheless, this progression must account for the varied needs of different optical systems. For example, in coherent communication systems, when the carrier frequency of the laser linewidth is not modulated it does not

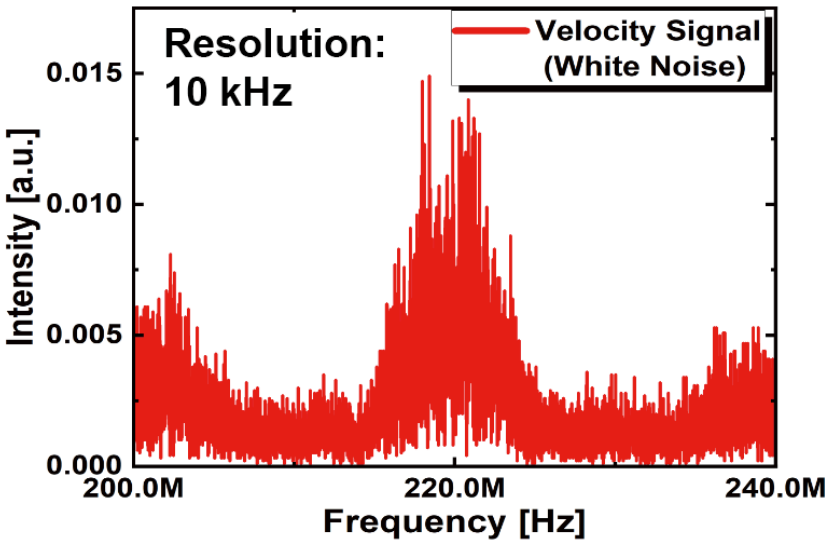

Figure 4.13: Velocity signal spectrum of white Gaussian noise.

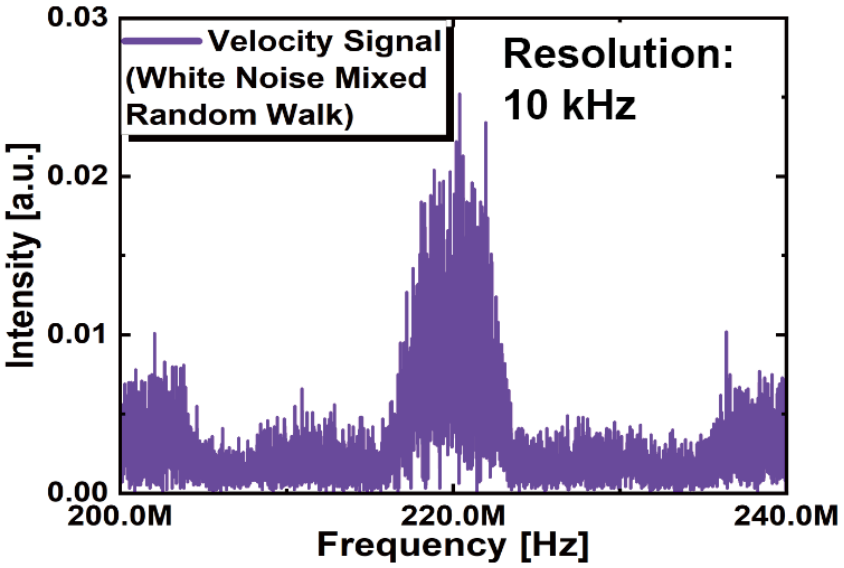

Figure 4.14: Velocity signal spectrum of white Gaussian noise mixed random walk noise.

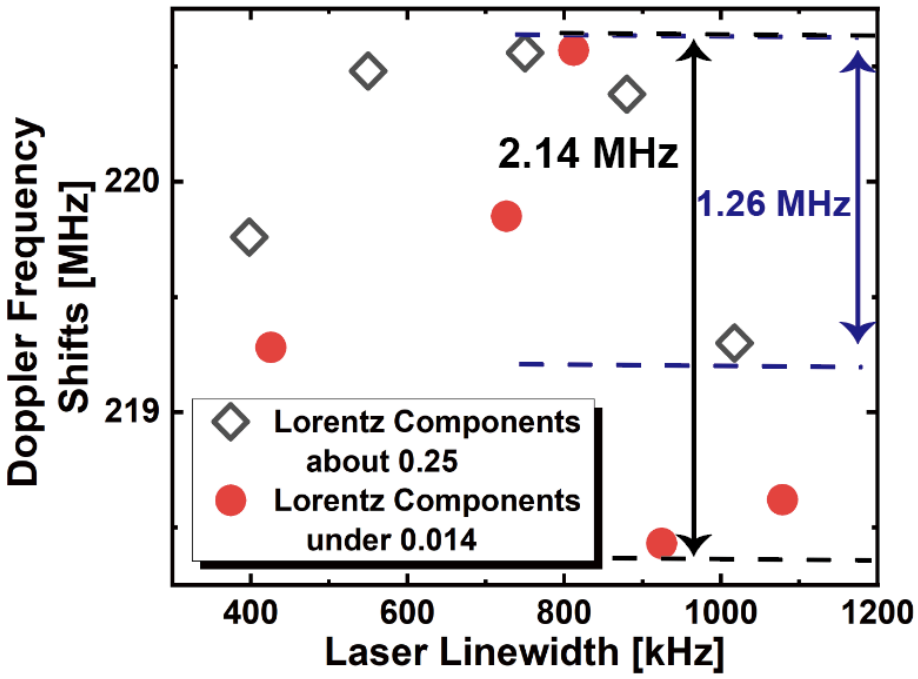

Figure 4.15: Relationship between laser linewidth, laser line shape, and velocity signal DFSs.

greatly affect the system performance. In contrast, whether the carrier frequency of the laser is modulated or not is essential for the accurate measurement of velocity and distance, which are vital for the effectiveness of system. This contrast highlights the need for customized laser linewidth designs that meet the specific requirements of the application.

4.4 Summary

This chapter investigates how varying linewidths and shapes of lasers affect FMCW LiDAR systems that use coherent receivers. The focus was on understanding how changes in laser linewidth influence the characteristics of the velocity signal. It was found that an increase in the linewidth leads to a reduction in signal intensity and a broadening of the signal's own linewidth. Moreover, it was observed that carrier frequency fluctuations become more noticeable as the laser linewidth widens.

Another key discovery from the investigation is how differently the velocity signal reacts to the laser line shape. Lasers with a Gaussian linew shape showed more significant carrier frequency fluctuations compared to those with a Lorentzian line shape, highlighting the importance of line shape on the performance of laser systems.

The digital noise has good performance on the low-frequency part and also has the digital filter to fit the random walk noise to achieve the good performance of the line shape, but its lack in the randomness makes it far from the actual laser noise. The analog noise has the randomness, but the low-frequency part is not so prefect and not easy to control the cutoff frequency and other parameters. Therefore, a new method should be proposed to combine both the advantages of them.

The detailed analysis and discussions presented in this chapter are recognized by their publication in the journal Optics Continuum,volume 2, in

2023, entitled ”Effects of a variable linewidth laser and variable line shape laser on coherent FMCW LiDAR” [61] (Section 4.2.2 and 4.3.2); and the 2022 Asia Communications and Photonics Conference (ACP), entitled ”Phase Noise Sensitivity of Coherent FMCW LiDAR Measured by Variable linewidth Laser with Low-Frequency Compensation and Mirror Method” [65] (Section 4.2.1 and 4.3.1)

Chapter 5 Conclusion

This dissertation examines the complex aspects of laser technology, focusing on the development and management of lasers with variable linewidth and lineshape, vital for improving coherent FMCW LiDAR.

A key aspect of this work is the application of an external LN phase modulator combined with an advanced electrical control system, proven to dynamically adjust laser linewidth from 400 kHz to 1 MHz. The adoption of the Pseudo-Voigt model as an analytic method has been effective for lineshape characterization, capable of achieving up to 29% Lorentzian components. These results have been supported by detailed simulations and real-world experiments, confirming the effectiveness of the proposed approach.

The study extended to evaluating the impact of the innovative laser system on FMCW LiDAR systems with coherent detectors. It was found that while the distance signal was unaffected by changes in laser linewidth, the velocity signal was highly sensitive due to the laser linewidth. A broader linewidth resulted in diminished quality of the velocity signal, with Gaussian shapes showing greater frequency disturbances than Lorentzian shapes.

In the search for economical and compact laser systems, the use of FPGAs has proved to be effective in generating both white Gaussian and random walk noise signals. This enhancement in the variable linewidth and lineshape laser highlights the system flexibility, enables the more actual like laser noise, and supports precise linewidth control.

The findings of this dissertation showcase the viability of a new method for producing lasers with adjustable linewidth. This approach is notable for its accuracy, cost-efficiency, and versatility in lineshape variation. It also has practical implications, shedding light on the connection between laser linewidth and its applications, potentially leading to cost savings in laser-equipped systems. The research offers a solid foundation for further advancements in variable linewidth laser technologies and is set to be an essential resource in tackling challenges associated with laser linewidth across different industrial and technological fields.

The conclusions of this dissertation highlight the practicality of a novel technique for making lasers with tunable linewidth. This method is distinguished by its precision, affordability, and the ability to vary lineshape. It has visible benefits, particularly for FMCW LiDAR systems with coherent receivers, as it provides a straightforward means to examine optical phase noise. Looking ahead, this approach holds promise for broader applications in other optical systems, potentially deepening the understanding of optical phase noise and its effects.

In the future, the aim is to identify an alternative low-frequency noise source

to compensate for the limitations of random walk noise with defined boundaries or using the new modulation method. For example, using the low-frequency phase modulator to achieve high power limitation, or using the IQ modulator to make the unlimited phase shifts. This effort is directed towards achieving pure Lorentzian components, which will enhance the understanding of pure Lorentzian line shapes in optical coherent systems. Additionally, FPGA-based lasers with variable linewidth will be applied in systems such as FMCW LiDAR, among others. Concurrently, the introduction of high sampling rate DACs is planned to enable the generation of a broader linewidth in lasers, utilizing FPGA technology.

REFERENCES

[1] Klaus Petermann. *Laser Diode Modulation and Noise*. en. Springer Science & Business Media, Apr. 1991. ISBN: 978-0-7923-1204-8.

[2] Hans Zappe. *Laser Diode Microsystems*. en. Springer Science & Business Media, 2004. ISBN: 978-3-540-40454-5.

[3] Colin McKinstrie, Trevor Stirling, and Amr S Helmy. "Laser linewidths: tutorial". In: *Journal of the Optical Society of America B* 38 (Dec. 2021), p. 3837.

[4] Mingyuan Xue and Juanning Zhao. "Laser linewidth measurement based on long and short delay fiber combination". In: *Optics Express* 29 (Aug. 2021), pp. 27118–27126. DOI: 10.1364/OE.428787.

[5] Zhenxu Bai et al. "A comprehensive review on the development and applications of narrow-linewidth lasers". In: *Microwave and Optical Technology Letters* 64 (2022), pp. 2244–2255. DOI: 10.1002/mop.33046.

[6] Xingkai Lang et al. “Advances in narrow linewidth diode lasers”. In: *Science China Information Sciences* 62 (May 2019), p. 61401. DOI: 10.1007/s11432-019-9870-0.

[7] Shihong Huang et al. “Precise measurement of ultra-narrow laser linewidths using the strong coherent envelope”. In: *Scientific Reports* 7 (Feb. 2017), p. 41988. DOI: 10.1038/srep41988.

[8] Bérengère Argence et al. “Quantum cascade laser frequency stabilization at the sub-Hz level”. In: *Nature Photonics* 9 (July 2015), pp. 456–460. DOI: 10.1038/nphoton.2015.93.

[9] Andrew D Ludlow et al. “Systematic study of the ^{87}Sr clock transition in an optical lattice”. In: *Physical Review Letters* 96 (Jan. 2006), p. 033003. DOI: 10.1103/PhysRevLett.96.033003.

[10] Henry Timmers et al. “Lasers for Deployed Optical Atomic Clocks”. In: *Quantum 2.0 Conference and Exhibition (2022), paper QTh3B.6*. Optica Publishing Group, June 2022, QTh3B.6. DOI: 10.1364/QUANTUM.2022.QTh3B.6.

[11] William Loh et al. “Operation of an optical atomic clock with a Brillouin laser subsystem”. In: *Nature* 588 (Dec. 2020), pp. 244–249. DOI: 10.1038/s41586-020-2981-6.

[12] Yufang Lei et al. “Si Photonics FMCW LiDAR Chip with Solid-State Beam Steering by Interleaved Coaxial Optical Phased Array”. In: *Micromachines* 14 (May 2023), p. 1001. DOI: 10.3390/mi14051001.

[13] Cenqin Jin et al. “Nonlinear Coherent Optical Systems in the Presence of Equalization Enhanced Phase Noise”. In: *Journal of Lightwave Technology* 39 (July 2021), pp. 4646–4653. DOI: 10.1109/JLT.2021.3076067.

[14] Ying Wu et al. “Narrow Linewidth External Cavity Laser Capable of High Repetition Frequency Tuning for FMCW LiDAR”. In: *IEEE Photonics Technology Letters* 34 (Nov. 2022), pp. 1123–1126. DOI: 10.1109/LPT.2022.3203063.

[15] Zhewei Zhang and Amnon Yariv. “A General Relation Between Frequency Noise and Lineshape of Laser Light”. In: *IEEE Journal of Quantum Electronics* 56.3 (2020), pp. 1–5. DOI: 10.1109/JQE.2020.2980011.

[16] Chen-Ting Liao et al. “Attosecond transient absorption in dense gases: Exploring the interplay between resonant pulse propagation and laser-induced line-shape control”. In: *Physical Review A* 93 (Mar. 2016), p. 033405. DOI: 10.1103/PhysRevA.93.033405.

[17] Christian Parigger, David Surmick, and Ghaneshwar Gautam. “Self-absorption characteristics of measured laser-induced plasma line shapes”. In: *Journal of Physics: Conference Series* 810 (Feb. 2017), p. 012012. DOI: 10.1088/1742-6596/810/1/012012.

[18] Beiersdorfer Peter et al. “Lineshape measurements of He-β spectra on the ORION laser facility”. In: *Physics of Plasmas* 23 (Oct. 2016), p. 101211. DOI: 10.1063/1.4965233.

[19] Shihong Huang et al. “Laser Linewidth Measurement Based on Amplitude Difference Comparison of Coherent Envelope”. In: *IEEE Photonics Technology Letters* 28.7 (2016), pp. 759–762. DOI: 10.1109/LPT.2015.2513098.

[20] Xian Zhou et al. “Theoretical Analysis of Phase Noise Induced by Laser Linewidth and Mismatch Length in Self-Homodyne Coherent Systems”. In: *J. Lightwave Technol.* 39 (Mar. 2021), pp. 1312–1321.

[21] Valeriy Yudin et al. “Frequency shift caused by the line-shape asymmetry of the resonance of coherent population trapping”. In: *Physical Review A* 108 (July 2023). Publisher: American Physical Society, p. 013103. DOI: 10.1103/PhysRevA.108.013103.

[22] Gianni Di Domenico, Stéphane Schilt, and Pierre Thomann. “Simple approach to the relation between laser frequency noise and laser line shape”. In: *Applied Optics* 49 (Sept. 2010), pp. 4801–4807. DOI: 10.1364/AO.49.004801.

[23] Yongkang Gao et al. “High-Power, Narrow-Linewidth, Miniaturized Silicon Photonic Tunable Laser With Accurate Frequency Control”. In: *Journal of Lightwave Technology* 38 (Jan. 2020), pp. 265–271.

[24] Nikola Bucalovic et al. “Experimental validation of a simple approximation to determine the linewidth of a laser from its frequency noise spectrum”. In: *Applied Optics* 51 (July 2012), pp. 4582–4588. DOI: 10.1364/AO.51.004582.

[25] Steffan Gwyn et al. “Dynamic Device Characteristics and Linewidth Measurement of InGaN/GaN Laser Diodes”. In: *IEEE Photonics Journal* 13 (Feb. 2021), pp. 1–10. DOI: 10.1109/JPHOT.2020.3045218.

[26] Hans Wenzel et al. “Semiconductor Laser Linewidth Theory Revisited”. In: *Applied Sciences* 11 (2021). DOI: 10.3390/app11136004.

[27] Zhou Meng, George Stewart, and Gillian Whitenett. “Stable Single-Mode Operation of a Narrow-Linewidth, Linearly Polarized, Erbium-Fiber Ring Laser Using a Saturable Absorber”. In: *J. Lightwave Technol.* 24 (May 2006), p. 2179.

[28] Benjamin Rein and Thomas Walther. “Frequency stabilized diode laser with variable linewidth at a wavelength of 404.7 nm”. In: *Opt. Lett.* 42 (Apr. 2017), pp. 1508–1511. DOI: 10.1364/OL.42.001508.

[29] Koji Igarashi et al. “Measurement of Laser Phase Noise for Ultra-Long Period of 0.8 Seconds With 800-ps Temporal Resolution Using Optical Coherent Detection With FPGA-Implemented Data Acquisition”. In: *Journal of Lightwave Technology* 39.20 (2021), pp. 6539–6546. DOI: 10.1109/JLT.2021.3101546.

[30] Nicolas Von Bandel et al. “Time-dependent laser linewidth: beat-note digital acquisition and numerical analysis”. In: *Opt. Express* 24 (Nov. 2016), pp. 27961–27978. DOI: 10.1364/OE.24.027961.

[31] Sarat Gundavarapu et al. “Sub-hertz fundamental linewidth photonic integrated Brillouin laser”. In: *Nature Photonics* 13 (Jan. 2019), pp. 60–67. DOI: 10.1038/s41566-018-0313-2.

[32] R Sri Durga et al. “Design and Synthesis of LFSR based Random Number Generator”. In: *2020 Third International Conference on Smart Systems and Inventive Technology (ICSSIT)*. Aug. 2020, pp. 438–442. DOI: 10.1109/ICSSIT48917.2020.9214240.

[33] Analog Devices. *AD9695 Datasheet*. https://www.analog.com/media/en/technical-documentation/data-sheets/ad9695.pdf. 2023.

[34] Pravin Zode, Pradnya Zode, and Raghavendra Deshmukh. “FPGA Based Novel True Random Number Generator using LFSR with Dynamic Seed”. In: *2019 IEEE 16th India Council International Conference (INDICON)*. Dec. 2019, pp. 1–3. DOI: 10.1109/INDICON47234.2019.9029049.

[35] Balsam Abdulkadhim Hameedi, Anwar Abbas Hattab, and Muna M. Laftah. “A Pseudo-Random Number Generator Based on New Hybrid LFSR and LCG Algorithm”. In: *Iraqi Journal of Science* (May 2022), pp. 2230–2242. DOI: 10.24996/ijs.2022.63.5.35.

[36] Christopher Panuski, Dirk Englund, and Ryan Hamerly. “Fundamental Thermal Noise Limits for Optical Microcavities”. In: *Physical Review X* 10 (Dec. 2020), p. 041046. DOI: 10.1103/PhysRevX.10.041046.

[37] John M Robinson et al. “Crystalline optical cavity at 4 K with thermal-noise-limited instability and ultralow drift”. In: *Optica* 6 (Feb. 2019), pp. 240–243. DOI: 10.1364/OPTICA.6.000240.

[38] Guanjun Xu et al. “Thermal Noise in Cubic Optical Cavities”. In: *Photonics* 8 (July 2021), p. 261. DOI: 10.3390/photonics8070261.

[39] Dongdong Jiao et al. “Research on Brownian Thermal Noise Limit of a Cylindrical Ultra-Stable Cavity with Support Pads”. In: *Crystals* 12 (Nov. 2022), p. 1682. DOI: 10.3390/cryst12111682.

[40] R Sri Durga et al. “Design and Synthesis of LFSR based Random Number Generator”. In: *2020 Third International Conference on Smart Systems and Inventive Technology (ICSSIT)*. 2020, pp. 438–442. DOI: 10.1109/ICSSIT48917.2020.9214240.

[41] Md Mahbub Alam, Mark Tehranipoor, and Domenic Forte. “Recycled FPGA Detection Using Exhaustive LUT Path Delay Characterization and Voltage Scaling”. In: *IEEE Transactions on Very Large Scale Integration (VLSI) Systems* 27.12 (2019), pp. 2897–2910. DOI: 10.1109/TVLSI.2019.2933278.

[42] Mohammad Ebrahimi, Rezgar Sadeghi, and Zainalabedin Navabi. “LUT Input Reordering to Reduce Aging Impact on FPGA LUTs”. In: *IEEE Transactions on Computers* 69.10 (2020), pp. 1500–1506. DOI: 10.1109/TC.2020.2974955.

[43] Asmita Poojari and Nagesh HR. “FPGA implementation of random number generator using LFSR and scrambling algorithm for lightweight cryptography”. In: *International Journal of Applied Science and Engineering* 18 (2021), pp. 1–9. DOI: 10.6703/IJASE.202112_18(6).001.

[44] Analog Devices. *AD9734/AD9735/AD9736 Datasheet*. https://www.analog.com/media/en/technical-documentation/data-sheets/AD9734_9735_9736.pdf. Accessed: 2023-11-22. 2023.

[45] Christopher Allen et al. “Fast-Time Clutter Suppression in mm-Wave Low-IF FMCW Radar for Fast-Moving Objects”. In: *2020 IEEE International Radar Conference (RADAR)*. IEEE, Apr. 2020, pp. 244–249. DOI: 10.1109/RADAR42522.2020.9114714.

[46] Naoya Kuse and Martin E Fermann. “Frequency-modulated comb LIDAR”. In: *APL Photonics* 4 (Oct. 2019), p. 106105. DOI: 10.1063/1.5120321.

[47] You Li and Javier Ibanez-Guzman. “Lidar for Autonomous Driving: The Principles, Challenges, and Trends for Automotive Lidar and Perception

Systems”. In: *IEEE Signal Processing Magazine* 37 (July 2020), pp. 50–61. DOI: 10.1109/MSP.2020.2973615.

[48] Corneliu I Rablau. “Lidar: a new self-driving vehicle for introducing optics to broader engineering and non-engineering audiences”. In: *Fifteenth Conference on Education and Training in Optics and Photonics: ETOP 2019*. Ed. by Anne-Sophie Poulin-Girard and Joseph A. Shaw. SPIE, July 2019, p. 138. DOI: 10.1117/12.2523863.

[49] Brent Schwarz. “Mapping the world in 3D”. In: *Nature Photonics* 4 (July 2010), pp. 429–430. DOI: 10.1038/nphoton.2010.148.

[50] Patrick Feneyrou et al. “Frequency-modulated multifunction lidar for anemometry, range finding, and velocimetry−1. Theory and signal processing”. In: *Applied Optics* 56 (Dec. 2017), pp. 9663–9675. DOI: 10.1364/AO.56.009663.

[51] Xiang Chen, Tong Shao, and Jianping Yao. “Digital Phase Noise Cancellation for a Coherent-Detection Microwave Photonic Link”. In: *IEEE Photonics Technology Letters* 26 (Apr. 2014), pp. 805–808. DOI: 10.1109/LPT.2014.2306065.

[52] Tongqing Liao, Mahmood Hameed, and Rongqing Hui. “Bandwidth efficient coherent lidar based on phase-diversity detection”. In: *Applied Optics* 54 (Apr. 2015), pp. 3157–3161. DOI: 10.1364/AO.54.003157.

[53] Zhongyang Xu et al. “FMCW Lidar Using Phase-Diversity Coherent Detection to Avoid Signal Aliasing”. In: *IEEE Photonics Technology Letters* 22 (Nov. 2019), pp. 1822–1825. DOI: 10.1109/LPT.2019.2948471.

[54] Shuang Gao, Maurice O’Sullivan, and Rongqing Hui. “Complex-optical-field lidar system for range and vector velocity measurement”. In: *Optics Express* 20 (Nov. 2012). Publisher: Optica Publishing Group, pp. 25867–25875. DOI: 10.1364/OE.20.025867.

[55] BM La Lone et al. “Simultaneous broadband laser ranging and photonic Doppler velocimetry for dynamic compression experiments”. In: *Review of Scientific Instruments* 86 (Feb. 2015), p. 023112. DOI: 10.1063/1.4908306.

[56] Diego Pierrottet et al. “Linear FMCW Laser Radar for Precision Range and Vector Velocity Measurements”. In: *MRS Online Proceedings Library (OPL)* 1076 (Jan. 2008), p. 1076. DOI: 10.1557/PROC-1076-K04-06.

[57] Lukas Kral, Ivan Prochazka, and Karel Hamal. “Optical signal path delay fluctuations caused by atmospheric turbulence”. In: *Optics Letters* 30 (July 2005), pp. 1767–1769. DOI: 10.1364/OL.30.001767.

[58] Po-Tsung Shih et al. “Optical Millimeter-Wave Signal Generation Via Frequency 12-Tupling”. In: *Journal of Lightwave Technology* 28.1 (2010), pp. 71–78. DOI: 10.1109/JLT.2009.2035452.

[59] Shang Gao and Rongqing Hui. “Frequency-modulated continuous-wave lidar using I/Q modulator for simplified heterodyne detection”. In: *Optics Letters* 37 (June 2012), pp. 2022–2024. DOI: 10.1364/OL.37.002022.

[60] Jun Mochizuki et al. “Variable-linewidth light source based on Brownian motion random walk in optical phase”. In: *IEICE Electronics Express* 17.16 (2020), pp. 20200216–20200216. DOI: 10.1587/elex.17.20200216.

[61] Yu Zhou et al. “Effects of a variable linewidth laser and variable linewidth shape laser on coherent FMCW LiDAR”. In: *Optics Continuum* 2 (May 2023), p. 1122. DOI: 10.1364/OPTCON.490071.

[62] Siying Chen et al. “Approximate Voigt function formula for laser-induced breakdown spectroscopy fitting”. In: *Applied Optics* 60 (May 2021), pp. 4120–4126. DOI: 10.1364/AO.416677.

[63] Fritz Riehle. *Frequency Standards: Basics and Applications*. John Wiley & Sons, Mar. 2006.

[64] YAN Jing-tao et al. “Laser Spectrum Broadening Method Based on Phase Modulation of Gaussian White Noise”. In: *SPECTROSCOPY AND SPECTRAL ANALYSIS* 42 (2022), pp. 665–671. DOI: 10.3964/j.issn.1000-0593(2022)03-0665-07.

[65] Yu Zhou et al. “Phase Noise Sensitivity of Coherent FMCW LiDAR Measured by Variable linewidth Laser with Low-Frequency Compensation

and Mirror Method". In: *2022 Asia Communications and Photonics Conference (ACP)*. Nov. 2022, pp. 2013–2016. DOI: 10.1109/ACP55869.2022.10088600.

[66] Tetsuya Kawanishi. *Electro-optic Modulation for Photonic Networks: Precise and high-speed control of lightwaves*. Springer International Publishing, 2022. DOI: 10.1007/978-3-030-86720-1.

[67] Xiang Chen and Jianping Yao. "A High Spectral Efficiency Coherent Microwave Photonic Link Employing Both Amplitude and Phase Modulation With Digital Phase Noise Cancellation". In: *Journal of Lightwave Technology* 33.14 (2015), pp. 3091–3097. DOI: 10.1109/JLT.2015.2419456.

[68] Yu Zhou, Zu-Kai Weng, and Tetsuya Kawanishi. "Effects of the Programmable Real-Time White Gaussian Noise Generated by FPGA on the Laser Linewidth Spectrum". In: *2023 Opto-Electronics and Communications Conference (OECC)*. 2023, pp. 1–3. DOI: 10.1109/OECC56963.2023.10209912.

[69] Yu Zhou et al. "FPGA-driven random walk noise generation for tunable laser linewidth control". In: *IEICE Electronics Express* advpub (2023), p. 20.20230245. DOI: 10.1587/elex.20.20230245.

Acknowledgements

The scholarly endeavors documented within this dissertation were pursued under the esteemed tutelage of Professor Tetsuya Kawanishi (川西哲也教授) at the Department of Electronic and Physical Systems within the hallowed halls of the Graduate School of Fundamental Science and Engineering at Waseda University.

I am profoundly indebted to Professor Kawanishi for his sagacious counsel and altruistic mentorship, which have been the compass guiding my daily research endeavors. Equally, I am grateful for the insightful critiques and constructive feedback provided by Professor Katsuyuki Utaka (宇高勝之教授) and Professor Itsuro Morita (森田逸郎教授) during the rigorous scrutiny of my dissertation defense.

My intellectual sojourn has been further enriched by the erudite contributions of Dr. Zu-kai Weng (翁祖凱博士) and Dr. Keizo Inagaki (稲垣恵三博士) from the National Institute of Information and Communications Technology (NICT), whose perspicacious suggestions have immeasurably enhanced the quality of this research.

Heartfelt appreciation is also extended to my colleague, Kaisen An (安 开 森), for his invaluable assistance with data processing and high-performance computing, and to Kun Cao (曹锟) for his adept support with FPGA implementations.

In closing, I tender my deepest gratitude to my family—my parents, 周章柏 and 鲍芝花—whose boundless support and sacrifices have been the bedrock of my academic journey. This doctoral achievement is a tribute to your unwavering faith in me, and every page of this dissertation is imbued with my gratitude for your love and encouragement.

Publication List

Journals

[1] **Yu Zhou*,** Chen Zheng, Zu-Kai Weng, Keizo Inagaki, and Tetsuya Kawanishi, ”Effects of a variable linewidth laser and variable linewidth shape laser on coherent FMCW LiDAR,” Optics Continuum 2, 1122-1136 (2023). (DOI: https://doi.org/10.1364/OPTCON.490071).

Conferences

[1] **Yu Zhou*,** Zu-Kai Weng, Keizo Inagaki, Atsushi Kanno, and Tetsuya Kawanishi, ,”Phase Noise Sensitivity of Coherent FMCW LiDAR Measured by Variable linewidth Laser with Low-Frequency Compensation and Mirror Method,” 2022 Asia Communications and Photonics Conference (ACP), Shenzhen, China, 2022, Poster paper,pp. 2013-2016. (DOI: 10.1109/ACP55869.2022.10088600).

[2] **Yu Zhou*,** Zu-Kai Weng, and Tetsuya Kawanishi, ”Effects of the Programmable Real-Time White Gaussian Noise Generated by FPGA on the Laser Linewidth Spectrum,” 2023 Opto-Electronics and Communications Conference (OECC), Shanghai, China, 2023, Poster paper, pp. 1-3, (DOI:

10.1109/OECC56963.2023.10209912).

Letters

[1] **Yu Zhou*,** Zu-Kai Weng and Keizo Inagaki and Tetsuya Kawanishi, ”FPGA-driven random walk noise generation for tunable laser linewidth control,” IEICE Electronics Express, pp. 20.20230245, 2023. (DOI: https://doi.org/10.1587/elex.20.20230245).